UNIVERSIDAD DE SALAMANCA

AVANCE EN TÉCNICAS GEOFÍSICAS PARA LA CARACTERIZACIÓN DE ESTRUCTURAS HIDROGEOLÓGICAS

TESIS DOCTORAL

Autor: Javier Carrasco García

ESCUELA POLITÉCNICA SUPERIOR DE ÁVILA

PROGRAMA DE DOCTORADO: GEOTECNOLOGIAS APLICADAS A LA CONSTRUCCIÓN, ENERGÍA E INDUSTRIA

DEPARTAMENTO DE INGENIERIA CARTOGRÁFICA Y DEL TERRENO

Directores de Tesis:

Dr. Pedro Carrasco García

Dr. Ignacio Martin Nieto

Dra. Cristina Sáez Blázquez

Ávila, junio de 2024

Esta Tesis Doctoral es parte de los proyectos de Investigación: PGC2018-094566-B-C21 y PID2022-14713NB-100 financiados por el MCIN/ AEI/10.13039/501100011033/ y FEDER "Una manera de hacer Europa".

Informe de los supervisores de la Tesis Doctoral

"AVANCE EN TÉCNICAS GEOFÍSICAS PARA LA CARACTERIZACIÓN DE ESTRUCTURAS HIDROGEOLÓGICAS"

Presentada en el departamento de Ingeniería Cartográfica y del Terreno por Javier Carrasco García

La Tesis Doctoral titulada "Avance en técnicas geofísicas para la caracterización de estructuras hidrogeológicas", presentada por Javier Carrasco García, se engloba dentro de la línea de investigación de "Integración de técnicas no destructivas (geofísica, geoquímica y termografía) en ingeniería civil y medioambiental. Actualización, optimización y normalización de las distintas aplicaciones" del Programa de Doctorado "Geotecnologías Aplicadas a la Construcción, Energía e Industria".

La línea de investigación abordada se considera de gran relevancia para la comunidad científica internacional, ofreciendo una propuesta clara y sólida para la aplicación de metodologías avanzadas en la resolución de problemas variados en el campo de la hidrogeología. Estas metodologías no solo abordan desafíos actuales, sino que también tienen el potencial de innovar y mejorar las prácticas existentes, proporcionando soluciones para la gestión de recursos hídricos subterráneos de toda índole, incluida la hidrogeotermia.

A través de la presente Tesis Doctoral, se ha podido identificar el potencial de aplicabilidad de las técnicas y metodologías desarrolladas, destacando su importancia en el ámbito científico. Este hecho se constata por los artículos científicos publicados en revistas internacionales de alto impacto, los cuales han sido sometidos a rigurosos procesos de revisión y evaluación crítica por parte de expertos internacionales de reconocida trayectoria. Estos logros no solo validan la calidad y relevancia de los hallazgos, sino que también subrayan la contribución significativa de esta investigación al avance del conocimiento en geofísica e hidrogeología.

Finalmente, la Tesis Doctoral presenta un apartado de conclusiones que detalla las principales aportaciones de las investigaciones realizadas. Estas conclusiones están expuestas de manera que puedan ser objeto de un análisis crítico, proporcionando una base sólida para el desarrollo de futuros trabajos integrados en esta línea de investigación. Los hallazgos y metodologías presentados no solo enriquecen el conocimiento actual en el campo de la hidrogeología, geofísica e hidrogeotermia, sino que también abren nuevas perspectivas y desafíos que invitan a la continuación y expansión de estos estudios.

Ávila, 4 de junio de 2024

Dr. Pedro Carrasco García   Dr. Ignacio Martín Nieto   Dra. Cristina Sáez Blázquez

Listado de Publicaciones

La tesis doctoral por compendio de artículos consta de cinco artículos científicos publicados en diferentes revistas de impacto, los cuales se enumeran a continuación:

- Drone Magnetic and Time Domain Electromagnetic Exploration in Metamorphic Formations: Tool for the Identification of Strategic Sites for Aquifer Exploitation. Appl. Sci. 2023,13, 10949. https://doi.org/10.3390/app131910949

- Time-Domain Electromagnetics as a Geophysical Tool in Hydrogeological Exploitation Projects in Mesozoic Formations. Appl. Sci. 2022, 12, 8655. https://doi.org/10.3390/app12178655

- TDEM Soundings as a Tool to Determine Seasonal Variations of Groundwater Salinity (Villafáfila Lakes, Spain). Water 2022, 14, 2402. https://doi.org/10.3390/w14152402

- Hidrogeología del entorno de las lagunas del Oso (Ávila). Geogaceta, 72, 2022. https://doi.org/10.55407/geogaceta98432

- Electrical-Resistivity Tomography Techniques for the Exploration of Medium- and Low-Geothermal Energy Resources. Energies 2024, 17, 1836. https://doi.org/10.3390/en17081836

Agradecimientos

Quiero expresar mi más profundo agradecimiento a mis directores de tesis, Ignacio Martin Nieto, Cristina Sáez Blázquez y Pedro Carrasco García, por su orientación, paciencia y dedicación a lo largo de este extenso proceso. En especial, agradezco a mi hermano por su constante influencia y apoyo, los cuales fueron cruciales para alcanzar este logro académico.

Agradezco sinceramente a mi familia por su comprensión y apoyo inquebrantable durante todos estos años de estudio. Especialmente, quiero destacar el constante apoyo aportado por mi madre y la ayuda técnica proporcionada por mi padre, cuyo extenso conocimiento en este campo resultó de gran valor.

Deseo expresar mi gratitud a Daniel Porras y Pedro Huerta por su colaboración y disposición para compartir sus experiencias y conocimientos. Sin su valiosa contribución, este trabajo no habría sido posible.

Asimismo, quiero agradecer a todas las personas que, de una u otra manera, contribuyeron a este proyecto, aunque no estén mencionadas explícitamente. Sus aportes no pasaron desapercibidos y son profundamente valorados.

Abstract

Geophysics is a fundamental technology for exploring the constitution and structure of the subsoil through the interpretation of geophysical fields such as electrical and geomagnetic fields.

Although its application in groundwater research has not yet reached full recognition in the scientific community, this doctoral thesis aims to demonstrate its value as an effective tool in the resolution of hydrogeological problems when used appropriately.

It is emphasised that geophysics is not limited to an exact science; the quality of its results depends on the level of resolution used, careful data processing and expert interpretation of the data. Furthermore, the crucial role of the researchers' experience and prior knowledge of the local geology in the success of these investigations is recognised.

In the current context, the availability of a wide range of software for the representation of geospatial data facilitates the efficient visualisation and analysis of terrain structure, further supporting the potential of Geophysics in hydrogeology and hydrogeothermal energy.

This thesis proposes to advance the application of Geophysics through innovation in methodology, technology and geospatial information management tools, recognising the need to use advanced geophysical equipment and to investigate a variety of locations in Spain with different geological issues to achieve significant advances in this field.

Resumen

La Geofísica se erige como una tecnología fundamental para explorar la constitución y estructura del subsuelo mediante la interpretación de campos geofísicos como los eléctricos y geomagnéticos.

Aunque su aplicación en la investigación de aguas subterráneas aún no ha alcanzado pleno reconocimiento en la comunidad científica, esta tesis doctoral se propone demostrar su valía como una herramienta efectiva en la resolución de problemas hidrogeológicos cuando se emplea de manera adecuada.

Se enfatiza que la Geofísica no se limita a una ciencia exacta; la calidad de sus resultados depende del nivel de resolución utilizado, del cuidadoso procesamiento de datos y de la experta interpretación de estos. Además, se reconoce el papel crucial de la experiencia de los investigadores y del conocimiento previo de la geología local en el éxito de estas investigaciones.

En el contexto actual, la disponibilidad de una amplia gama de software para la representación de datos geoespaciales facilita la visualización y el análisis eficiente de la estructura del terreno, respaldando aún más el potencial de la Geofísica en la hidrogeología y energía hidrogeotermal.

Esta tesis propone avanzar en la aplicación de la Geofísica mediante la innovación en metodología, tecnología y herramientas de gestión de información geoespacial, reconociendo la necesidad de utilizar equipos geofísicos avanzados y de investigar una variedad de ubicaciones en España con diferentes problemáticas para lograr avances significativos en este campo.

INDICE

CAPÍTULO 1
INTRODUCCIÓN

1.1. Introducción

La caracterización de estructuras hidrogeológicas es esencial para la gestión y el aprovechamiento sostenible de los recursos hídricos subterráneos. Ante el aumento de la demanda de agua y los efectos del cambio climático, comprender la dinámica y distribución de los acuíferos se ha convertido en una prioridad tanto para la comunidad científica como para los organismos públicos y las entidades privadas.

La geofísica aplicada ofrece un conjunto de herramientas y técnicas que permiten explorar y analizar las características del subsuelo de manera indirecta y no destructiva. A través de métodos eléctricos, electromagnéticos, magnéticos y otros, es posible obtener información detallada sobre la geología e hidrogeología de una región específica. Estas técnicas facilitan la identificación de diversas formaciones geológicas, cuyo análisis contribuye a la caracterización hidrogeológica de la zona de estudio.

Los artículos presentados en esta tesis demuestran diversas metodologías aplicadas en diferentes contextos geológicos, proponiendo un enfoque sistemático que puede servir de guía para futuras investigaciones y trabajos en el ámbito hidrogeológico e hidrogeotérmico.

Este estudio no solo aportará conocimientos valiosos sobre las características hidrogeológicas del área de estudio, sino que también demostrará la efectividad de las técnicas geofísicas en la exploración y gestión de acuíferos. Además, establecerá un precedente para futuras investigaciones en otras regiones con condiciones geológicas similares.

Esta tesis propone el uso de tanto nuevas metodologías de trabajo como técnicas tradicionales con el fin de caracterizar estructuras hidrogeológicas de la manera más cómoda y eficiente posible. Este estudio busca proporcionar una actualización y apoyo a los diferentes estamentos, tanto públicos como privados, para abordar los problemas hídricos actuales y futuros.

1.2. Motivación y Objetivos

La motivación principal para la realización de esta tesis radica en la contribución a la comunidad científica mediante el intercambio de la experiencia acumulada durante años de trabajo y estudios. Se busca abordar de manera efectiva los problemas hidrogeológicos contemporáneos y dar inicio a un recorrido académico más enfocado en la investigación y la colaboración universitaria. Este compromiso continuo refleja nuestra determinación por avanzar en el conocimiento y la comprensión del campo de la hidrogeología.

Los objetivos de esta tesis se centran en los siguientes puntos:

- Proponer la aplicación de diversas metodologías de investigación en distintos contextos geológicos, con el fin de definir las características hidrogeológicas de manera eficiente, precisa y actualizada. Estas técnicas se adaptarán a las condiciones específicas de cada enclave geológico, lo que permitirá optimizar los resultados y proporcionar información crucial para una mejor gestión de los recursos hídricos.
- Plasmar los diferentes resultados de manera accesible para la comunidad científica, presentando la información de forma clara, concisa y fácil de entender. El objetivo es garantizar que los hallazgos sean accesibles y útiles para los investigadores y profesionales del área, facilitando así su aplicación práctica y promoviendo un mayor avance en el campo de la hidrogeología.

CAPÍTULO 2
ARTÍCULOS

ARTICULO 1: Drone Magnetic and Time Domain Electromagnetic Exploration in Metamorphic Formations: Tool for the Identification of Strategic Sites for Aquifer Exploitation

Resumen:

En la actualidad, la explotación de los acuíferos en el sector agrícola ha cobrado cada vez más importancia. En respuesta, los investigadores han dirigido sus esfuerzos hacia la formulación de metodologías eficaces, surgiendo la prospección geofísica como herramienta fundamental, para localizar los mejores yacimientos subterráneos. La técnica de prospección magnética puede discriminar entre diferentes formaciones metamórficas, lo que facilita la localización de contactos geológicos, un factor esencial para la localización estratégica de las perforaciones, mientras que la prospección electromagnética en el dominio del tiempo ayuda a definir los estratos sedimentarios. Los rendimientos variables registrados en los pozos de la zona que han dado buenos resultados son una clara evidencia de la presencia de acuíferos. Sin embargo, es importante señalar que se han realizado numerosos pozos en esta región que han arrojado caudales insignificantes o incluso nulos. La elección de la ubicación y la profundidad de los pozos es esencial para garantizar una gestión adecuada de este recurso. El uso de drones equipados con magnetómetros es una herramienta para acelerar el proceso de cartografía espacial. Los resultados corroboran la clasificación precisa de las unidades litológicas, facilitando así la selección de lugares para la extracción de aguas subterráneas. Estos estudios sirven para validar las hipótesis iniciales y enriquecer profundamente nuestra comprensión de la dinámica hidrogeológica del yacimiento, proporcionando así vías de explotación óptima y sostenibles.

applied sciences

MDPI

Article

Drone Magnetic and Time Domain Electromagnetic Exploration in Metamorphic Formations: Tool for the Identification of Strategic Sites for Aquifer Exploitation

Javier Carrasco García [1], Pedro Carrasco García [2,*], Daniel Porras Sanchiz [3], Ignacio Martín Nieto [2], Cristina Sáez Blázquez [2] and Pedro Huerta Hurtado [2]

1 Técnicas Geofísicas S.L., 05003 Avila, Spain; tgeofisicas@gmail.com
2 Department of Cartographic and Land Engineering, Higher Polytechnic School of Avila, University of Salamanca, Hornos Caleros 50, 05003 Avila, Spain; nachomartin@usal.es (I.M.N.); u107596@usal.es (C.S.B.); phuerta@usal.es (P.H.H.)
3 Geoland Services S.L., 28008 Madrid, Spain; dporras@geoland.es
* Correspondence: retep81@usal.es; Tel.: +34-920353500

Abstract: In the contemporary era, the exploitation of aquifers in the agricultural sector has become increasingly important. In response, researchers have directed their efforts towards the formulation of effective methodologies, with geophysical prospecting emerging as a fundamental tool in locating the best underground deposits. The magnetic prospecting technique can discriminate between different categories of rocks, which facilitates the localisation of geological contacts—an essential factor in determining the strategic location of boreholes, while electromagnetic time-domain prospecting helps in the definition of sedimentary strata. In particular, this process reveals the important influence of tertiary and metamorphic formations on the regional hydrogeological framework of the studied area. The variable yields recorded in the wells in the area that have yielded good results are a clear indication of the presence of aquifers. However, it is important to note that numerous wells have been drilled in this region that have yielded negligible or even zero flow rates. Prudent selection of the location and depth of boreholes is essential to ensure proper management of this resource. The use of drones equipped with magnetometers is essential to speed up the spatial mapping process. Empirical results corroborate the accurate classification of lithological units, thus facilitating the selection of sites for groundwater abstraction. These studies serve to validate initial hypotheses and profoundly enrich our understanding of the hydrogeological dynamics of the site, thus providing avenues for optimal and sustainable exploitation and future academic research.

Keywords: aeromagnetics; drone survey; geophysical prospecting; hydrogeology

check for updates

Citation: García, J.C.; García, P.C.; Sanchiz, D.P.; Nieto, I.M.; Blázquez, C.S.; Hurtado, P.H. Drone Magnetic and Time Domain Electromagnetic Exploration in Metamorphic Formations: Tool for the Identification of Strategic Sites for Aquifer Exploitation. *Appl. Sci.* **2023**, *13*, 10949. https://doi.org/10.3390/app131910949

Academic Editors: Domenico Patella and Paolo Mauriello

Received: 9 September 2023
Revised: 25 September 2023
Accepted: 30 September 2023
Published: 4 October 2023

1. Introduction

In the 21st century, the exploitation of aquifers has become one of the main objectives of the agricultural sector, both to expand and improve existing farms. This growing trend has sparked a keen interest among researchers, who are focused on finding different methods to address this issue in different geological contexts [1–6].

Currently, the techniques used, such as geophysics, require considerable physical effort and face difficulties of access due to topography or vegetation. Therefore, one of the main concerns among geophysicists is the need to adopt methods that are more convenient, faster and able to cover larger areas.

In this paper, we propose an advanced methodology for the effective characterisation of geological strata. We focus in particular on the application of electromagnetic soundings in order to deepen the understanding of the Tertiary strata located in the study region. These soundings are presented as a valuable complement to magnetometry techniques. We also integrate the use of unmanned aerial vehicles (drones) as an essential component in the generation of detailed mapping of the metamorphic materials found in this research area.

In general, metamorphic materials tend to be aquifers with low levels of permeability, making them difficult to exploit. In many cases, they are hardly viable for use. To obtain more interesting flow rates, it is necessary to locate fracture zones or contacts between different materials [7–9]. In this sense, the mapping of the area by means of magnetic prospecting is of great help in the strategic location of these boreholes.

Indeed, magnetic surveying has the ability to differentiate between different types of metamorphic rocks, a feature that can be difficult to achieve using other geophysical variables. This distinguishing ability makes magnetic surveying a valuable tool for the characterisation and detailed study of metamorphic formations, which in turn helps to improve accuracy in the identification of potential aquifers and areas of interest for exploitation [10].

2. Geological and Hydrogeological Context

2.1. Geological Context

The region between the Sierra Albarrana and Obejo-Valsequillo-Puebla de la Reina domains hosts metamorphic materials with a dynamothermal evolution that differs markedly from the rest of the area. These rocks are delimited by large-scale longitudinal faults and include a varied range of formations, including volcanic, detrital and granitic materials of Carboniferous and Tertiary–Quaternary age.

In this geographical area (Figure 1), two distinct groups of metamorphic rocks have been identified: The Higuera de Llerena-Hinojosa del Valle Group and the Atalaya Group. These groups represent a significant geological unit that has been the subject of extensive research due to their unique evolution and composition. The presence of these metamorphic rocks, together with the specific tectonic configuration of the area, makes this place an exciting field of study to deepen the understanding of the geological processes that have shaped this region [11].

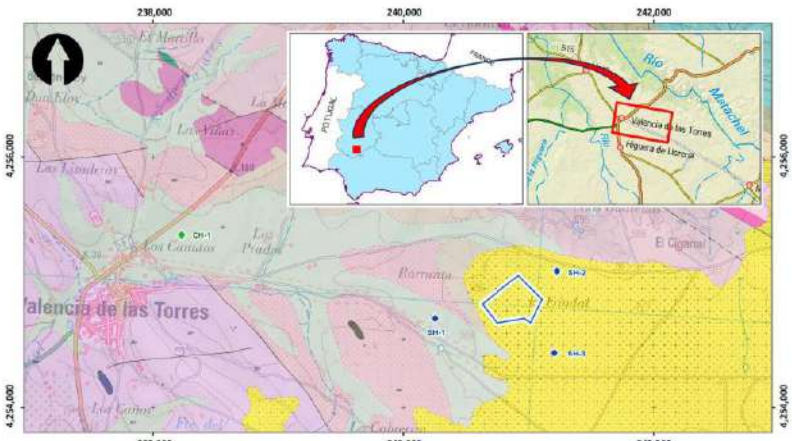

Figure 1. IGME MAGNA. Usagre sheet (855). Geological Map of Spain (E. 1:50,000). Precambrian (Formation 1 and 2), Tertiary (Formation 3) and Quaternary (Formation 4 and 5) [11].

The study area is located in the Higuera de Llerena-Hinojosa del Valle Group. Here, different types of metamorphic rocks can be identified. On the one hand, there are metagranites, quartz schists and/or ultramylonites (Formation 1). These metamorphic rocks have a schistose appearance and are mainly composed of minerals such as quartz, feldspar and a pelitic matrix.

On the other hand, in the same area, there are also orthogneisses (Formation 2) that have their origin in granites, tuffs or acid volcanic rocks. These orthogneisses are rocks that have undergone a process of metamorphism and are characterised by a distinctive texture and composition.

The presence of this diversity of metamorphic rocks in the study area offers a valuable opportunity to investigate and understand the geological processes that have been at work in this region, as well as to analyse the transformations and evolution that these formations have undergone over time.

In the upper part of these materials is a Tertiary formation (Formation 3) that is mainly composed of siltstones and argillites, which originated from the decalcification of limestone outcrops. Towards the base of this tertiary formation, levels of sandstones and conglomerates with calcareous cement are observed.

This set of Tertiary formations adds an additional layer of geological interest in the study area. The process of limestone decalcification and the subsequent deposition of siltstones and argillites have contributed to the present configuration of the area, while the presence of sandstones and conglomerates with calcareous cement provides valuable information on the sedimentary and paleoenvironmental conditions that prevailed during their formation.

In the vicinity of the municipality of Valencia de las Torres, there is an interesting alluvial formation (Formation 4). This formation is characterised by thick deposits found in rivers and flood plains. These deposits are mainly composed of quartzite gravels and sand.

In addition to this, in the areas with steeper relief near Valencia de las Torres, colluvial deposits and alluvial soils can be observed (Formation 5). These colluvial deposits and alluvial soils are interpreted as the result of the accumulation of materials from the erosion of Plio–Quaternary materials in the region. It is important to highlight that, in these areas, the influence of human activities has played a relevant role in the configuration of these deposits.

Although bibliographical data exists on the geology of the area, there are still unknowns regarding the arrangement of the metamorphic rocks in the areas of Tertiary and Quaternary cover. These unknowns add a level of intrigue to the understanding of the geological history of the region, and this is an area where continued research can provide valuable insights into the geological evolution of Valencia de las Torres and the surrounding area.

2.2. Hydrogeological Context

In the research area, Precambrian and Palaeozoic terrains are mostly impermeable, with the exception of Cambrian limestone outcrops, which have the capacity to store significant amounts of water. Highly competent rocks can also act as good aquifers if they are highly fractured. However, most other materials present very little potential as aquifers from a general point of view. Only small water uptakes can be expected, especially in areas where fracture zones exist or in areas that have undergone high geological alteration.

In summary, the region has limited availability of significant aquifers, with the most significant being Cambrian limestone outcrops and highly fractured rocks. It is important to take these geological characteristics into account when approaching any water resource exploitation project in the area.

Tertiary and/or quaternary deposits are materials that are characterised by their crumbly nature, i.e., their composition is brittle and easily eroded. These materials are deposited or formed on an impermeable substrate, resulting in what is known as a hanging deposit. These deposits, being on an impermeable base, allow water to flow into the existing streams in the area. This situation is clearly perceptible, and a series of springs can be identified at the same level, indicating the level of contact between these materials and the impermeable substrate.

Water abstractions in these reservoirs tend to be quite shallow, generally with depths ranging from 0 to 20 m. The flows obtained from these catchments tend to be moderate, as the permeable nature of the reservoirs does not allow for the accumulation of large volumes of water.

It is very interesting to know that in the surroundings of the study area, there is a borehole catalogued by the Guadiana Hydrographic Confederation (CH-1). This borehole represents a valuable source of information on the availability and quality of water in the region. The cataloguing by the confederation indicates that these boreholes have been subject to rigorous monitoring and analysis, which provides a reliable database for the hydrogeological study and sustainable management of water resources in the area.

We are thankful for the information provided on the borehole present in the study area. According to the data provided, this borehole has a depth of approximately 50 m, while the water level is around 10 m. The recorded flow rates are 11 L/s. It is important to note that the lithology of the borehole is composed of metagranites, quartz schists and/or ultramylonites, according to the data provided by the data platform [12].

This information is relevant for the hydrogeological analysis of the region, as it indicates the existence of aquifers in the area. The depth of the boreholes suggests that the groundwater is at an accessible distance, which may favour its use by means of appropriate extraction techniques.

Variable flows are indicative of the dynamics of groundwater flow, which can be influenced by various factors such as seasonality and local hydrological characteristics. These moderate flows represent a significant source of water, which can satisfy various water requirements, provided they are managed in a responsible and sustainable manner.

The presence of metagranites, quartz schists and/or ultramylonites in the borehole is relevant, as these metamorphic rocks have the capacity to contain and transport groundwater. These lithological characteristics offer promising potential as natural aquifers in the region.

It is relevant to mention that, in addition to the boreholes catalogued by official bodies, additional research was carried out in boreholes close to the study area carried out by private individuals. These boreholes are not officially registered, which means that it is not possible to be absolutely certain about the quality and reliability of their data.

Nevertheless, the information obtained through this research is valuable, as it sheds light on the existence of SH-1 flows of 2–2.5 L/s, SH-2 of 1–1.5 L/s and SH-3 of 1 L/s. The variability in flow rates points to the natural dynamics of groundwater flow in the area, which may be influenced by different hydrological and geological factors. In addition, it is important to note that numerous boreholes have been drilled in this region that have yielded negligible or even zero flow rates.

In conclusion, we can see that, in general, the flow rate of the boreholes depends on the metamorphic formation in which they are located, ignoring the small tertiary cover of no more than 20 m in some cases. It should be noted that the supply borehole (CH-1) is located on a Quaternary formation which the rest do not have, in addition to the Tertiary, which may indicate a thickening of the thickness of this formation and be the factor for this increase in flow. For our assessment we will not take this borehole into account, as it yields data that are probably not consistent with the metamorphic rocks.

3. Materials and Methods

3.1. Site Conditions

The data used in this study were collected during the spring of 2020, on a day that was partly cloudy but mostly sunny. During data collection, the temperature remained at a pleasant average of 19 degrees Celsius, while wind speed remained constant at 5 m per second. The location is characterised by spring weather, with average temperatures varying between 20 and 30 degrees Celsius, and wind speeds generally below 5 m per second. These climatic conditions favoured data acquisition and ensured the accuracy of the results.

The study was carried out over a three-hour period in a large rain-fed agricultural area. In this area the presence of trees is scarce, except in the plots located to the east, which contain vineyards and olive groves that were not the subject of our analysis. The topography of the region shows minimal variations, with a difference of less than 2 m from north to south, making it gentle and practically flat. This topography provided optimal conditions for data collection, greatly simplifying our research.

To mitigate possible risks (although they were not considered particularly relevant in our study area, such as collisions of the drone with topographic elements or vegetation), a digital elevation model (DEM) of the area was previously elaborated. In this flight the most essential geometric criteria for photogrammetric applications [13] were applied, which guaranteed the obtaining of high-quality cartographic data and a Ground Sampling Resolution (GSD) of 4 centim per pixel.

DEM generation was carried out using a DJI Mavic 2 Pro drone equipped with a 1-inch CMOS sensor, flying at an altitude of 150 m above ground level (AGL). This approach ensured a stable and safe flight, which allowed us to obtain accurate and reliable results for our research.

In addition, a short electromagnetic sounding campaign was conducted to assess the possible thickness of the Tertiary strata [14,15]. This campaign consisted of three electromagnetic soundings arranged in a 75 × 75 m profile.

3.2. *Platform and Flight Planning*

In the current study, the Dji Matrice 600 Pro multi-rotor hexacopter was used (Figure 2), which has an A3Pro flight controller and is compatible with UgCS mission planning software. This device has a total take-off weight of 9.6 kg and a maximum payload capacity of 6 kg, and is powered by 6 lithium polymer batteries with a capacity of 4500 mAh.

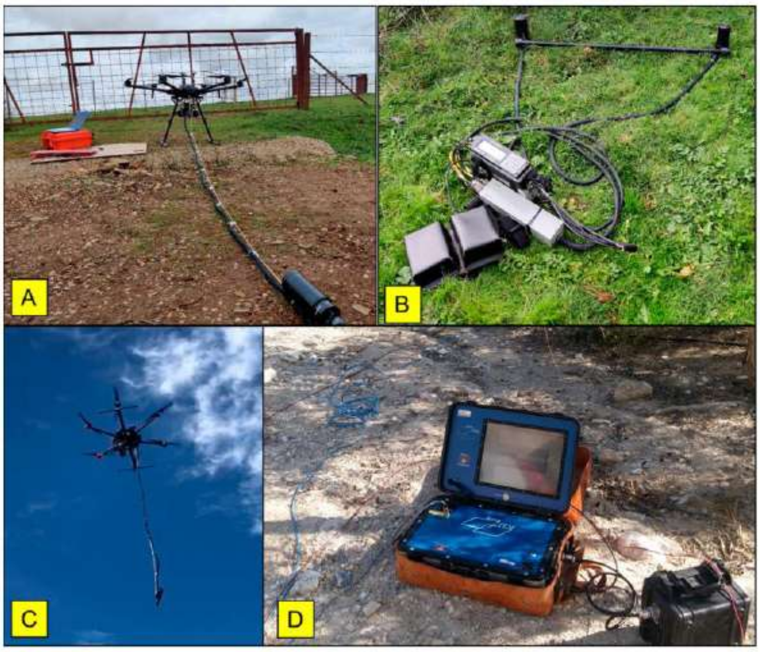

Figure 2. Registration system. (**A**) Mavic Matrice 600 Pro hexacopter drone; (**B**) base magnetometer for diurnal corrections; (**C**) static drone position with the magnetometer hanging below; (**D**) Terra-Tem equipment.

The flight speed was set at 5 m per second, with a sampling interval of 200 milliseconds, allowing measurements to be taken at one-metre intervals along the recorded profile. A flight altitude of 20 m above ground level (AGL) was selected to maximise sensor resolution and ensure safety from potential obstacles. In addition, the previously acquired digital elevation model was incorporated into the flight plan. Finally, a tolerance level of 1 m was defined for altitude adjustments during the flight.

The design and control of the project was carried out using UgCS flight software. Seven parallel survey lines of varying lengths were implemented, oriented in a N45E direction and perpendicular to the regional geological structure. A distance of 25 m was maintained between each line to achieve high spatial resolution and to capture variations in the target magnetic field (Figure 3). Given the vastness of the study area, the total flight was divided into two blocks, choosing a take-off and landing point considering the capabilities of the batteries.

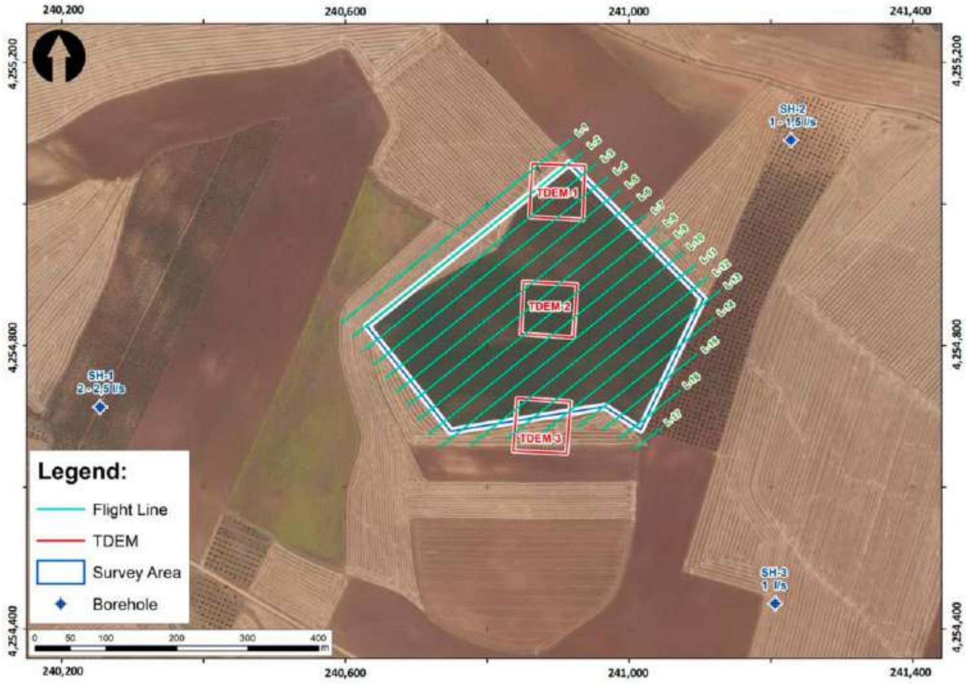

Figure 3. Flight plan made for magnetometry.

The resulting effect of the separation between the sensor and the surface leads to a slight reduction in spatial resolution and intensity, in contrast to ground-based investigations [16,17]. However, this decrease is compensated by a constant and higher density data acquisition.

3.3. *Magnetometry*

The drone was equipped with a GEM-Systems GSMP-35U potassium vapour magnetometer, which has a sensitivity of 0.0002 nT/1 Hz. This system also has the capability to simultaneously record the magnetic field and to incorporate a real-time single-frequency (L1) GPS receiver.

This equipment consists of multiple components, including a sensor connected by cable to a controller, a data logger, a 5 V battery power supply and a GPS receiver, with a total weight not exceeding 2 kg. To ensure the stability and safety of the system, careful adjustments were made to locate and balance the data logger and batteries inside the drone's cargo compartment. In addition, the GPS antenna was placed on top of the drone to ensure continuous signal reception.

Regarding the accuracy of the magnetic sensor, it is important to note that interference from vegetation, topography, soil moisture and rock features is negligible. However, it is crucial to keep in mind that topography plays a decisive and essential role in the generation of the three-dimensional (3D) model.

Due to the presence of magnetic interference generated by the electromagnetic motors inside the drone platform, significant measures were implemented to counteract this effect [18,19]. The magnetic sensor was placed at a distance of 3 m from the base of the drone and connected to the main system via a cable. This strategic arrangement allowed the influence of the magnetic field produced by the motors to be minimised, preventing it from affecting the measurements made by the GSMP-35U magnetometer [20].

To prevent pendulum motion of the sensor, which could cause variations in roll, pitch and yaw axes, additional 25 m segments were added at each end of the flight lines during 180-degree turns. This approach allowed greater leeway and reduced the likelihood of sudden or unexpected movements affecting the measurements.

The installation of the magnetic sensor was carried out without rotation restrictions on any of the axes, which provided greater freedom of movement during operations. Specific measures were implemented in the project design to ensure the accuracy of the measurements and minimise any possible interference.

In addition, the flight speed was reduced, which contributed to a more stable and controlled operation. The lower speed facilitated better control of the drone, which in turn helped to minimise unwanted sensor oscillations.

Simultaneously, a fixed magnetometer was installed in a nearby location free from sources of magnetic interference. Its purpose was to calculate the correction for the diurnal effect, which occurs due to the temporal variation of the magnetic field throughout the day (Figure 2B).

The fixed magnetometer was set up with a total field recording interval of 1 s.

3.4. TDEM

A series of 75 × 75 m electromagnetic soundings were carried out using a "coincident loop" type measuring device. Data were acquired using Terra-Tem equipment designed by Monex GeoScope (Figure 2D).

Time domain electromagnetic surveying (TEDM) is performed by introducing a constant current into a closed circuit or transmitter coil (Tx). This action gives rise to a constant primary magnetic field. Then, when the current flowing through the transmitter coil (Tx) is abruptly interrupted, the previously constant primary magnetic field begins to decay gradually over time.

Following the principles of Faraday's Law, when a body is exposed to a time-varying magnetic field, electric currents are generated in the subsurface. These currents follow closed paths underground, moving both in depth and laterally. Over time, the strength of these currents decreases, giving rise to a transient secondary magnetic field that also vanishes at the surface.

This secondary magnetic field induces a temporary variation in the voltage within the receiver circuit (Rx). The way this voltage decreases provides valuable information about the resistivity of the subsurface. Both the magnitude and the distribution of the induced currents are closely related to the resistivity properties of the medium. It is important to note that this process is depth–migratory, which implies that short duration stresses provide information about the resistivity of the shallow layers, while longer duration stresses provide knowledge about the resistivity of the deeper layers of the subsurface [21–23].

3.5. Data Processing

The magnetometry data were processed using OASIS Montaj 9.8 software, using conventional methods to calculate anomalies and produce residual anomaly maps through a variety of filters. In an initial phase, inaccurate values resulting from drone position, take-off and landing manoeuvres, orientation, excessive roll and temporal discrepancies between the sensor and the drone were filtered out. Points located at the most extreme extensions of the survey lines and other outliers were excluded using a one-dimensional median filter. Finally, a correction using the diurnal variation of the Earth's magnetic field values, caused by solar activity, was applied to adjust the data collected during the study period [24].

Regarding the TDEM data, they were acquired using a "coincident loop" configuration and square loops (both emitter and receiver) of 75 m length per side. A minimum of 1000 measurement repetitions per channel were performed, and tests were carried out at different gain levels in order to minimise any influence of electromagnetic noise present in the environment. The results of the various decay curves obtained in the field were presented using the Monex GeoScope "TEM Plotting Program v 2.0.0". In addition, the same program was used to generate the corresponding geoelectric profile [25].

4. Results

4.1. Total Magnetic Field and Reduction to Pole

The data interpretation process starts with the calculation of the Total Magnetic Field (TMF) from the filtered records (Figure 4A), followed by the application of the Reduction to Pole (RP). By combining the magnetic inclination and declination data in the sampling area, together with the use of the International Geomagnetic Model Reference Magnetic Field (IGRF), it is possible to obtain a direct representation of the primary magnetic sources responsible for the generating bodies (Figure 4B) [26,27].

By examining both representations, a variation in the magnetic field that delimits the study area into two distinct formations stands out. Formation 1 is composed of metagranites, quartz schists and/or ultramylonites (target formation), while Formation 2 corresponds to orthogneisses (very impermeable formation with low hydrogeological possibilities).

The results reveal a disparity of up to 20 nT in the magnetic field between these two geological structures. Interpretation of these data suggests that the lower magnetic field values are linked to the metagranites, quartz schists and/or ultramylonites that make up Formation 1 due to their lower magnetic propensity, compared to the orthogneisses of Formation 2. [28,29] This conclusion is strengthened by the location of nearby drill holes, which indicate a higher permeability in Formation 1.

A critical aspect is the precise identification of the contact point between these two geological structures. The proximity to this transition zone is crucial, as a decrease in flow is anticipated due to the limited aquifer capacity of Formation 2.

This analysis provides valuable information to guide decisions in planning the exploitation of groundwater resources. This enables a more informed choice in the selection of sites for well drilling and a deeper understanding of the local hydrogeology, thus enriching the knowledge base for sustainable groundwater resources management.

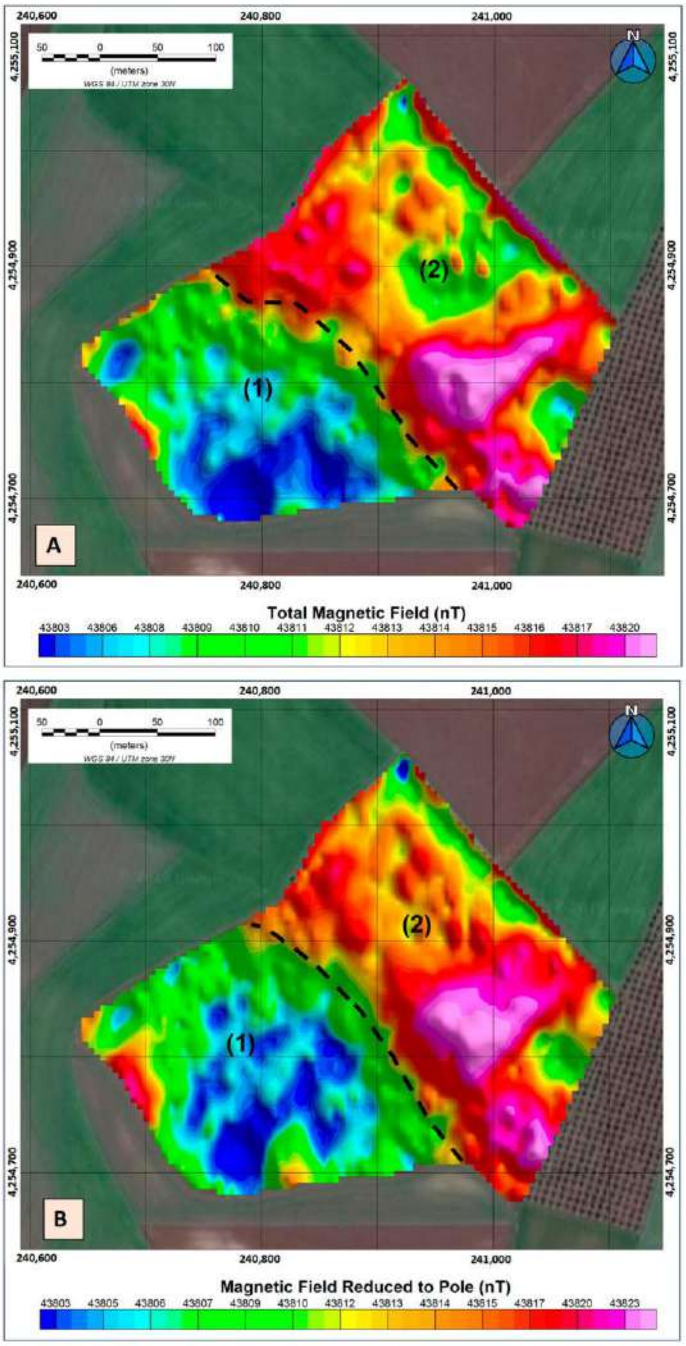

Figure 4. Total magnetic field (**A**) and pole reduction (**B**).

4.2. D Inversion Model

The generation of a high-resolution uniform grid using drones has enabled the creation of three-dimensional models that visualize the magnetic susceptibility by applying an advanced inversion technique [30]. The resulting model has been built using the VOXI Earth Modelling software from OASIS Montaj. This tool has greatly simplified the identification and spatial delimitation of the magnetic bodies of interest.

The results obtained from this modelling process (Figure 5) show the existence of two geological bodies with contrasting magnetic susceptibilities. These findings are of great relevance for the discrimination of the different geological formations present in the study region. It is noteworthy that the lowest magnetic susceptibility corresponds to Formation 1, while the highest susceptibility is associated with Formation 2. It is noteworthy that the metagranites, quartz schists and/or ultramylonites exhibit a markedly lower iron content compared to the orthogneisses, which is essential for the accurate interpretation of our geological model. Moreover, this distinction manifests itself continuously as one goes deeper into the subsurface.

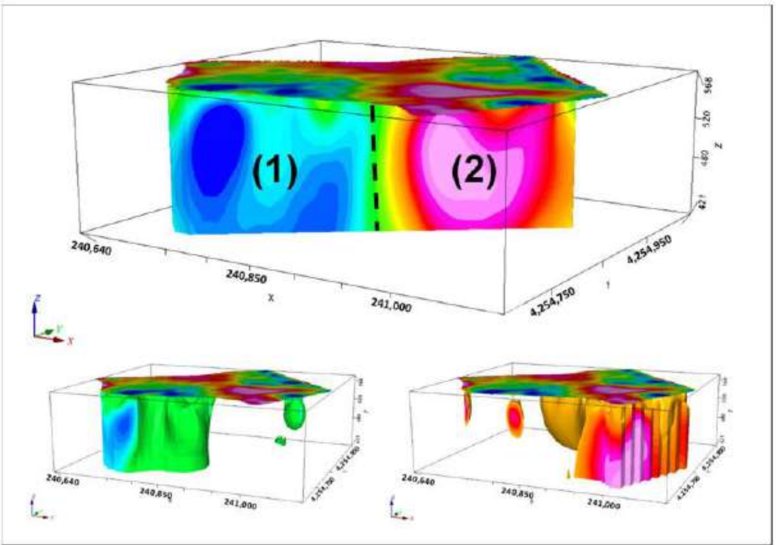

Figure 5. 3D model of the study area.

4.3. TDEM

Three electromagnetic soundings (Figure 6) were carried out to acquire information about the Tertiary stratum in order to gain a more precise understanding of the geological column present in our investigation. These tests reveal a more conductive portion corresponding to the Tertiary stratum, followed by an abrupt transition to a more resistive material of a rocky nature, although no changes in it are discernible as anticipated [31,32].

These results show a limited thickness in the Tertiary stratum, which lacks sufficient entity to be considered an aquifer. Moreover, its composition is made up of materials of little hydrogeological interest.

As for the contact between the Precambrian formations, it is not possible to determine its position by TEDM or any other geophysical method from which the resistivity parameter is obtained, given the lack of resistivity contrast between the Precambrian formations present.

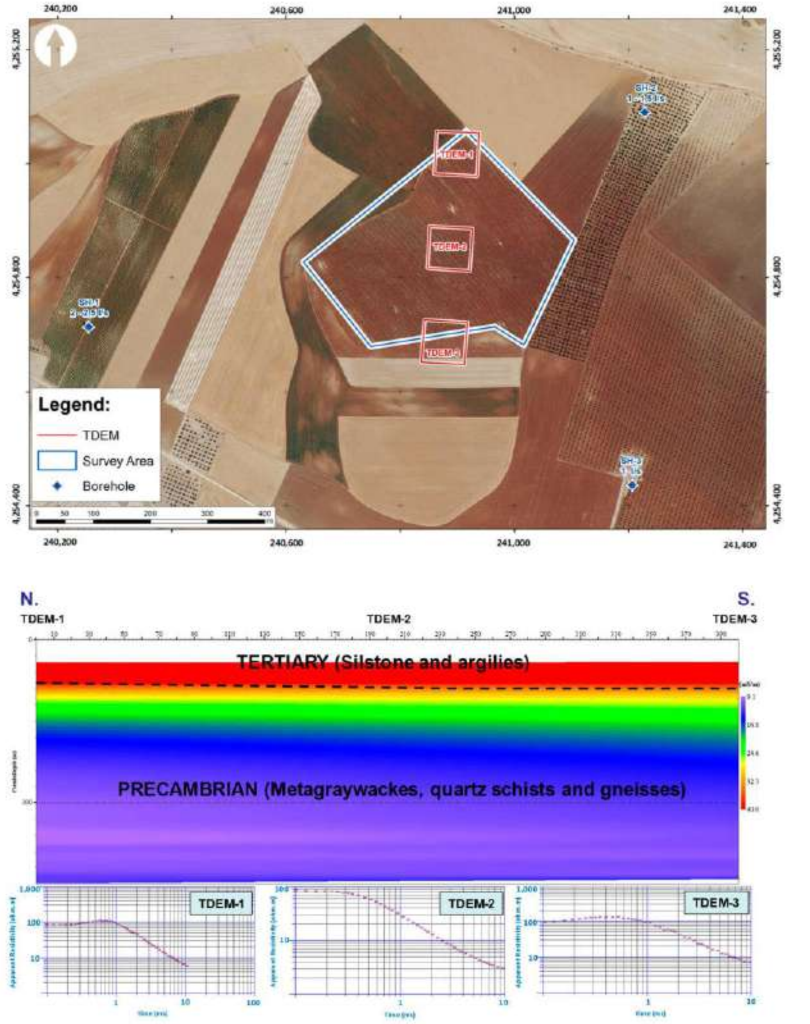

Figure 6. Situation of electromagnetic soundings and interpreted electrical conductivity profile formed by the electromagnetic soundings and apparent resistivity curves of the different electromagnetic soundings.

4.4. Geological Interpretation, Site Location and Drilling Results

TDEM tests in our study area have yielded results consistent with the presence of a Tertiary cover, as shown in the geological map of the area. However, the configuration of the contact between the Precambrian formations remains an unresolved enigma.

Fortunately, thanks to the application of magnetic investigation techniques, we have been able to identify the point of contact between the formations below the Tertiary layer. This contact is clearly and distinctly in the northwest direction, as can be seen on the geological map. By superimposing our findings on the map, together with a precise extrapolation of this contact point, we have managed to visualise how it aligns relatively coherently with the previously determined trajectory of this particular contact. This interesting result can be seen in Figure 7.

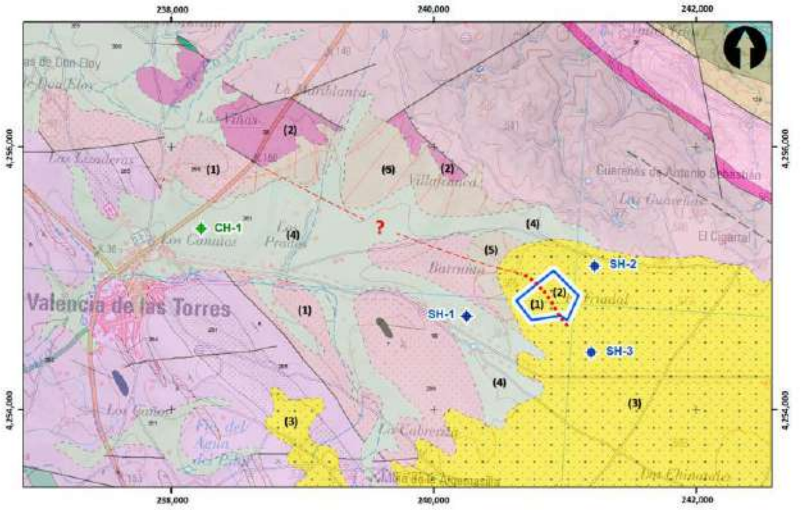

Figure 7. Contact path image between Formation 1 and 2. Precambrian (Formation 1 and 2), Tertiary (Formation 3) and Quaternary (Formation 4 and 5).

This breakthrough represents a significant step forward in our understanding of the geological layout of the area. By linking the magnetic data with existing geological mapping, we have been able to infer the location of the contact between strata in the subsurface, providing valuable information for the characterisation of the region studied.

Using these results and the information gathered from boreholes, we can propose sites for exploitation of the aquifer of greatest interest (Figure 8).

The selection of drilling sites is based on two main criteria supported by magnetic scanning data, while electromagnetic (TDEM) data were not useful in this respect. These criteria focus on the most favourable lithology (S-1) and the point of contact between geological formations, which could indicate a more fractured zone (S-2).

It is important to note that the location of borehole S-1 is determined on the basis of the lower magnetic susceptibility recorded in the results, looking for a greater presence of material of higher permeability. On the other hand, borehole S-2 is located in the contact zone between both geological formations, but within the formation of greatest interest.

In relation to borehole S-1, the data collected indicate an estimated flow rate of around 2–3 L per second (L/s), which coincides with nearby boreholes and previous boreholes drilled in the same geological formation. As for borehole S-2, due to its location between two formations and its greater degree of alteration, the estimate of the flow rate is less certain, although its proximity to an impermeable edge suggests a lower estimate than in the previous borehole.

Both boreholes (Figure 9) were drilled to a depth of 100 m in both cases, revealing an approximate flow rate of 3 L/s in borehole S-1 and 2 L/s in borehole S-2. These data, although requiring careful consideration due to the absence of regular testing throughout different seasons of the year, provide valuable context to support our site selection hypotheses and rationale.

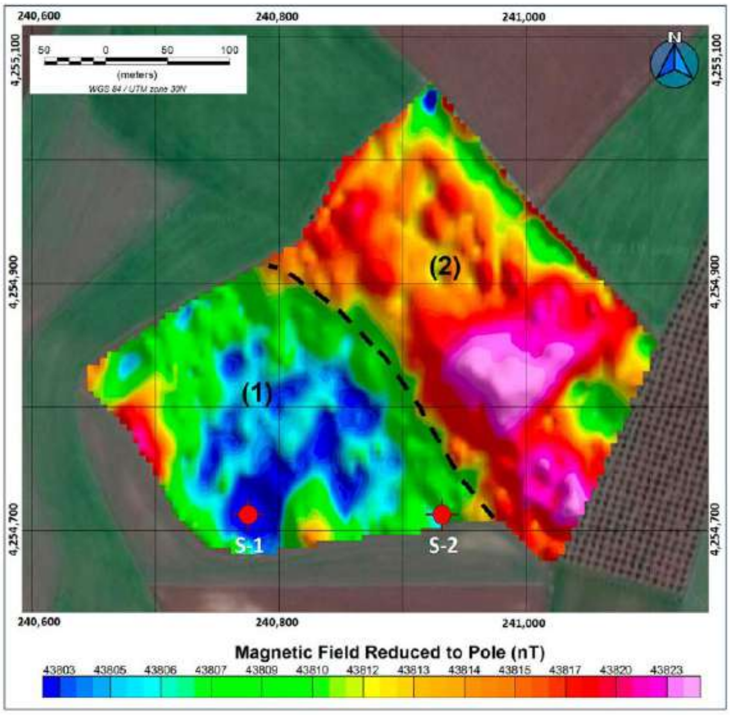

Figure 8. Location of soundings (S-1 and S-2).

Figure 9. Image of drilling rig at site S-1.

The higher flow rate recorded in borehole S-1 supports the initial assumption of higher permeability at this location. On the other hand, the lower flow rate obtained in borehole S-2 evidences the nature of the contact between both formations. In addition, it is relevant to note that the material drilled in borehole S-1 was mostly identified as greywackes, whereas borehole S-2 passed through an alteration zone composed of quartz schists, greywackes and ultramylonites.

5. Conclusions

The findings of this current study, based on the application of magnetometric technology using drones to map metamorphic formations for the purpose of identifying locations suitable for drilling groundwater extraction wells, constitute an immensely valuable tool that effectively and rapidly facilitates the mapping of lithological variations in the terrain. In addition, it should be noted that the application of airborne methods enables us to explore much larger geographical areas in significantly reduced time intervals. These methods are particularly effective in the analysis of areas that are difficult to access, either due to complex topographic conditions or dense vegetation, while minimising the physical effort compared to traditional geophysical techniques. The synergy of these elements leads to significant economic savings in the investigation of large areas.

In this specific investigation, it has been possible to distinguish precisely between the different types of materials present, such as orthogneisses, metagranites, quartz schists and ultramylonites. This detailed mapping, which shows the spatial arrangement of these materials, is of considerable importance in the process of selecting and locating extraction pits. This is achieved by proposing the identification of the materials with the highest water potential, as well as the location of contact points between the geological strata. In addition, it is noteworthy that this technology also allows the detection of fractured zones in other types of geological materials.

It is particularly significant to highlight the results obtained by magnetic investigation under a tertiary layer, which was an uncertainty from a bibliographical point of view, and which we have had the opportunity to verify effectively.

It is relevant to underline that the results obtained, presented in their direct form, have contributed substantially to the confirmation of our previous hypotheses, thus enriching our understanding of the hydrogeological behaviour of the studied environment. These findings have not only validated our initial theories, but have also opened new perspectives to broaden our knowledge in this particular field.

Author Contributions: Conceptualization, J.C.G. and P.C.G.; methodology, J.C.G., P.C.G. and D.P.S.; validation, I.M.N., P.C.G., P.H.H. and C.S.B.; formal analysis, P.C.G. and J.C.G.; investigation, J.C.G. and P.C.G.; resources, P.C.G. and J.C.G.; software, P.C.G., D.P.S. and J.C.G.; data curation, J.C.G.; writing—original draft preparation, J.C.G. and D.P.S.; writing—review and editing, P.C.G., D.P.S., I.M.N., P.H.H. and C.S.B.; visualization, I.M.N., P.C.G., C.S.B. and P.H.H.; supervision, P.C.G., P.H.H., I.M.N. and C.S.B.; project administration, P.C.G. and J.C.G. All authors have read and agreed to the published version of the manuscript.

Funding: This research received no external funding.

Institutional Review Board Statement: Not applicable.

Informed Consent Statement: Not applicable.

Data Availability Statement: Not available.

Conflicts of Interest: The authors declare no conflict of interest.

References

1. D'Odorico, P.; Chicarelli, D.D.; Rosa, L.; Bini, A.; Zilberman, D.; Rulli, M.C. The global value of water in agriculture. *Proc. Natl. Acad. Sci. USA* **2020**, *117*, 21985–21993. [CrossRef] [PubMed]
2. Basso, B.; Kendall, A.D.; Hyndman, D.W. The future of agriculture over the Ogallala Aquifer: Solutions to grow crops more efficiently with limited water. *Earth's Future* **2013**, *1*, 39–41. [CrossRef]

3. Smidt, S.J.; Haacker, E.M.K.; Kendall, A.D.; Deines, J.M.; Pei, L.; Cotterman, K.A.; Li, H.; Liu, X.; Basso, B.; Hyndman, D.W. Complex water management in modern agriculture: Trends in the water-energy-food nexus over the High Plains Aquifer. *Sci. Total Environ.* **2016**, *566–567*, 988–1001. [CrossRef] [PubMed]
4. Othman, A.; Sultan, M.; Becker, R.; Alsefry, S.; Alharbi, T.; Gebremichael, E.; Alharbi, H.; Abdelmohsen, K. Use of Geophysical and Remote Sensing Data for Assessment of Aquifer Depletion and Related Land Deformation. *Surv. Geophys.* **2018**, *39*, 543–566. [CrossRef]
5. Calderón Palma, H.; Bentley, L.R. A regional-scale groundwater flow model for the Leon-Chinandega aquifer, Nicaragua. *Hydrogeol. J.* **2007**, *15*, 1457–1472. [CrossRef]
6. Rad, M.R.; Brozovic, N.; Foster, T.; Mieno, T. Effects of instantaneous groundwater availability on irrigated agriculture and implications for aquifer management. *Resour. Energy Econ.* **2020**, *59*, 101129. [CrossRef]
7. Ofterdinger, U.; MacDonald, A.M.; Comte, J.C.; Young, M.E. Groundwater in fractured bedrock environments: Managing catchment and subsurface resources- an introduction. *Geol. Soc. Lond. Spec. Publ.* **2019**, *479*, 1–9. [CrossRef]
8. Font Capó, J.; Vázquez Suñe, E.; Carrera, J.; Herms, I. Groundwater characterization of a heterogenous granitic rock massif for shallow tunneling. *Geol. Acta Int. Earth Sci. J.* **2012**, *10*, 395–408. Available online: https://dialnet.unirioja.es/servlet/articulo?codigo=4138023 (accessed on 17 August 2023).
9. Gobashy, M.M.; Metwally, A.M.; Abdelazeem, M.; Soliman, K.S.; Abdelhalim, A. Geophysical Exploration of Shallow Groundwater Aquifers in Arid Regions: A Case Study of Siwa Oasis, Egypt. *Nat. Resour. Res.* **2021**, *30*, 3355–3384. [CrossRef]
10. Nabighian, M.N.; Grauch, V.J.S.; Hansen, R.O.; LaFehr, T.R.; Li, Y.; Peirce, J.W.; Phillips, J.D.; Ruder, M.E. The historical development of the magnetic method in exploration. *Geophysics* **2005**, *70*, 33–61. [CrossRef]
11. IGME MAGNA. Geological and Mining Institute of Spain (IGME). Hoja de Usagre (855). In *Mapa Geológico de España (E. 1:50.000)*; Servicio de Publicaciones del Ministerio de Industria y Energía: Madrid, Spain, 1981.
12. BD Puntos de Agua v2.0 IGME. Available online: https://info.igme.es/BDAguas/ (accessed on 19 August 2023).
13. Hernandez-Lopez, D.; Felipe-Garcia, B.; Gonzalez-Aguilera, D.; Arias-Perez, B. An automatic approach to UAV flight planning and control for photogrammetric applications. *Am. Soc. Photogramm. Remote Sens.* **2013**, *1*, 87–98. [CrossRef]
14. Elwaheidi, M. Geophysical Imaging of a Buried Tertiary Valley Aquifer in an Arid Region Using Time Domain Electromagnetic Method. *J. Geosci. Environ.* **2020**, *8*, 195–206. [CrossRef]
15. Hamada, L.R.; Porsani, J.L.; Bortolozo, C.A.; Rangel, R.C. TDEM and VES soundings applied to a hydrogeological study in the central region of the Taubaté Basin, Brazil. *First Break* **2018**, *36*, 49–54. [CrossRef]
16. Cunningham, M.; Samson, C.; Wood, A.; Cook, I. Aeromagnetic Surveying with a Rotary-Wing Unmanned Aircraft System: A Case Study from a Zinc Deposit in Nash Creek, New Brunswick, Canada. *Pure Appl. Geophys.* **2018**, *175*, 3145–3158. [CrossRef]
17. Walter, C.A.; Braun, A.; Fotopoulos, G. Impact of three-dimensional attitude variations of an unmanned aerial vehicle magnetometry system on magnetic data quality. *Geophys. Prospect.* **2019**, *67*, 465–479. [CrossRef]
18. Mu, Y.; Chen, L.; Xiao, Y. Small Signal Magnetic Compensation Method for UAV-Borne Vector Magnetometer System. *IEEE Trans. Instrum. Meas.* **2023**, *72*, 1–7. [CrossRef]
19. Walter, C.A.; Braun, A.; Fotopoulos, G. High-resolution unmanned aerial vehicle aeromagnetic surveys for mineral exploration targets. *Geophys. Prospect.* **2020**, *68*, 334–349. [CrossRef]
20. Zheng, Y.; Li, S.; Xing, K.; Zhang, X. Unmanned Aerial Vehicles for Magnetic Surveys: A Review on Platform Selection and Interference Suppression. *Drones* **2021**, *5*, 93. [CrossRef]
21. Huerta, P.; Carrasco-García, P.; Armenteros, I.; Recio, C.; Carrasco-García, J.; Rodríguez-Jiménez, E. TDEM Soundings as a Tool to Determine Seasonal Variations of Groundwater Salinity (Villafáfila Lakes, Spain). *Water* **2022**, *14*, 2402. [CrossRef]
22. Nieto, I.M.; Carrasco García, P.; Sáez Blázquez, C.; Farfán Martín, A.; González-Aguilera, D.; Carrasco García, J. Geophysical Prospecting for Geothermal Resources in the South of the Duero Basin (Spain). *Energies* **2020**, *13*, 5397. [CrossRef]
23. Sheriff, R.E. *Geophysical Methods*, 1st ed.; Prentice Hall: Englewood Cliffs, NJ, USA, 1989.
24. Porras, D.; Carrasco, J.; Carrasco, P.; Alfageme, S.; Gonzalez-Aguilera, D.; Lopez Guijarro, R. Drone Magnetometry in Mining Research. An Application in the Study of Triassic Cu-Co-Ni Mineralizations in the Estancias Mountain Range, Almería (Spain). *Drones* **2021**, *5*, 151. [CrossRef]
25. Carrasco-García, J.; Porras-Sanchiz, D.; Carrasco-García, P.; Herrero-Pacheco, J.L.; Martín-Nieto, I.; Benito-Herrero, J.M.; Huerta-Hurtado, P. Time-Domain Electromagnetics as a Geophysical Tool in Hydrogeological Exploitation Projects in Mesozoic Formations. *Appl. Sci.* **2022**, *12*, 8655. [CrossRef]
26. Subasinghe, N.D.; Charles, W.K.D.G.D.R.; De Silva, S.N. Analytical Signal and Reduction to Pole Interpretation of Total Magnetic Field Data at Eppawala Phosphate Deposit. *J. Geosci. Environ. Prot.* **2014**, *2*, 3. [CrossRef]
27. Munazyi, D.; Suparman, R.; Abiyudo, R. Application of Magnetic Method (Reduced to Pole and Analytic Signal) to Extract Specific Geology Information (Young Lava, Alteration and Quarternary Older Rock). Case Study: Mount Lamongan. In Proceedings of the 4th Indonesia International Geothermal Convention & Exhibition 2016, Cendrawasih Hall—Jakarta Convention Center, Jakarta, Indonesia, 10–12 August 2016.
28. Telford, W.M.; Geldart, L.P.; Sheriff, R.E. *Applied Geophysics*; Cambridge University Press: Cambridge, UK, 1990.
29. Clark, D.A.; Emerson, D.W. Notes on Rock Magnetization Characteristics in Applied Geophysical Studies. *Explor. Geophys.* **1991**, *22*, 547–555. [CrossRef]

30. MacLeod, I.N.; Ellis, R.G. Magnetic Vector Inversion, a Simple Approach to the Challenge of Varying Direction of Rock Magnetization. Australian Society of Exploration Geophysicists, Extended Abstracts. 2013, pp. 1–4, Melbourne. Available online: https://www.semanticscholar.org/paper/Magnetic-Vector-Inversion-%2C-a-simple-approach-to-of-Macleod-Ellis/9cd186fe7e6843baeb43c706d80fc64ffed3109a (accessed on 1 December 2021).
31. Porras, D.; Carrasco, J.; Carrasco, P.; Herrero-Pacheco, J.L. Deep TDEM Study for Structural and Mining Purposes: A Case Study of the Barbastro Saline-Evaporitic Formation, Spain. *Appl. Sci.* **2023**, *13*, 6385. [CrossRef]
32. Mendoza, R.; Rey, J.; Martínez, J.; Hidalgo, M.C.; Sandoval, S.S. Geophysical characterisation of geologic features with mining implications from ERT, TDEM and seismic reflection (Mining District of Linares-La Carolina, Spain). *Ore Geol. Rev.* **2021**, *139*, 104581. [CrossRef]

ARTICULO 2 Time-Domain Electromagnetics as a Geophysical Tool in Hydrogeological Exploitation Projects in Mesozoic Formations

Resumen:

La necesidad de utilizar los recursos hídricos subterráneos para las explotaciones agrícolas y ganaderas es un tema en constante crecimiento, ya que, estos recursos condicionan el desarrollo socioeconómico de muchas zonas con regímenes climáticos y recursos hídricos superficiales limitados. Las decisiones sobre la ubicación y características de obras de extracción de aguas subterráneas se basan en estudios hidrogeológicos, en los que las técnicas geofísicas son una herramienta muy útil. En nuestro estudio se utilizó la técnica de sondeos electromagnéticos en el dominio del tiempo (TDEM), que mejora notablemente la precisión y la seguridad a la hora de planificar perforaciones para la extracción de agua en formaciones mesozoicas gracias al importante contraste de resistividad entre sus diferentes unidades hidrogeológicas. La realización de una campaña de investigación mediante TDEM permite obtener perfiles geoeléctricos 2D perfiles que definen la estructura hidrogeológica de la zona de estudio y los materiales que la componen, permitiendo la selección de un emplazamiento en el que realizar los sondeos con las mejores perspectivas de éxito. Este artículo muestra la utilidad de esta metodología de estudio, aplicada a las formaciones mesozoicas en una zona concreta situada en el término municipal de Liceras (Soria, España).

applied sciences

MDPI

Article

Time-Domain Electromagnetics as a Geophysical Tool in Hydrogeological Exploitation Projects in Mesozoic Formations

Javier Carrasco-García [1], Daniel Porras-Sanchiz [2], Pedro Carrasco-García [3,*], José Luis Herrero-Pacheco [3], Ignacio Martín-Nieto [3], Juan Manuel Benito-Herrero [4] and Pedro Huerta-Hurtado [5]

1 Técnicas Geofísicas S.L., 05003 Ávila, Spain
2 Geoland Services S.L., 28008 Madrid, Spain
3 Department of Cartographic and Terrain Engineering, Geology, Polytechnic School of Avila, University of Salamanca, Av. Hornos Caleros, n° 50, 05003 Ávila, Spain
4 Inserma Ingenieros S.L., Av. Sotillo, n° 2ª, 2° D, 40196 La Lastrilla, Spain
5 Department of Geology, Higher Polytechnic School of Ávila, University of Salamanca, Av. Hornos Caleros, n° 50, 05003 Ávila, Spain
* Correspondence: retep81@usal.es; Tel.: +34-920353500

Abstract: The need to use groundwater resources for agricultural and livestock farms is a constantly growing issue, as these resources condition the socio-economic development of many areas with limited climatic regimes and surface water resources. Decisions on the location and characteristics of groundwater extraction works are based on hydrogeological studies, in which geophysical techniques are a very useful tool. In our study, the Time-Domain Electromagnetics technique (TDEM) was used, which significantly improves the precision and safety when planning to drill for water extraction in Mesozoic formations thanks to the significant resistivity contrast among its different hydrogeological units. The performance of a research campaign using TDEM allows for obtaining 2D geoelectrical profiles which define the hydrogeological structure of the study area and the materials of which it is composed, enabling the selection of a site where drilling can be carried out with the best prospects of success. This article shows the usefulness of this study methodology, applied to Mesozoic formations in a specific area located in the municipality of Liceras (Soria, Spain).

Keywords: geophysics; TDEM; hydrogeology; Liceras (Soria)

Citation: Carrasco-García, J.; Porras-Sanchiz, D.; Carrasco-García, P.; Herrero-Pacheco, J.L.; Martín-Nieto, I.; Benito-Herrero, J.M.; Huerta-Hurtado, P. Time-Domain Electromagnetics as a Geophysical Tool in Hydrogeological Exploitation Projects in Mesozoic Formations. *Appl. Sci.* **2022**, *12*, 8655. https://doi.org/10.3390/app12178655

Academic Editor: Arcady Dyskin

Received: 14 July 2022
Accepted: 23 August 2022
Published: 29 August 2022

1. Introduction

Research in the field of hydrogeology has been increasing in recent decades due to the growing needs of farmers, livestock breeders and municipalities [1–3]. In this respect, there is a great deal of ignorance, which has led to considerable failures and economic losses. For this reason, it is common to find sites for water catchment works whose location techniques have been based on dowsing [4], while in recent decades, the use of geophysical techniques has become more widespread with the use of mostly vertical electrical soundings [5–7].

Currently, there is a greater variety of tools for the resolution of this type of problem, depending on the geological structure of the basin to be studied. In this case, we wanted to test the use of Transient Electromagnetics or Time-Domain Electromagnetic (TEM/TDEM) soundings in Mesozoic formations. With this tool, we wanted to check and corroborate the initial bibliographic data found in the Geological and Mining Institute of Spain to locate future exploitations and solve hydrogeological problems in this type of geological formation.

The Electromagnetic Sounding technique is a methodology that emerged in the 1980s, using analogue equipment [8]; it is quite unknown to many today, and in the 21st century, it has evolved to a greater extent compared to its predecessors [9–13].

In the same way as vertical electrical soundings, this type of method is commonly used for the definition of sub-horizontal structures, although Electromagnetic Soundings show a greater focalisation and less affection of lateral changes, which makes it a technique of greater accuracy in such geological contexts where faults are frequent. This is our main reason for choosing this geophysical prospecting system since we also aimed to validate its potential for the execution of future projects of the same nature.

In order to confirm this tool in this type of geological environment, we carried out a study in the municipality of Liceras (Soria, Spain). For some time now, the population of Liceras has suffered high levels of arsenic contamination from the current catchment. In addition to this main catchment, the municipality has two other secondary catchments in a Triassic formation that have been set up over time. The lack of hydrogeological studies for the location of these boreholes has meant that very poor-quality water is obtained from these complementary catchments.

Aware of this problem, the Liceras Town Council requested the help of the Regional Government of Castile and Leon to solve the issue. The municipality has always located the boreholes to the south of Liceras, in a very unfavourable area from a hydrogeological point of view.

Until now, the main supply point in the area has been a catchment located on Triassic outcrops, capturing the resources available in the Upper Triassic materials: sandstones of the "Lutitas con yesos y Valderromán" formation. Their low hydrochemical quality, together with the insufficient flow, has led to the need to explore the use of resources from the Liassic formations outcropping to the northeast. There, the "Imón and Cortes de Tajuña" formation, with its folded dolomites and carniolas, has become the target formation.

The determination of a new site for water extraction is conditioned by two factors: the identification of the position of the target formation and the avoidance of entering the underlying Triassic formations of low water quality, thereby ensuring the best prospects from the point of view of usable flows and hydrochemical quality.

A geological-geophysical study using the Time-Domain Electromagnetic technique was carried out with the aim of structurally delimiting the formations defined by the geological map so that, on the basis of the results, the best possible location for the new borehole could be determined, as well as its depth. The study results combine the pre-existing data with the geophysical data obtained to show the value of a tool that can solve similar problems in Mesozoic formations due to the significant resistivity contrast among the Cretaceous, Jurassic and Triassic. Therefore, this methodology can produce savings for both public and private institutions in their investment in hydrogeological Mesozoic resources.

2. Geological Context

The study area is located in the southeastern sector of the tertiary basin of the Duero River, on Triassic, Jurassic and Cretaceous outcrops belonging to the Mesozoic cover that fossilises the bedrock.

The Mesozoic succession outcropping in the study area presents a slightly dipping structure (10–20°) towards the northeast. The lower base is made up of materials of the Keuper facies, on top of which Jurassic carbonate materials are found, and finally, the Cretaceous formation.

The Keuper is composed of shales with gypsum and sandstones from the "Lutitas con yesos de Valderroman" formation. This is a sequence of some 60–70 m in thickness whose base is located on a level of sandstone on which the town of Liceras is located. There are various metric sandstone sections with silt intercalations producing topographic reliefs, as well as sections of shales and siltstones and dolomitic clayey loams with secondary gypsum crystals.

The Keuper facies culminate in a dolomitic section present throughout the northern sector of the Castilian branch of the Iberian Mountain Range (Cordillera Ibérica), "Dolomías tableadas de Imón" formation, still from the Upper Triassic (Norian) [14]. From a cartographic point of view, this formation is integrated with the Cortes de Tajuña Fm., formed by dolomitic breccias and dolomites of massive aspect; they show a combined thickness of about 112 m that can be divided into up to four sections or members.

The Middle Jurassic, Lower Pleinsbachian Sinemurian, appears in a concordant contact, formed by the "Cuevas Labradas" Fm. [14], consisting of limestones and folded dolomites, which at some points, can reach over 100 m in thickness.

Finally, and in the case of the Jurassic, on the sharply folded limestones of the "Cuevas Labradas" Fm., the Upper Jurassic materials appear, made up of marls and bioclastic limestones of the "Cerro del Pez" Fm. and bioclastic limestones of Barahona, with an approximate thickness of around 20 m. The entire Jurassic section is considered the target for any catchment.

Above the Jurassic, we find the Cretaceous sequence belonging to the "Proto-Atlantic Domain" of the Iberian Basin, and within this, to the North-Castilian Plateau [15], whose base is made up of the clayey sands of the Lower Cretaceous ("Utrillas Fm".), followed by the marls and marly limestones of the "Margas" Fm. plus limestones from the "Picofuentes" Fm., and limestones and dolomites of the Lower Cretaceous.

3. Geology of the Study Area

The analysis of the geology in the vicinity of the study area defines a relatively simple structure in which the outcropping Mesozoic sequence dips gently to the northeast. The contact between the Triassic and Jurassic materials (the target formation of the catchment) can be defined with some clarity on the surface, given the topographic contrast between those materials generated by the sandy sections and the lithological banks between them, in addition to the topographic relief that occurs just to the north of the town of Liceras.

Geological cartography (Figure 1) allows the generation of geological cross-sections that initially show the structure, position and height of the geological formations, including the main target formation (Jurassic materials).

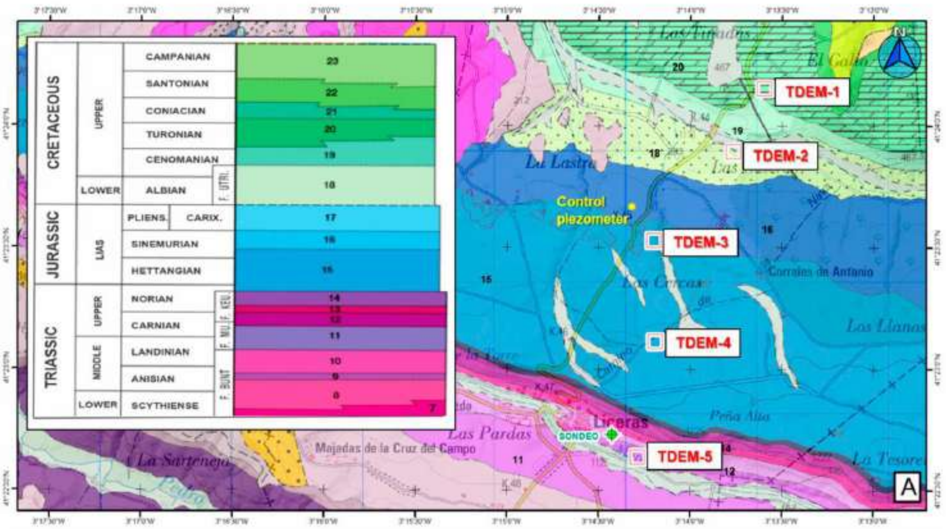

Figure 1. *Cont.*

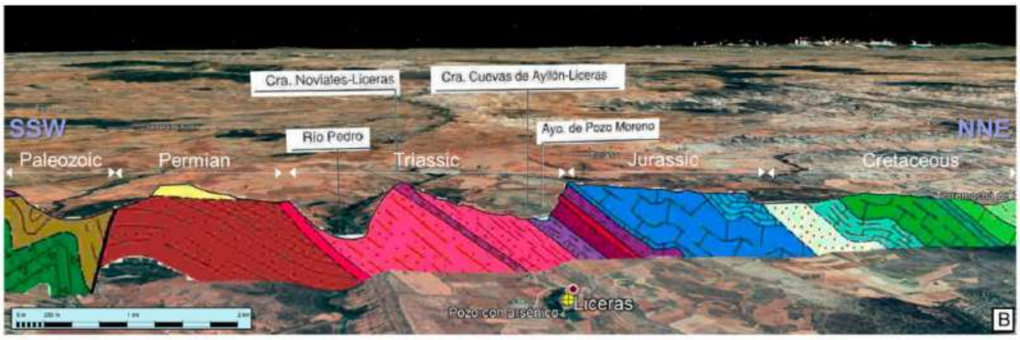

Figure 1. (**A**) Geological Cartography (Geological Map of Spain 1:50,000, sheet n° 404 (Ayllón) [16]) with the position of the TDEM surveys carried out (**B**) and interpretative geological cross-section showing the main structural features over the TDEM survey line.

4. Hydrogeological Context

From the hydrogeological point of view, the study area belongs to the Almazán Sur Groundwater Body (ES020MSBT000400050), belonging to the Duero River Basin, with a defined surface area of 1032 km^2 and in which two groundwater formations of interest are defined:

- The main aquifer—Jurassic—is made up of dolomites, carniolas and limestones of the formations corresponding to the "Infralías" and "Lías" of the Iberian Mountain Range (Cordillera Ibérica). They have sections of variable permeability due to fissuring and/or karstification, and they behave as free aquifers.
- From a hydrogeological point of view, the Upper Cretaceous carbonate series of the domain of the Northern Edge of the Central System (Sistema Central), with permeability associated with fissuring and/or karstification, are of interest. They constitute a—Cretaceous—aquifer that overlaps and disconnects from the Jurassic aquifer due to the existence of a low-permeability detrital formation between the two, made up of the sands of the "Utrillas" Fm.

The Jurassic aquifer formation is confined and disappears to the north, under the Cretaceous aquifer formation, which, at the same time, goes under Tertiary materials towards the Almazán basin. There, it constitutes the main deep aquifer, which feeds the Tertiary detrital materials and significant springs and watercourses, constituting the important Groundwater Body of the Almazán Basin, as well as that of the Páramo de Escalote. The following figure (Figure 2) shows the definition of the Almazán Sur Groundwater Body and the bordering bodies, as well as the location of the research area within the body.

The present research focuses on the Jurassic aquifer formation shortly before it is confined by Cretaceous materials, as it is expected to provide a higher quality source of resources and solve the existing problems at Liceras associated with the poor hydrogeological characteristics of the Triassic materials with a high content of salts due to their lutitic and gypsum materials. In the area, the public body Confederación Hidrográfica del Duero has a borehole used as a control piezometer for the Jurassic materials, called PZ0250005, located 1.6 km to the north of Liceras. This borehole is 205 m deep and with very plastic red and grey clays at the bottom (possibly Keuper). The piezometric level is monitored periodically (Figure 3), with the base level at 103 m depth in the driest periods and around 70 m depth in the periods of greatest recharge.

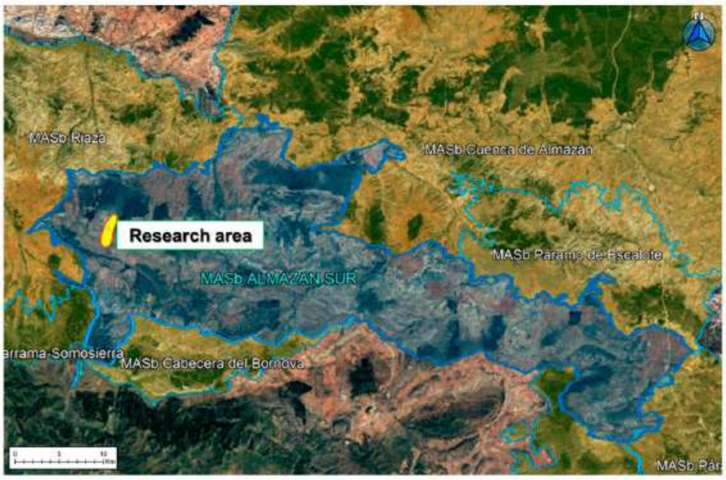

Figure 2. Definition of the Almazán S. groundwater boundaries and location of study area.

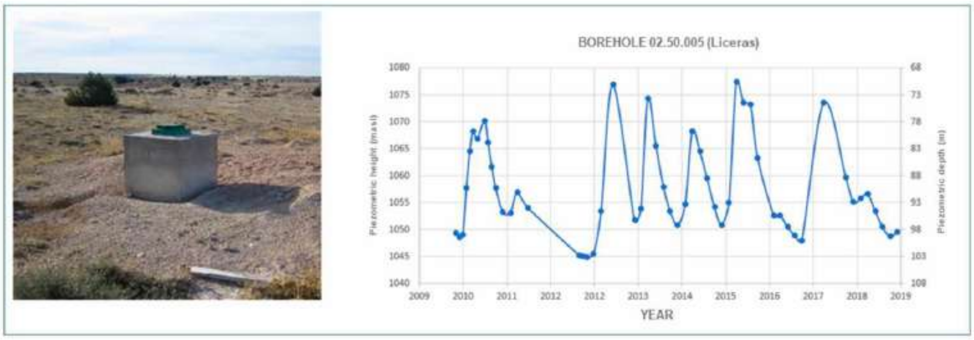

Figure 3. Liceras control piezometer (**left**) and piezometric evolution (**right**) [17].

5. Geophysical Technique Used: Time-Domain Electromagnetic Sounding (TDEM)

According to Carrasco [18], time-domain electromagnetic sounding, commonly referred to as TDEM, consists of injecting a constant current into a loop or transmitting coil (TX), generating a constant primary magnetic field. When the current flowing through the transmitting coil (TX) is suddenly interrupted, the primary magnetic field is no longer constant and decreases in value over time until reaching zero. According to Faraday's law, when a body is exposed to a time-varying magnetic field, a series of electromagnetic inductions of electric currents occur in the subsurface (Figure 4). These currents flow in closed paths through the subsurface, migrating in depth and laterally, decreasing in strength over time and, in turn, generating a decreasing transient secondary magnetic field at the surface [19].

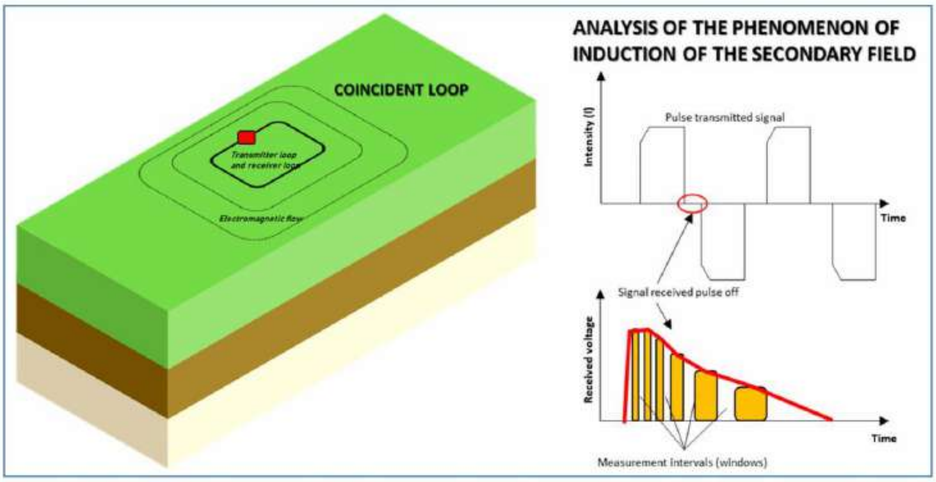

Figure 4. General arrangement of an electromagnetic sounding [20].

This secondary field induces a time-varying voltage in the receiving loop (RX). The way the voltage decays contains information about the resistivity of the subsurface since the magnitude and distribution of the induced currents depend on the resistivity of the medium [21]. The depth migratory character, i.e., short time voltages, provide information on the resistivity of shallow layers, while long time voltages provide information on the resistivity of deeper layers [22].

In more detail, the process of an electromagnetic survey would be as follows:

1. A current is circulated through the transmitting loop (Tx), which creates a time-varying primary magnetic field (Figure 5).

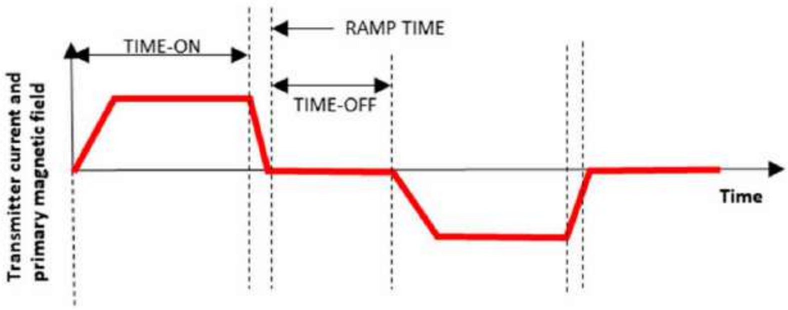

Figure 5. Transmitter current and primary magnetic field vs. time [23].

2. According to Faraday's law, a rapid decrease of the transmitted current and thus of the primary magnetic field induces an electromotive force (emf.) in the subsurface (Figure 6).

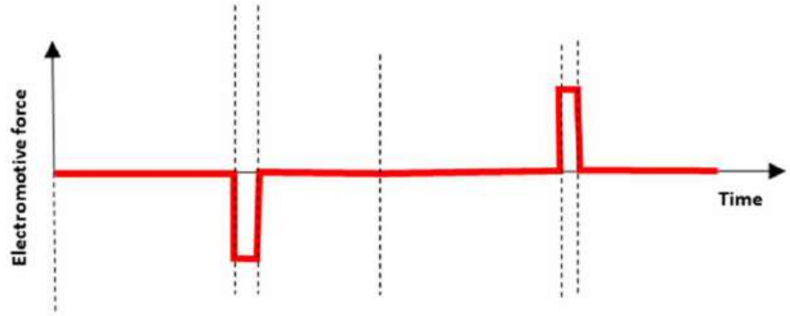

Figure 6. Electromotive force vs. time [23].

3. These induced currents generate, in turn, a secondary magnetic field whose variation over time is measured in the receiving coil (Rx) (Figure 7).

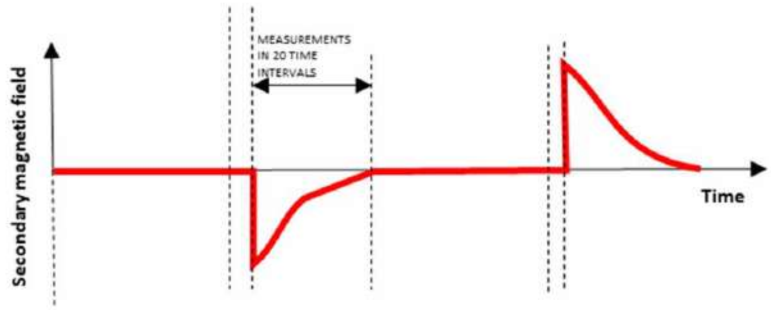

Figure 7. Secondary magnetic field vs. time [23].

6. Results from Time-Domain Electromagnetic Surveys

An electromagnetic profile was carried out in a N-S direction, in the direction of the presumed dominant geological structure in the area, starting at the Triassic facies and ending at the Cretaceous terms. The length of the profile was 3200 m, and it was produced from the execution of a total of five TDEM surveys. To place the TDEM's 100 × 100 loops accurately, a compass Silva SSM360LA Professional Optical Compass was used. This is a high-precision and high-sensitivity compass with sapphire bearings and quick position adjustment.

The TDEM surveys were carried out using the Terra-Tem equipment (Figure 8) designed by Monex GeoScope, with a "coincident loop" configuration and with square loops (transmitter and receiver) of 100 m on each side, using a minimum stacking of 1000 measurement repetitions per channel and testing various gains to minimise the effect of any environmental electromagnetic noise. The results of the different decay curves obtained in the field are shown using the Terratem equipment software "TEM Plotting Program v 2.0.0" from Monex GeoScope (Figure 9).

Figure 8. Terra-Tem equipment in the process of measurement.

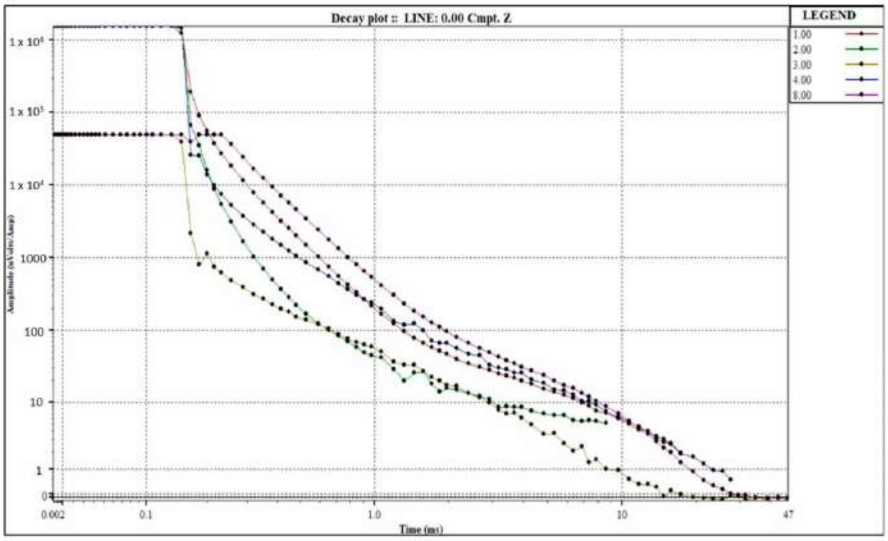

Figure 9. Decay curves obtained in the field.

After the measurements, the resistivity/time curves were obtained and processed using the IX1D software from Interpex to obtain the geoelectric resistivity/depth column for each TDEM survey carried out (Figure 10). These data were used, also through the IX1D software, to obtain a geoelectric profile, through which a geological and hydrogeological interpretation of the studied area could be made.

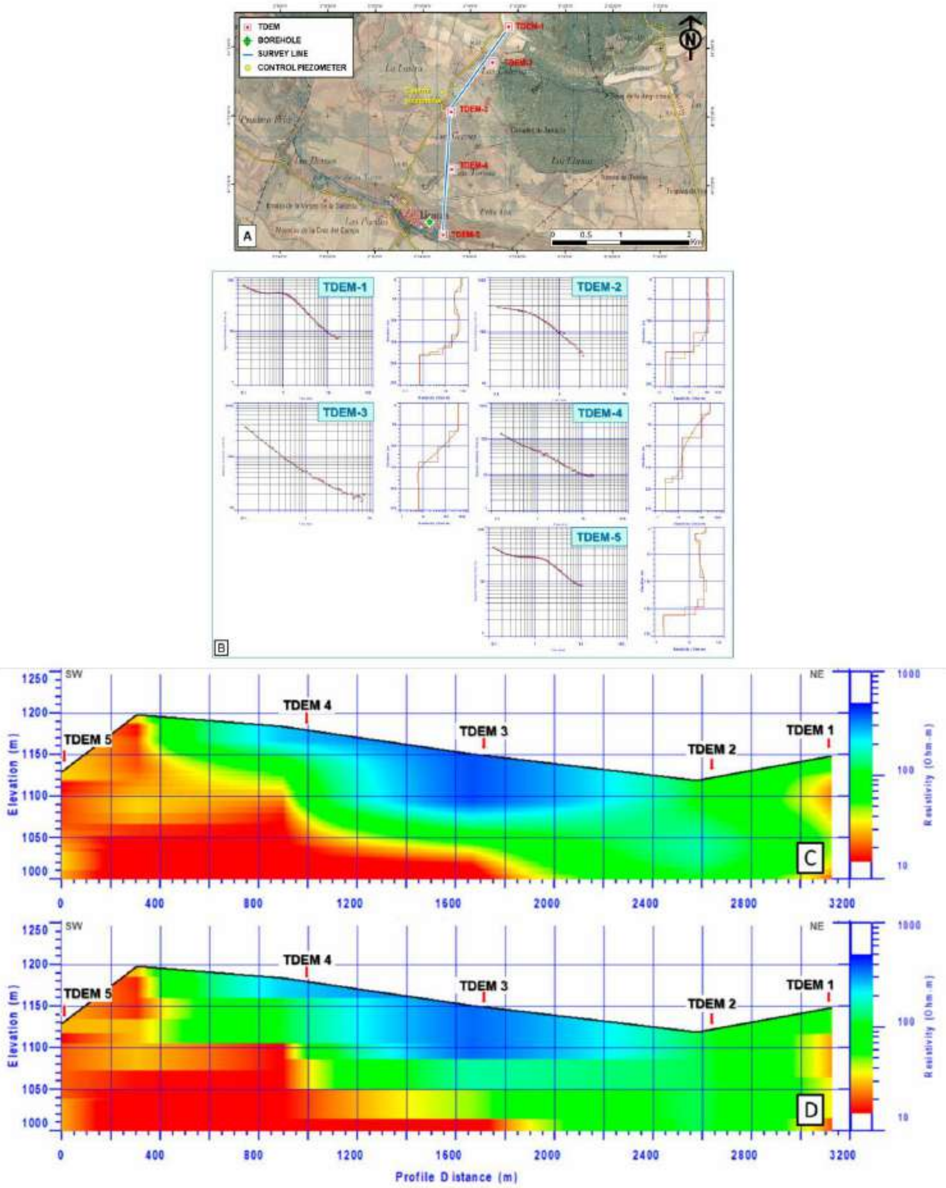

Figure 10. TDEM location map with borehole and control piezometer and pseudo-2D profile (**A**), resistivity-time curves and their respective resistivity/depth profiles processed with Occam inversion (green) and quantitative layered inversion (red) (**B**). Pseudo-2D profiles build on the data from the processed with Occam inversion (**C**) and quantitative layered inversion (**D**).

We chose Occam inversion [24] on this occasion for its greater simplicity and softness when comparing the geological profile. The profile obtained (Figure 11) identified the presence of a total of three geoelectric units:

- Geoelectric Unit 1: present at the SW end of the profile, is of a conductive nature, with resistivities below 30 Ohm.m, corresponding to Triassic materials (shales, gypsum and sandstones). The low resistivities of this unit may be influenced by the low hydrochemical quality.
- Geoelectric Unit 2: corresponding to the Finitriassic and Jurassic carbonate resistive materials (limestones and dolomites). This is a unit located on top of the previous one, appearing between metres 400 and 2600 of the profile, with more than 140 m of thickness. The high resistivities of this unit (100–500 Ohm.m) indicate a high proportion of permeable materials (limestones and dolomites) compared to impermeable materials (marls and marl-limestones). In addition, high resistivities are usually indicative of the good chemical quality of the groundwater.
- Geoelectric Unit 3: appears around metre 2600 of the profile and extends to the end of the profile. The unit shows a resistivity that is intermediate to the previous ones and corresponds to Cretaceous materials (sands, marls, marlstones and limestones).

The general structure observed, according to the geophysical data, is concordant with the geologically predefined one, in which the Mesozoic sequence appears normal in character, dipping slightly, about 15 degrees to the northeast, with all the terms of the series progressively outcropping in that direction.

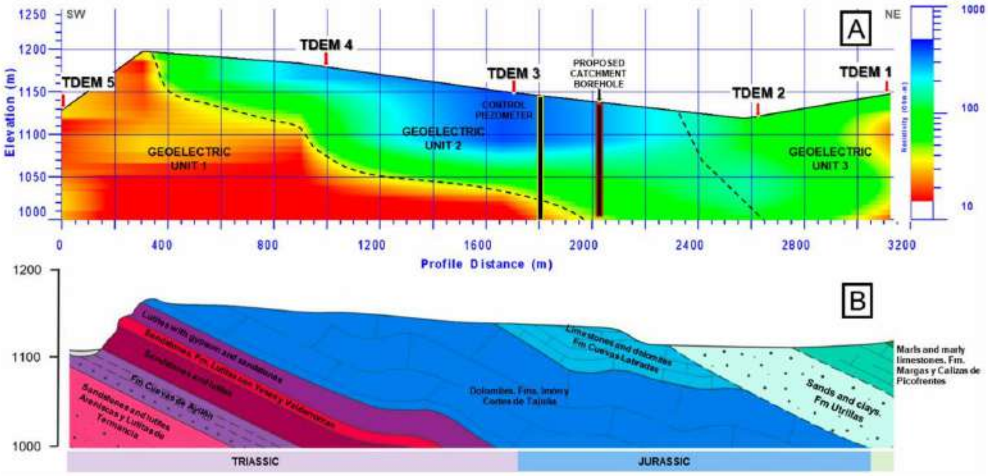

Figure 11. Interpreted TDEM geoelectric profile (occam inversion data), including position of the proposed catchment borehole (**A**) and geological cross-section of the TDEM profile based on the 1:50,000 geological cartography of Spain (**B**).

7. Discussion

The geophysical profile obtained shows concordance (Figure 11) with the available geological information (Geological Map of Spain 1:50,000, sheet n° 404 Ayllón); as an improvement, it allows us to define the position and depth of the materials belonging to the three existing geological (Cretaceous, Jurassic and Triassic) and geoelectric formations. This has been possible thanks to the important resistivity contrast among the Mesozoic formations. However, other geological contexts present geoelectrical similarities that do not allow the efficient use of this TDEM technique for hydrogeological purposes.

In this case, the target formation of the catchment, corresponding to geoelectric unit number two of a resistive nature, and formed by Finitriassic and Jurassic limestones and dolomites, is the main aquifer of the area, corresponding to the "Infralías" and "Lías" of the Iberian Mountain Range (Cordillera Ibérica). The high resistivities of this unit indicate a high proportion of permeable materials (limestones and dolomites) and a high hydrochemical quality of the groundwater. This aquifer has sections of variable permeability due to fissuring and/or karstification, and it behaves as a free aquifer. This geoelectric unit has an approximate thickness of about 140 m, dipping slightly to the northeast, with an apparent dip of about 15 degrees. Given that the catchment should be located in the place where it reaches the greatest possible depth within the profile under study, it is recommended that it be carried out at around metre 2000 of the profile, with an approximate depth of 140 m.

On the other hand, it is important to avoid the geoelectric unit number one, associated with the poor known hydrogeological characteristics of the Triassic materials (low hydrochemical quality and insufficient flow). Triassic materials are the low permeability substrate with the contribution of substances of an evaporitic nature that particularly influence the quality of the resource. Therefore, the objective is to drill the maximum possible thickness of saturated Jurassic materials without touching the Triassic materials (Figure 12).

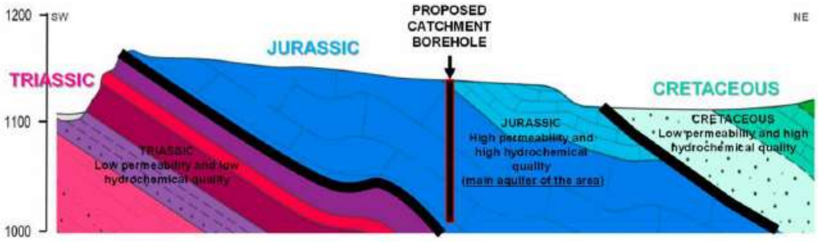

Figure 12. Hydrogeological Interpretation based on the 1:50,000 geological cartography of Spain, including position of the proposed catchment borehole.

Drilling in the final part of the profile could also be considered so that the Cretaceous and Jurassic materials are crossed, which would allow the permeable sections of the entire cross-section to be captured, allowing for higher flow rates. However, this option is discarded, in view of the results of the geoelectric study, on observing the poor prospects obtained by TDEM 1, in which the Cretaceous materials showed relatively conductive values related to the presence of predominantly loamy materials as a whole, with lower prospects from the hydrogeological point of view. This would require, at the same time, much deeper and more costly drilling, both in execution and exploitation, to capture resources in the Jurassic materials (geoelectric unit number two).

8. Conclusions

The geophysical study carried out by means of TDEM sounding in Liceras (Soria, Spain) demonstrates the value of this geophysical research system as a support for hydrogeological studies in Mesozoic formations. The difference in resistivity of the Cretaceous, Jurassic and Triassic formations allows for obtaining geoelectric profiles that can be correlated with the local and regional geological and hydrogeological structure, which allows for the definition of the structure and position in the subsurface of the Mesozoic sequence outcropping in the study area. In addition, the low resistivities could indicate a low hydrochemical quality of the groundwater, usually associated with the gypsum of the Triassic formation.

This spatial information obtained by Time-Domain Electromagnetic is essential when considering the design of works to capture hydrogeological Mesozoic resources in order to solve the quality and supply problems existing in the area, as it defines the ideal location and depth for the execution of potential works.

Therefore, combining the pre-existing geological data with TDEM geophysical data has shown to be a methodology that can solve similar problems in Mesozoic formations and can produce savings for both public and private institutions in their investment in hydrogeological resources.

Author Contributions: Conceptualisation, J.C.-G., D.P.-S. and J.M.B.-H.; methodology, J.C.-G., D.P.-S. and J.L.H.-P.; software, J.C.-G. and P.C.-G.; validation, J.C.-G.; formal analysis, J.C.-G. and P.H.-H.; investigation, J.C.-G., P.C.-G., D.P.-S., J.M.B.-H., J.L.H.-P., I.M.-N. and P.H.-H.; resources, J.C.-G., J.C.-G. and P.C.-G.; writing—original draft preparation, J.C.-G., D.P.-S., J.L.H.-P. and P.C.-G.; writing—review and editing, P.C.-G. and I.M.-N.; visualisation, J.C.-G.; supervision, P.C.-G.; project administration, J.C.-G. and P.C.-G.; funding acquisition, J.C.-G. and J.M.B.-H. All authors have read and agreed to the published version of the manuscript.

Funding: This research received no external funding.

Acknowledgments: The authors would like to thank the Water Supply Service of the Regional Government of Castile and Leon (Servicio de Abastecimiento de Aguas de la Junta de Castilla y León) for supporting the above research project and for their consent to show the results obtained in a research article. This paper is part of the Research Project I+D+i/PGC2018-094566-B-C21, supported by the MCIN/AEI/10.13039/501100011033/ and FEDER "Una manera de hacer Europa".

Conflicts of Interest: The authors declare no conflict of interest.

References

1. Howard, K.W.F. Sustainable cities and the groundwater governance challenge. *Environ. Earth Sci.* **2015**, *73*, 2543–2554. [CrossRef]
2. Madramootoo, C.A. Sustainable groundwater use in agriculture. *Irrig. Drain.* **2012**, *61*, 26–33. [CrossRef]
3. Mahmoud, M.A. Groundwater and Agriculture in the Nile Delta. In *Groundwater in the Nile Delta. The Handbook of Environmental Chemistry*; Negm, A., Ed.; Springer: Berlin/Heidelberg, Germany, 2017; Volume 73.
4. Chevalier, R. *Alumbramiento de Aguas Ocultas*; Sintes: Barcelona, Spain, 1984.
5. Layade, G.O.; Adegoke, J.A.; Oladewa, F.C. Hydro geophysical Investigation for groundwater development at Gbongudu Area, Akobo Ojurin, Ibadan, Southwestern Nigeria. *J. Appl. Sci. Environ. Manag.* **2017**, *21*, 527–535. [CrossRef]
6. Soomro, A.; Qureshi, A.L.; Jamali, M.A.; Ashraf, A. Groundwater investigation through vertical electrical sounding at hilly area from Nooriabad toward Karachi. *Acta Geophys.* **2019**, *67*, 247–261. [CrossRef]
7. Varamashvili, N.D.; Tarkhan-Mouravi, A.G.; Ghlonti, N.Y. Efficiency of Vertical Electrical Sounding in Water Prospecting Problems in Adjara Region (Khelvachauri Municipality). *J. Georgian Geophys. Soc.* **2021**, *24*.
8. Fitterman, D.V.; Stewart, M.T. Transient electromagnetic sounding for groundwater. *Geophysics* **1986**, *51*, 995–1005. [CrossRef]
9. Amato, F.; Pace, F.; Vergnano, A.; Comina, C. TDEM prospections for inland groundwater exploration in semiarid climate, Island of Fogo, Cape Verde. *J. Appl. Geophys.* **2021**, *184*, 104242. [CrossRef]
10. Descloitres, M.; Chalikakis, K.; Legchenko, A.; Moussa, A.M.; Genthon, P.; Favreau, G.; Le Coz, M.; Boucher, M.; Oï, M. Investigation of groundwater resources in the Komadugu Yobe Valley (Lake Chad Basin, Niger) using MRS and TDEM methods. *J. Afr. Earth Sci.* **2013**, *87*, 71–85. [CrossRef]
11. Guevara Mansilla, O.; Ventura Houle, R.; Andrade Limas, E.C. Uso de sondeos electromagnéticos en la caracterización hidrológica del acuífero del altiplano de Tula, Tamaulipas. *Investig. Y Cienc. Univ. Autónoma Aguascalientes* **2017**, *70*, 23–30. [CrossRef]
12. Huerta, P.; Carrasco-García, P.; Armenteros, I.; Recio, C.; Carrasco-García, J.; Rodríguez-Jiménez, E. TDEM Soundings as a Tool to Determine Seasonal Variations of Groundwater Salinity (Villafáfila Lakes, Spain). *Water* **2022**, *14*, 2402. [CrossRef]
13. Martínez-Moreno, F.J.; Monteiro-Santos, F.A.; Madeira, J.; Bernardo, I.; Soares, A.; Esteves, M.; Adão, F. Water prospection in volcanic islands by Time Domain Electromagnetic (TDEM) surveying: The case study of the islands of Fogo and Santo Antão in Cape Verde. *J. Appl. Geophys.* **2016**, *134*, 226–234. [CrossRef]
14. Goy, A.; Gomez, J.J.; y Yébenes, A. El Pliensbachiense y Toarciense en la Rambla del Salto (Sierra Palomera, Teruel). *Estud. Geol.* **1976**, *32*, 391–423.
15. Vilas, L.; Mas, R.; García, A.; Arias, C.; Alonso, A.; Meléndez, N.; y Rincón, R. *El Cretácico de España*; Universidad Complutense de Madrid: Madrid, Spain, 1982; p. 457514.
16. Mozal Martín, F.; y Rubio Pascual, F.J. *Mapa Geológico de España 1:50.000, Hoja nº 404 (Ayllón) y Memoria*; IGME: Madrid, Spain, 1997; 119p.
17. Confederación Hidrográfica del Duero Borehole Control Piezometric Information. 2019. Available online: https://www.chduero.es/documents/20126/0/Piezometria_Red_Nivel_CHD.xlsx/5088b7a0-39ca-09da-eaca-edf17b423388?t=1641227734531 (accessed on 10 April 2022).
18. Carrasco García, P. Avance en Técnicas Geofísicas para la Caracterización del Subsuelo Mediante Innovación y el uso de Herramientas de Gestión de Información Espacial. Ph.D. Thesis, Escuela Politécnica Superior de Ávila, Universidad de Salamanca, Salamanca, Spain, 2013.
19. McNeill, J.D. *Applications of Transient Electromagnetic Technics*; Technical Note TN-7; Geonics Ltd.: Mississauga, ON, Canada, 1980; 17p.
20. Navarro Luna, R.A. Aplicación de Pruebas Electromagnéticas en el Dominio de Tiempo (TDEM) para Caracterización de Recursos Hídricos en Venezuela. Ph.D. Thesis, Universidad Simón Bolívar, Barranquilla, Colombia, 2006; 86p.
21. Nieto, I.M.; Carrasco García, P.; Sáez Blázquez, C.; Farfán Martín, A.; González-Aguilera, D.; Carrasco García, J. Geophysical Prospecting for Geothermal Resources in the South of the Duero Basin (Spain). *Energies* **2020**, *13*, 5397. [CrossRef]

22. Sheriff, R.E. *Geophysical Methods*, 1st ed.; Prentice Hall: Englewood Cliffs, NJ, USA, 1989.
23. Ward, S.H.; Wannamaker, P.E. *The MT/AMT Electromagnetic Method in Geothermal Exploration*; Report 5; UNU-GTP: Reykjavik, Iceland, 1983; 107p.
24. Constable, S.C.; Parker, R.L.; Constable, C.G. Occam's inversion: A practical algorithm for generating smooth models from electromagnetic sounding data. *Geophysics* **1987**, *52*, 289–300. [CrossRef]

ARTICULO 3 TDEM Soundings as a Tool to Determine Seasonal Variations of Groundwater Salinity (Villafáfila Lakes, Spain)

Resumen:

La interacción entre las aguas subterráneas con diferentes salinidades y los lagos muestra variaciones estacionales impulsadas por los cambios en las precipitaciones y la evapotranspiración. En las proximidades de los lagos de Villafáfila, las aguas subterráneas regionales locales, dulces y salobres, alimentan los lagos, formando una salmuera en los sedimentos lacustres. Se realizaron dos campañas de prospección mediante TDEM (verano 2019 e invierno 2020). En cada campaña se realizaron cinco sondeos TDEM en la misma ubicación para cada investigación, formando un perfil desde las colinas hasta la orilla del lago. Simultáneamente a los sondeos TDEM, se midió la conductividad eléctrica del agua del lago y del agua subterránea. El límite de resistividad entre el agua dulce local (10-35 Ohm/m) y el agua subterránea salobre regional (2-5 Ohm/m) está diferenciada a 600 m sobre el nivel del mar (msnm) por debajo de las colinas, y a 650 m por debajo de las tierras bajas que rodean el lago. Durante el verano, las aguas subterráneas dulce-salobres aumentan debido al bombeo por evaporación que se produce en las zonas a menor cota. Esto aumenta la salinidad del agua subterránea cerca de la superficie del terreno favoreciendo la precipitación de eflorescencias de halita. El registro anual en un piezómetro confirma el ascenso estival de la salmuera contenida en el acuitardo del lago. Los sondeos electromagnéticos son una técnica rápida y sencilla para controlar las variaciones estacionales de la interfase agua subterránea dulce-salobre y detectar posibles salinizaciones de los pozos de consumo y los cambios ambientales.

water

MDPI

Article

TDEM Soundings as a Tool to Determine Seasonal Variations of Groundwater Salinity (Villafáfila Lakes, Spain)

Pedro Huerta [1,*], Pedro Carrasco-García [2], Ildefonso Armenteros [3], Clemente Recio [3], Javier Carrasco-García [4] and Esther Rodríguez-Jiménez [3,5]

1 Dpto. Geología, Escuela Politécnica Superior de Ávila, Universidad de Salamanca, Av. Hornos Caleros, n° 50, 05003 Ávila, Spain
2 Dpto. Ingeniería Cartográfica y del Terreno, Escuela Politécnica Superior de Ávila, Universidad de Salamanca, Av. Hornos Caleros, n° 50, 05003 Ávila, Spain
3 Dpto. Geología, Facultad de Ciencias, Universidad de Salamanca, Pza. de la Merced S/N, 37008 Salamanca, Spain
4 Técnicas Geofíscas, S.L. Paseo de San Roque 21, 3°1, 05003 Ávila, Spain
5 Confederación Hidrográfica del Duero, Avda. de Italia, 1, 37007 Salamanca, Spain
* Correspondence: phuerta@usal.es

Abstract: Interaction between groundwaters with different salinities and lakes show seasonal variations driven by changes in precipitation and evapotranspiration. In the vicinity of Villafáfila lakes, local fresh and brackish regional groundwaters feeds the lakes, forming a brine in the lake sediments aquitard. Two TDEM surveys (summer 2019 and winter 2020) were carried out. Five TDEM soundings were acquired at the same location for each survey, forming a profile from the hills to the lake-shore. Simultaneously to the TDEM surveys, electric conductivity of lake water and groundwater was measured. The resistivity boundary between the local fresh (10–35 Ohm/m) and regional brackish groundwater (2–5 Ohm/m) is well marked at 600 m above sea level (masl) below the hills, and at 650 masl below the lowlands surrounding the lakes. During the summer, fresh-brackish groundwater interphase rises due to evaporative pumping occurring in the lowlands. This increases groundwater salinity close to the terrain surface favoring precipitation of halite efflorescences. Annual record of EC in a piezometer confirms the summer ascendant of the brine contained in the lake aquitard. TDEM sounding is fast and simple technique to monitor seasonal variations in fresh-brackish groundwater interphase and to detect possible salinization of consumption wells and environmental changes.

Keywords: electromagnetism; electric conductivity; duero; groundwater; wetland; saline

check for updates

Citation: Huerta, P.; Carrasco-García, P.; Armenteros, I.; Recio, C.; Carrasco-García, J.; Rodríguez-Jiménez, E. TDEM Soundings as a Tool to Determine Seasonal Variations of Groundwater Salinity (Villafáfila Lakes, Spain). *Water* **2022**, *14*, 2402. https://doi.org/10.3390/w14152402

Academic Editor: Ryan Bailey

Received: 6 July 2022
Accepted: 29 July 2022
Published: 2 August 2022

1. Introduction

Many lakes show interactions between their waters and groundwaters which sometimes have different salinities, densities, and compositions [1–4]. Time domain electromagnetism (TDEM) is a geophysical technique that is able to determine the lateral and vertical (depth) variations in electric resistivity (ρ) of the subsoil. Since the beginning of its application, TDEM has proven useful in research fields such as hydrogeology [5,6], mining [7], underground environmental pollution [8], and archaeology [9]. TDEM technique is useful to identify the interface of groundwaters with different salinities due to its high capacity to discriminate between units with high electric conductivity (EC) [10–13]. The dynamics of groundwaters and the lake-groundwater interaction can show seasonal and multi-annual changes due to the variations in evapotranspiration and precipitation along the year. Such variability can result in lateral and vertical changes in ground- and lake-water salinity and circulation [14]. Villafáfila lakes in Zamora province (Spain) are brackish to saline lakes located in a saline grassland. These lakes are protected by several environmental protections such as Natural Park, area of special protection for birds, and a Site of Community Interest (SCI) of the European Union, and are included in the intergovernmental RAMSAR treaty for protection of wetlands. These lakes are wintering place for migrant birds such as ducks and geese, and host one of world's largest populations of Great Bustard (*Otis tarda*) [15,16]. The aim of this study is to characterize, by means of TDEM surveys, the margins of the Salina Grande lake in Villafáfila, during both the dry and wet seasons and to compare simultaneously the ρ data with the EC of lake and groundwaters. This characterization is of interest for correlating the variations in soil and water salinity with faunal and plant changes. The location of the saline-freshwater interface will serve to the local and regional stakeholders to identify the areas and maximum depths to pump fresh groundwaters for human consumption.

2. Study Area

Villafáfila lakes are located in the northwestern part of the Duero river hydrological basin in northern Spain (Figure 1A), on Cenozoic sedimentary rocks that constitute a great aquifer system, with groundwaters flowing from the periphery of the basin toward the Duero river that flows westwards, to the Atlantic Ocean, along the central axis of the basin [17,18].

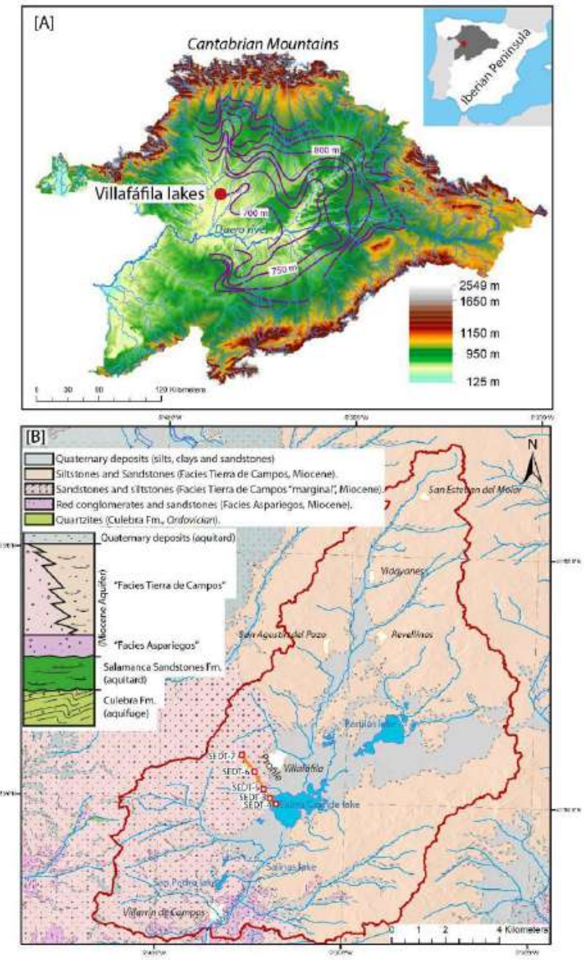

Figure 1. Location of the Duero hydrological basin and the Villafáfila basin. (**A**) Digital elevation model of the Duero hydrological basin and reference piezometry obtained from wells deeper than 200 m (purple lines). (**B**) Geological map and schematic stratigraphic section of the Villafáfila lakes basin. Location of the TDEM profiles represented in Figure 3 is marked with an orange line, and the different sounding sites with red squares. Note that Culebra Fm. crops out in the southwestern part of the map.

2.1. Climate

Villafáfila has a semi-arid, Continental Mediterranean climate, characterized by cold and wet winters (November–February) and hot and dry summers (June–September). During the winter, average monthly temperatures are about 4 °C, but minimum temperatures are commonly below zero. During the summer, average monthly temperatures are about 22 °C [19]. Mean annual evaporation is 720 mm and real evapotranspiration is 237 mm. Mean annual precipitation is 330 mm, largely concentrated from October to May. During this wetter period, when precipitation exceeds evapotranspiration, soil surplus occurs; the aquifer is recharged and the lakes fill up. On the other hand, during the summer, when evapotranspiration exceeds precipitation, the soils suffer water deficit and the lakes dry out [20].

2.2. Hydrogeology

Villafáfila lakes are brackish to saline lakes that occur in the Salado river valley, a tributary of the Valderaduey river, which discharges downstream into the Duero river. Villafáfila lakes occur in a flat area at 677 m above sea level (masl) surrounded by gently sloping hills that reach up to 730 masl [21]. The Miocene rocks outcropping in the area (Facies Tierra de Campos and Facies Aspariegos Units; mainly siliceous/litharenite sandstones and siltstones) constitute the main local aquifer, that belongs to the large Duero basin aquifer system. The clayey-sandy Quaternary lake deposits behaves as an aquitard at the bottom of the lakes (Figure 1B).

The water of the lakes comes mainly from the rain, but the ions dissolved are provided by shallow fresh groundwaters coming from the hills and regional deep brackish groundwaters. In Villafáfila, the regional component of the groundwater flow comes from the northeast (Figure 1A) and shows an increase in salinity southwestwardly [17]. Deep brackish groundwaters raise toward the lakes bottom and the lowland areas due to the presence of a near surface Paleozoic metamorphic basement elevation. This elevation is perpendicular to the general flow and locates in the southern zone of the Salina Grande Lake (Figure 1B) [20]. The basement is constituted by the Culebra Fm. and the Salamanca sandstone Fm. which does not crop out in the Villafáfila basin.

Groundwaters below the hills are of the calcium-bicarbonate type, with low salinities (TDS = 250 mg/L). Deep groundwaters, however, are sodium-chlorine waters with high salinities all year round (TDS = 3200–5000 mg/L). Lake waters have sodium-chlorine composition and show salinity variations along the year, with values ranging from 800–6200 mg/L. The brine contained in the Quaternary lake aquitard has salinities of 12,000–27,000 mg/L TDS [20].

3. Methodology

Two TDEM surveys were carried out, one during the winter (February 2020) and the other during the summer (July 2019) at the same five sounding sites. Soundings were placed aligned in a NNW-SSE trend, from higher in the hills to the lowlands around Salina Grande lake, close to the Villafáfila village (Figure 1B). The position of the different soundings was chosen to evaluate the distribution of salinities from the upper part of the hills (700 masl), where local groundwaters recharge, to the lowland areas (677 m), where the regional groundwaters discharge and mixing processes occur [20,22]. The soundings were placed 200–600 m apart from each other, at the same positions for the summer and winter surveys, to evaluate the ρ variations along the year. The surveys were carried out by the company Técnicas Geofísicas S.L. with a TerraTEM (MONEX GeoScope

Co., Ltd., Melbourne, Australia) transient electromagnetic survey system. Time domain electromagnetic sounding (TDEM) consists on injecting a constant electric current into a cable loop (transmitter coil). The transmitter loop generates an electromagnetic wave that propagates into the subsoil through the subsurface when the electric current is suddenly interrupted [23–25]. As the electromagnetic energy finds different materials underground, it induces eddy currents that generate secondary electromagnetic fields. These secondary electromagnetic fields are measured on the surface by a receiver loop or magnetic antenna and recorded as the induced energy diffuses into the earth. The resistivity of the subsurface materials depends on the rate of diffusion. The array consisted on 50 × 50 m square loops in the mode of coincident loops. Several 10 ms measurements were performed in every site, varying the number of stacks (up to 3000 stacks) to minimize electromagnetic noise. Similar arrangements have been performed for hydrogeological research [20,26,27]. Management of the obtained data and its conversion from apparent to real resistivities were made with IX1D V3 (INTERPEX Co., Ltd., Golden, CO, USA). A smooth model was generated for every TDEM site measured. Occam's inversion [28] was used to obtain the 30–40 layers smooth model (Figure 2). The obtained resistivities were used to construct the NNW-SSE profiles (Figure 3). Alongside TDEM survey acquisition, hydrogeological field measurements (groundwater level, temperature, and electric conductivity) were made in the Salina Grande lake, springs, boreholes and dug wells located closest to the TDEM sites (see next sections for more details). EC and temperature were measured with a Hanna HI 9835 m and probe. SGR-3 piezometer was monitored at 8 m depth with a conductivity, temperature, depth data logger (CTD) (OTT Hydromet Inc., Loveland, CO, USA). Local piezometry was measured during the summer of 2018 in dug wells screened at depths lower than 40 m. The data were interpolated with a convergent interpolation method and later manually redrawn to avoid inconsistencies due to the lack of data in certain areas. The piezometer SGR-3 is screened below the aquitard, and overflows at 0.4 m above lake bottom.

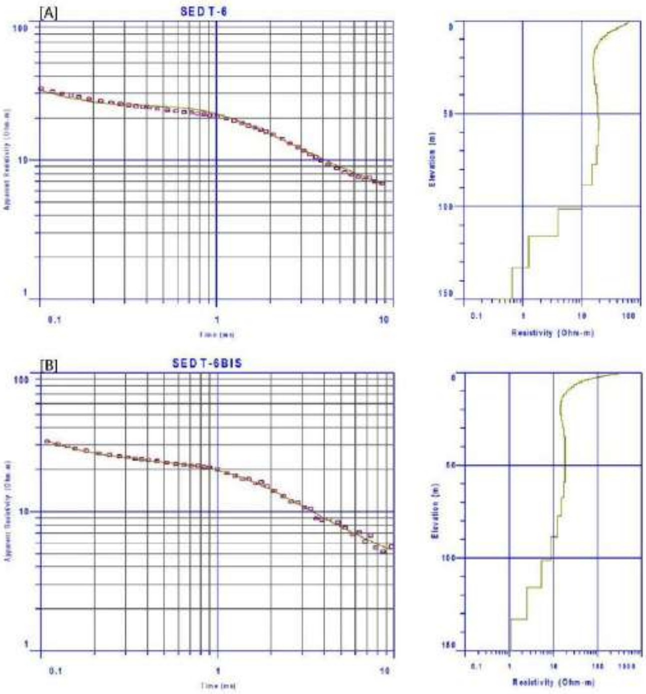

Figure 2. Example of TDEM soundings. (**A**) SEDT 6, (summer survey). Apparent resistivity curve versus time (**left**), Smooth inversion model (**right**). (**B**) SEDT 6BIS, (winter survey). Apparent resistivity curve versus time (**left**), Smooth inversion model (**right**).

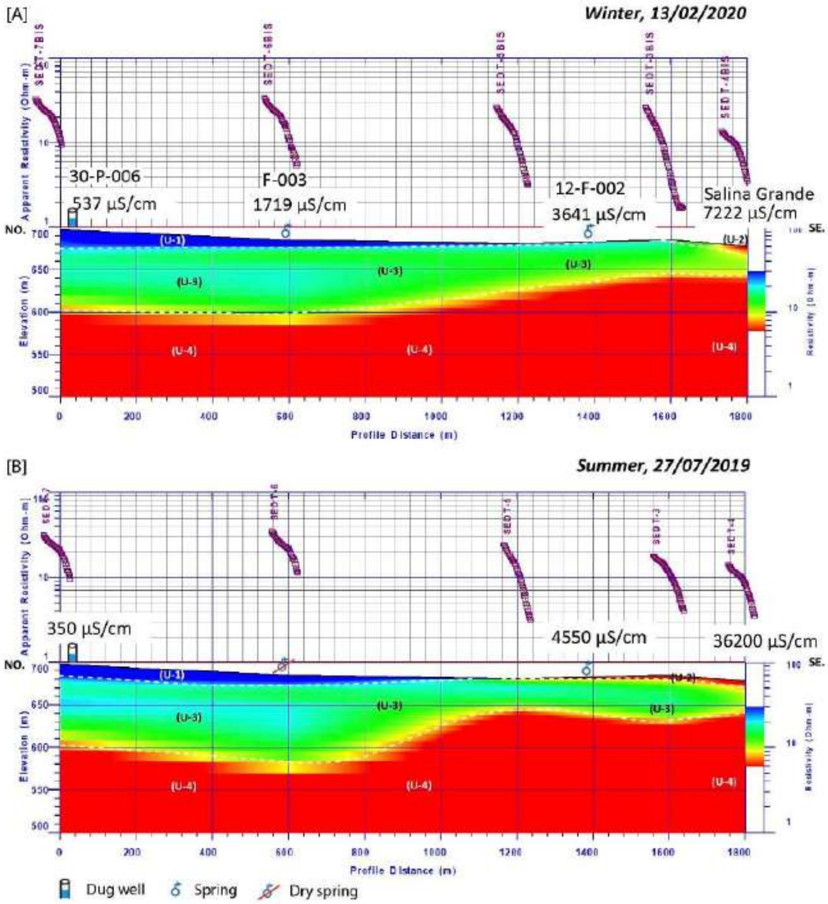

Figure 3. TDEM profiles measured from the hills to the lowlands and Salina Grande lake shore. Location in Figure 1. EC values measured in lake waters, dug wells and springs close to the profile path have been projected (Table 1). (**A**) TDEM profile acquired during the winter survey (13/02/2020), (**B**) TDEM profile acquired during the summer survey (27/07/2019). Note that red colors indicates low resistivity while blue colors means high resistivity values.

4. Results

4.1. Time Domain Electromagnetic Results

4.1.1. Winter Geoelectric Profile

Resistivities vary from 1 to 35 Ohm/m. The lowest values have been registered in the lowlands surrounding the lakes while the highest values have been measured in the upper part of the hills (SEDT-6BIS and 7BIS) (Figure 3A). 2D profiles show a decrease in ρ with depth in the soundings located in the upper parts of the hills (SEDT-6BIS and 7BIS) showing four geoelectric units that have been named from top to bottom as U-1, U-2, U-3, and U-4, in order to facilitate the description. U-1 appears in the upper part of the hills (700–680 masl), has ρ values ranging from 25 to 35 Ohm/m, and extends toward the toe of the hills. U-2 appears in the lowlands surrounding Salina Grande and in the lake shore and shows low resistivity values ($\rho < 5$ Ohm/m) in the upper part of the terrain. U-3 locates generally at an intermediate position between U-1 and U-4, below the upper parts of the hills (SEDT-6BIS and 7BIS), and between U-2 and U-4 in the lake shore. For the winter survey U-3 locates very close to the terrain surface (SEDT-3BIS and 4BIS). U-3 has ρ ranging from 10 to 25 Ohm/m and appears at 680–600 masl, below the hills and at 685–640 masl at the lowlands. U-4 appears at the lower part of the profile and is present at all sites; below the hills it is between 600–500 masl (SEDT-7BIS) and below the lake shore between 640–500 masl (SEDT-4BIS,) and has ρ lower than 5 Ohm/m (Figure 3A). The boundary between the U-3 and U-4 is almost horizontal between SEDT-6BIS and 7BIS (600 masl) and has a gentle slope between SEDT-6BIS and 3BIS. Below SEDT-3BIS and SEDT-4BIS is horizontal again.

4.1.2. Summer Geoelectric Profile

Resistivities measured during the summer survey have similar values (2–35 Ohm/m) to those recorded during the winter. The lowest ρ is registered in the lowlands surrounding Salina Grande and at the lake shore (SEDT-5, 4, 3) and the highest is recorded in the upper parts of the hills (SEDT-6 and 7), in the upper zone (Figure 3B). As in winter, in the upper parts of the hills there is a decrease in ρ from the upper parts of the terrain where geoelectric U-1 occurs toward the lower parts where U-4 appears. The boundary between U-1 and U-3 deepens slightly from the upper parts of the hills (SEDT-7) toward their toe (SEDT-6), but the boundary between U-3 and U-4 deepens 20 m from SEDT-7 (600 masl) to SEDT-6 (580 masl). The slope of this boundary is one of the main differences with the winter geoelectric profile, which is horizontal. In the lowland areas (SEDT-5, 4, 3) the upper part of the terrain (U-2) shows low ρ values (lower than 5 Ohm/m) and in comparison with the ρ data of the winter survey, U-2 extends from the lake shore (SEDT-4) to SEDT-5. U-3 has a similar thickness in SEDT-3, 4, and 5 and the ρ values are slightly lower (18 Ohm/m) towards the lake shore (SEDT-4). The interface between U-3 and U-4 in the lowland areas locates 20 m shallower in SEDT-5 (640 masl) relative to the winter survey, when it was located at 620 masl (SEDT-5BIS) (Figure 3). The geometry of the interface between U-3 and U-4 in the 2D profile shows a steeper slope between SEDT-6 and SEDT-5, in the summer (Figure 3B) than in the winter profile (Figure 3A).

4.2. Hydrogeological Data

4.2.1. Piezometry

Piezometry in the Duero hydrological basin indicates that regional groundwater flow in the northern half of the basin has a southwestward component, from recharge areas located in the Cantabrian Mountains and the northern edge of the Duero basin to the valley of the Duero river (Figure 1A) [17,18]. Local deep and brackish groundwater discharge occurs in Villafáfila due to the existence of an elevation of the Paleozoic impermeable basement [20].

Local piezometry also indicates a southwestern component of groundwater flow in the watershed of the Salado river, parallel to the river flow. The hills that surround the lakes have a local component flowing from the upper part of the hills toward the lowlands around the lakes (Figure 4). In the upper part of the hills the groundwater table locates about 700 masl, with depths between 5 and 10 m. In the lowlands around the lakes the groundwater table is at 680 masl, 10–30 cm below the surface. The hydraulic gradient in the upper part of the hills is about 0.1 and in the lowlands is about 0.001. The vertical component of the groundwater flow is downwards in the upper part of the hills, but it is upwards at its toe and in the lowlands (Figure 4). This is evidenced by the differences in hydraulic head between boreholes screened at more than 40 m depth and wells and dug wells screened at depths shallower than 15 m. In the upper part of the hills hydraulic head is lower in boreholes (screened > 40 m) than in dug wells (screened < 15 m). On the contrary, at the toe of the hills and in the lowlands hydraulic head in wells, some of which are flowing wells, is higher than in dug wells [20]. The occurrence of springs around Salina Grande lake shore is an additional evidence for the ascendant component of groundwater flow. Seasonal variations produce minor changes in groundwater level (about 10 cm) in the upper part of the hills. At the toe of the hills many springs dry out during the summer, and groundwater and Salina Grande lake level decrease by about 30–40 cm (Figure 4). Salina Grande lake is normally dry during the summer (from ≈ mid-July till October), although some years stays dry till December, when soils have surplus water and evapotranspiration is low. Lake level reaches maximum depth of 35 to 40 cm during the spring (April–May) (Figure 5). In SGR-3 piezometer, located in the lake shore (Figure 4), hydraulic head overflows with a minimum discharge at 0.4 m above lake floor. Some springs and flowing boreholes, all of them with brackish Na-Cl regional waters, maintain a constant discharge and temperature all year round.

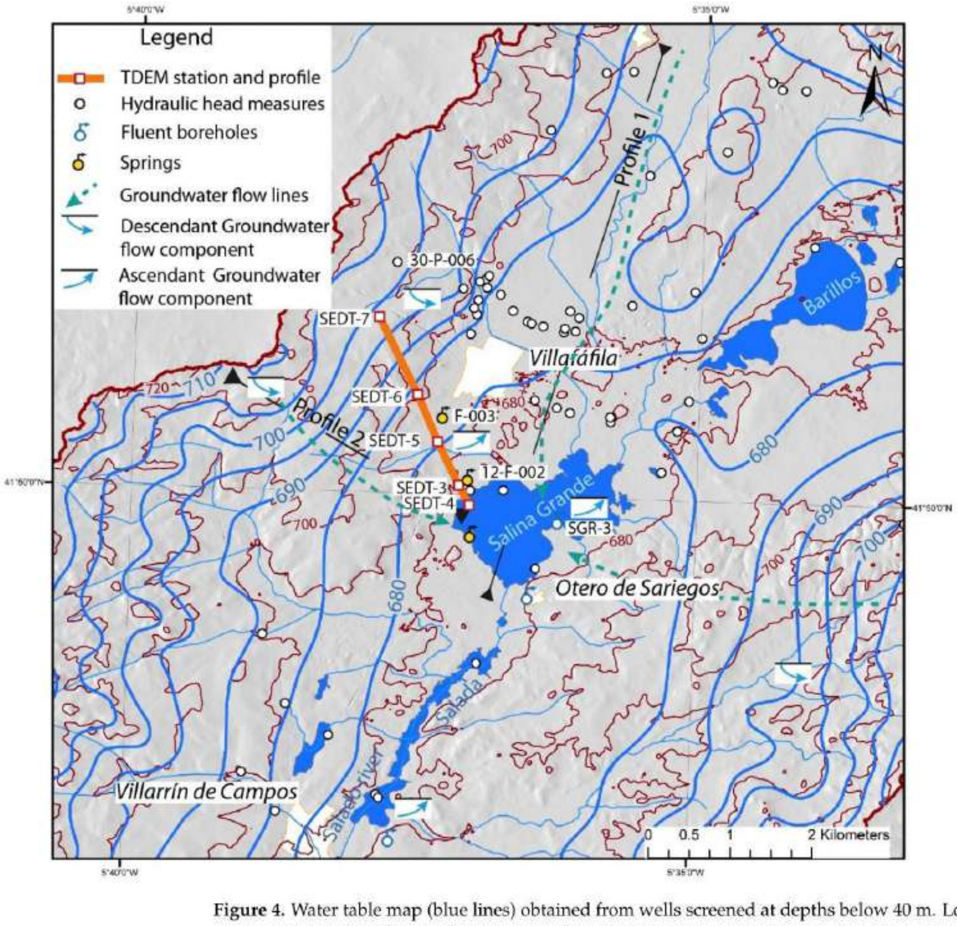

Figure 4. Water table map (blue lines) obtained from wells screened at depths below 40 m. Location of the TDEM profiles (orange line) the sounding sites, EC measurement sites and vertical components of groundwater flow are also indicated (see legend). Red lines indicate the altimetry. Black lines indicate the location of profile 1 and 2 in Figure 7.

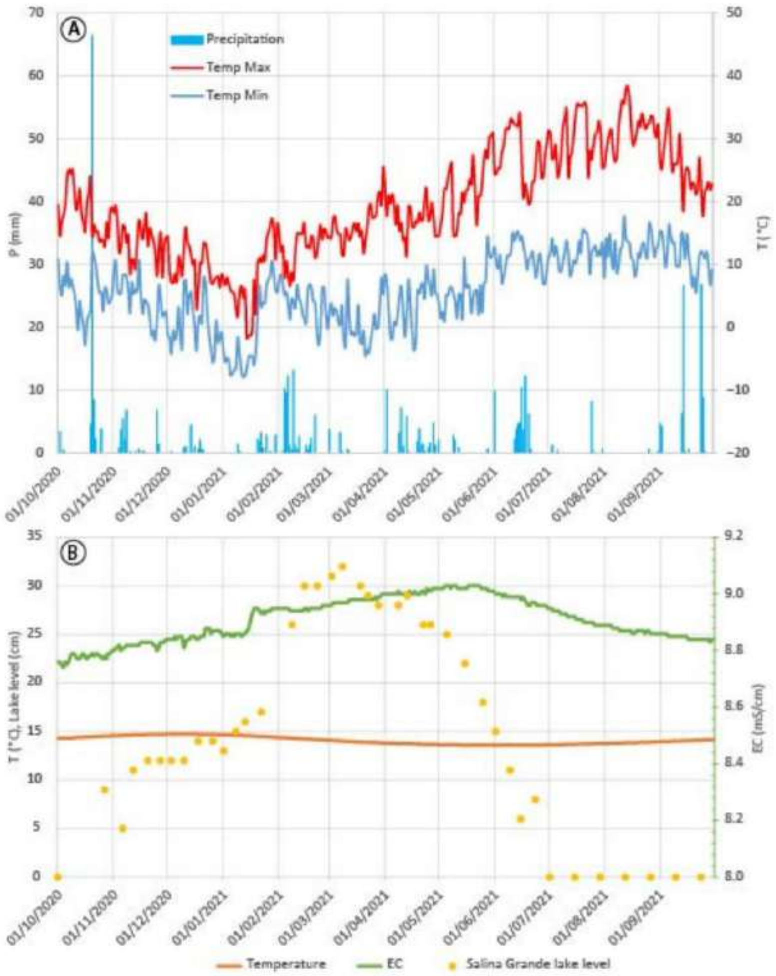

Figure 5. (**A**) Precipitation, minimum, and maximum temperatures measured in Villafáfila meteorological station along the 2020–2021 hydrologic year. (**B**) Record of the EC and temperature at 8 m depth in piezometer SGR-3. Hydraulic head in SGR-3 is constant and overflows to 0.4 m above lake bottom. Lake level in Salina Grande lake is marked by yellow points.

4.2.2. Electric Conductivity

Electric conductivity (EC) of shallow groundwaters in the Villafáfila area show an increasing trend from the lowest values measured in the upper parts of the hills, toward the lowlands surrounding the lakes and to the lake itself (Figure 6), where a brine occurs within the lake sediment's aquitard [20]. EC data, measured in the summer of 2018, were used to construct with a convergent interpolation method the EC map (Figure 6), that shows the lateral changes in this parameter. EC was also measured in lake waters, springs and dug wells in locations closest to the TDEM soundings at the time of the summer and winter surveys (in July 2019 and in February 2020) (Table 1). EC in the shallow groundwaters occurring below the upper part of the hills are between 300–600 μS/cm, with no significant variations along the year (Table 1). Towards the toe of the hills and lowlands around the lakes, EC of shallow groundwaters increases to 1000–6000 µS/cm (Figure 6). The brine within the lake sediment´s aquitard has values reaching 42,000 µS/cm during the summer, when the lake is dry. Lake waters in Salina Grande vary along the year from about 1000 to 20,000 µS/cm (Figure 6). Low EC values in lake waters are registered from February to May. On the other hand, high EC values in lake waters occur at the end of June or along July when the lake is concentrated by evaporation (Table 1). During December and January, there is an increase in lakes salinity, reaching values of 10,000 µS/cm. Groundwaters sampled from boreholes screened below 40 m has EC values ranging from 3000–6000 µS/cm, and show minor variations along the year [20].

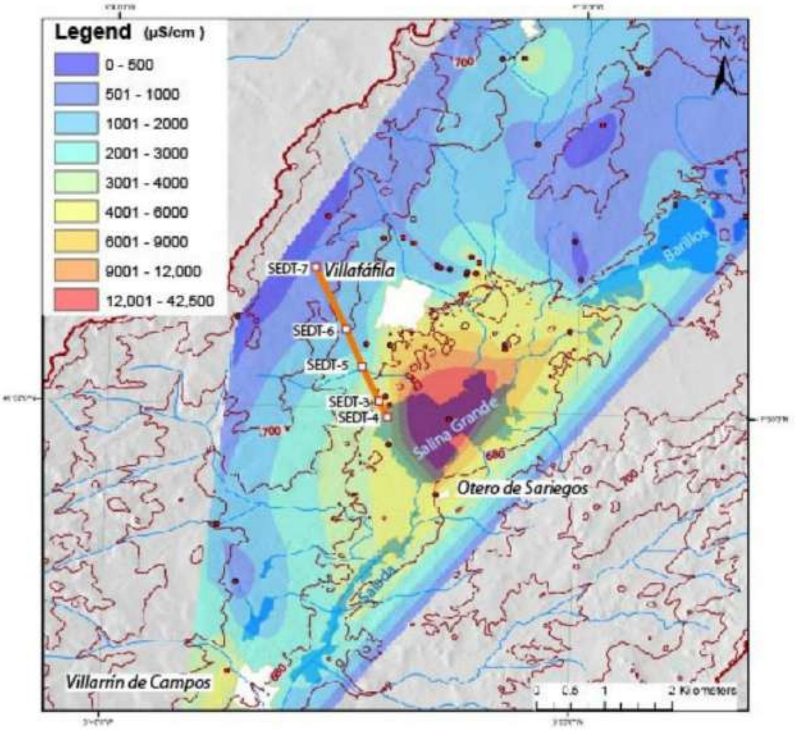

Figure 6. EC map of the surroundings of the Villafáfila lakes. Location of TDEM profile and soundings are marked with an orange line and red squares respectively.

Table 1. Electric conductivity (EC) values measured during the TDEM surveys in the lake, dug wells, and springs close to the different soundings. See location in Figure 4.

Name	Category	Location	Date	EC (µS/cm)
Salina Grande	Lake	Lake	27 July 2019	36,200
Salina Grande	Lake	Lake	13 February 2020	7222
12-F-002	Spring	Low lands	27 July 2019	4550
12-F-002	Spring	Low lands	13 February 2020	3641
F-003	Spring	Toe hills	27 July 2019	Dry
F-003	Spring	Toe hills	13 February 2020	1719
30-P-006	Dug well	Upper part hills	27 July 2019	350
30-P-006	Dug well	Upper part hills	13 February 2020	537

The electric conductivity record of SGR-3 piezometer along 2020–2021 has been measured at 8 m depth, below the aquitard (Figure 5). It shows values that vary between 8760 µS/cm and 9030 µS/cm (Figure 5). The lowest values occur during October while the highest ones are recorded in May and June (Figure 5). During the summer there is a trend toward decreasing EC, till the end of September–October. From October to June there is an increasing trend in EC. Groundwater temperature in SGR-3 has little variations along the year, from 13.5 °C to 14.7 °C. The highest temperatures occur during December and January, when the lowest air temperatures occur. On the other hand, the lowest groundwater temperatures in SGR-3 occur during May and June (Figure 5).

5. Discussion

5.1. Aquifer System Characterization

TDEM resistivity data and electric conductivity (EC) values of lake waters and groundwaters show a consistent spatial distribution. Field geological mapping and well logs indicate that the upper part of the Cenozoic rock record is a sandstone aquifer [18,29,30]. Background resistivity values measured in the Miocene aquifer in the southern part of the Duero aquifer system are about 20 Ohm/m for similar lithologies [26]. Estimates of formation ρ using the measured groundwater EC (Table 1) and Archie´s Law [31] for water saturated units with porosities of 0.35 for the Miocene unconsolidated sandstones and 0.2 for the Quaternary lake mudstones using Archie´s standard parameters (a = 1.2; m = 1.3) are shown in Table 2. Estimated formation resistivity values are similar to those obtained in the TDEM surveys except for those measured in the proximities of dug well 30-P-006 (SEDT-7 and 7BIS), for which the calculated formation resistivity of 87.5 Ohm/m is notably higher than the ρ measured (25 Ohm/m) for U-1 in the SEDT-7 sounding. This is probably due to the existence of a 7 m thick non-saturated zone above the groundwater table, that if were considered in calculations (Sw-n = 0.3) would reduce the formation resistivity. U-1 is interpreted as the non-saturated part of the Miocene aquifer in the hills (Figure 7). Previous geophysical surveys have revealed the existence of an elevated threshold in the Paleozoic metamorphic basement that forces regional brackish groundwater flow to rise [20] (Figure 7). TDEM profiles perpendicular to the lake's axis (Figure 3) show the occurrence of brackish regional groundwaters (<8 Ohm/m) below 600–550 masl (U-4). The upper parts of the profiles with ρ ranging between 20 to 10 Ohm/m are interpreted as the local fresh groundwaters recharged on the hills (U-3). Piezometry indicates lateral groundwater flow from the hills to the lowlands and to the lake. TDEM profiles evidence the gradual decrease in ρ from the upper part of the hills towards the lowlands. This is consistent with the increase in EC of groundwaters and is interpreted as an increased contribution of the brackish regional groundwaters that mix with fresh groundwaters locally recharged in the hills.

Table 2. Conversion of different EC values measured in waters into formation resistivities (ρf) using Archie's law [31]. Sw-n is the water saturation, φ is the porosity, and "a" and "m" are the parameters of Archie's formula that refers to tortuosity and cement respectively.

EC (µS/cm)	Site	Sw-n	φ (Porosity)	a	m	ρf (Ohm/m)
537	30-P-006	1	0.35	1.2	1.3	87.5
1719	F-003	1	0.35	1.2	1.3	27.3
3641	12-F-002	1	0.35	1.2	1.3	12.9
7222	Salina Grande	1	0.35	1.2	1.3	6.5
36,200	Salina Grande	1	0.2	1.2	1.3	2.7

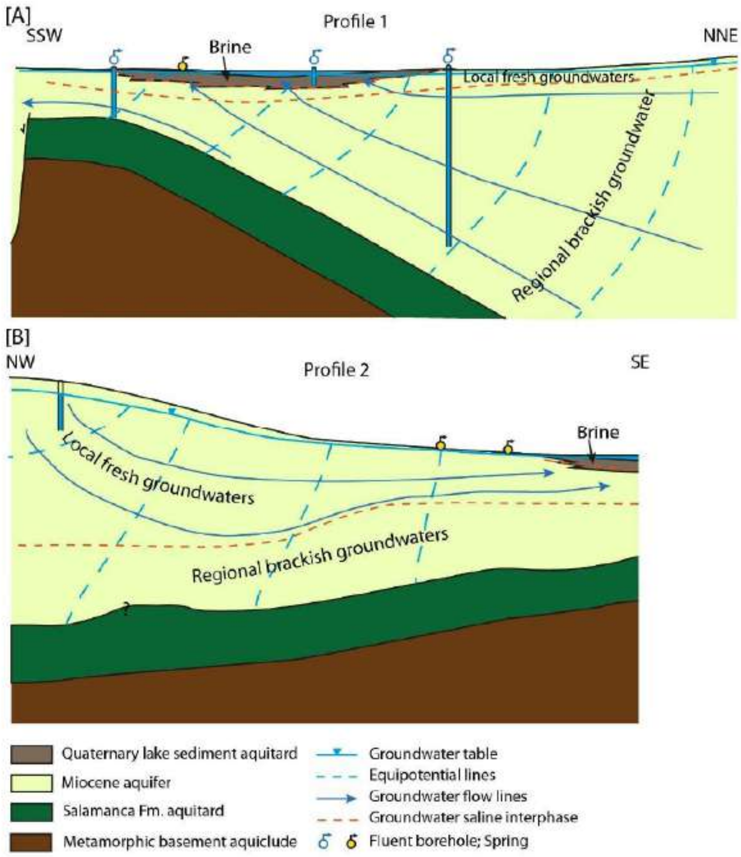

Figure 7. Schematic cross sections of the Villafáfila geological structure and groundwater flow. Location of (**A**) Profile 1 and (**B**) Profile 2 are indicated in Figure 4. Geological reconstruction is based on the data of [20].

Underneath the lowlands and the Salina Grande lake bottom, the low ρ values in the upper part of the profile (U-2) are interpreted as a concentrated brine contained within the Quaternary lake sediment aquitard [20] and highly saline capillary waters and the halite efflorescences that form within the soils of the lake margins by evapotranspirative concentration (Figure 7).

5.2. Seasonal Changes in Groundwater

TDEM profiles show a similar ρ distribution pattern during summer and winter, but there are some differences that are related to the different hydrological processes occurring in Salina Grande lake and its surroundings. At the lake (SEDT-4BIS) ρ values in the upper part of the profile are low (r < 5 Ohm/m) during winter, due to the occurrence of brackish waters and the presence of the brine contained in the lake sediment aquitard (U-2 in Figure 3). During summer this low ρ zone (U-2) extends to the lowlands surrounding the lake. This is interpreted as an effect of groundwater concentration by evaporation in the upper part of the vadose-capillary zone in an area with mixing of local and regional groundwaters. This agrees with the occurrence of halite efflorescences on the surface of the lowland areas. The summer profile (Figure 3B) also shows a rise of the interphase between the local groundwaters coming from the hills (U-3) and the regional brackish groundwaters (U-4), in the lowland areas. The annual record of SGR-3 piezometer (at 8 m depth) shows the highest EC values in May-June decreasing during the summer until reaching the minimum in October (Figure 5). This decrease in EC (Figure 5) is interpreted as the rise of the interphase between the brine (U-2) and the waters coming from the hills, that in the lake shore are mixed with the regional brackish groundwaters (U-3). The rise of the interphase is favored by evaporation pumping and capillary rise in the lake aquitard. This is consistent with the summer rise of the U-3/U-4 interphase observed in the TDEM profiles (Figure 3). In contrast, at the beginning of winter the salinity increases not only in SGR-3 but in the lake waters as well due to the dissolution of halite efflorescences in the lowland areas and the aquifer recharge that favors the transport of the groundwaters and their dissolved salts to the lake area. This processes favor the lowering of the U-2/U-3 interphase in the lake area. Similar processes have been described in other saline lakes where the most soluble salts, mainly halite, can show precipitation-dissolution cycles [32,33]. Other less soluble mineralogical phases can remain, as it occur with the loose calcite cementation observed in the lacustrine mudstones.

5.3. *Implications for Groundwater Use*

TDEM identifies the fresh groundwater domain and is an important tool to locate its contact with brackish or saline groundwaters. Many research papers have highlighted the importance of TDEM soundings to identify groundwater resources [34–36]. In Villafáfila, where regional brackish groundwaters occur in many boreholes that then have to be abandoned, it is important to identify the mentioned interphase, especially for the construction of new boreholes for human consumption. TDEM results reported in this paper indicate that the best places to drill boreholes for human consumption of groundwater are the upper part of the hills, and that the lowlands surrounding the lakes should be avoided. The maximum depth of boreholes should not reach below 600 masl on the hills, which is the depth of the fresh (U-3) and brackish groundwaters (U-4) interphase (Figure 3). Seasonal variations in groundwater dynamics do not affect severely the position of this boundary below the hills, but at the toe of the hills and in the lowlands this boundary can rise significantly during the summer. If intense groundwater pumping is planned in the area, monitoring the fresh-brackish groundwater boundary with TDEM is recommended. The collected data published in this paper and other previous hydrogeological, hydrochemical, and isotopic research in the area could be used to construct a hydrogeological model that will contribute to understand the role of groundwaters in the changes observed in this ecosystem.

6. Conclusions

TDEM profiles in the surroundings of Villafáfila lakes allowed identifying the lateral and vertical variations in terrain resistivity, which are mainly dominated by variations of groundwater salinity. The occurrence of high ρ zones below the hills (U-1 and U-3) show that these zones, dominated by fresh groundwaters, are the main recharge zones of the local aquifer. This is consistent with the piezometry which indicates that local groundwater flows go from the upper part of the hills toward the low lands and the lakes. The low ρ zones close to the surface toward the Salina Grande correspond to the brine contained in the Quaternary lake sediments aquitard (U-2). The deeper part of the terrain explored by the TDEM soundings shows low ρ that represent the regional brackish groundwater flows. The occurrence of a structural relief that elevates the metamorphic basement of the basin perpendicularly to regional groundwater flows forces the flow to increase, favoring the contribution of brackish groundwaters to the Villafáfila lakes [20,21].

Two TDEM surveys during summer (dry season) and winter (wet season), undertaken in the same location, from the hills toward the Salina Grande lake, have shown that there are some differences in ρ which are the response to the hydrological processes occurring in the lake vicinity. The summer expansion of the low ρ area (U-2) close to the surface in the lowland areas and in the lake is produced by the increase in salinity favored by the evapotranspiration of surficial groundwaters and from the capillarity zone. This evaporative groundwater pumping also produces the rise of the interphase between local fresh groundwaters and the regional brackish groundwaters. The continuous record of EC and temperature in the piezometer SGR-3 confirms the rise of the interphase between the saline brine in the aquitard and the local fresh groundwaters.

EC of groundwaters was measured alongside TDEM sounding acquisition. This has allowed correlating the ρ values of the terrain with those of water and groundwater salinity. The correlation between the measured EC of groundwaters and the ρf values obtained from Archie´s law formula is consistent with the ρ values obtained from TDEM soundings. This means that TDEM sounding is an excellent tool to monitor the seasonal changes of groundwater salinity. This can help to prevent aquifer salinization problems. EC map reveals that surficial groundwaters in the low lands has values between 6000 and 9000 μS/cm and the brine below the Salina Grande Lake reaches 42,000 μS/cm.

The best places in the area to obtain fresh groundwaters are the hills that surround the Villafáfila lakes. Below 600 masl in the hills, brackish regional groundwaters are present. In the low lands, the brackish regional groundwaters can be found below 640 masl.

Author Contributions: Conceptualization, P.H.; methodology, P.H., P.C.-G. and J.C.-G.; software, P.C.-G. and J.C.-G.; validation, P.H. and P.C.-G.; investigation, P.H., P.C.-G., I.A., C.R., J.C.-G. and E.R.-J.; resources, E.R.-J.; data curation, P.C.-G. and J.C.-G.; writing—original draft preparation, P.H. and P.C.-G.; writing—review and editing, P.H., P.C.-G., I.A. and C.R.; project administration, P.H.; funding acquisition, P.H. All authors have read and agreed to the published version of the manuscript.

Funding: This paper is part of the Research Project I+D+i/ PGC2018-094566-B-C21, supported by the MCIN/ AEI/10.13039/501100011033/ and FEDER "Una manera de hacer Europa".

Data Availability Statement: Not applicable.

Acknowledgments: The research acknowledges the Consejería de Fomento y Medio Ambiente, Junta de Castilla y León, and the Casa del Parque (Villafáfila) for permission to do fieldwork in the Villafáfila Natural Reserve. Authors acknowledge the anonymous reviewers and the editor of water for the improvement of the manuscript.

Conflicts of Interest: The authors declare no conflict of interest.

References

1. Kohfahl, C.; Rodriguez, M.; Fenk, C.; Menz, C.; Benavente, J.; Hubberten, H.; Meyer, H.; Paul, L.; Knappe, A.; López-Geta, J.A.; et al. Characterising flow regime and interrelation between surface-water and ground-water in the Fuente de Piedra salt lake basin by means of stable isotopes, hydrogeochemical and hydraulic data. *J. Hydrol.* **2008**, *351*, 170–187. [CrossRef]
2. Cartwright, I.; Hall, S.; Tweed, S.; Leblanc, M. Geochemical and isotopic constraints on the interaction between saline lakes and groundwater in southeast Australia. *Hydrogeol. J.* **2009**, *17*, 1991. [CrossRef]
3. Marazuela, M.A.; Vázquez-Suñé, E.; Custodio, E.; Palma, T.; García-Gil, A.; Ayora, C. 3D mapping, hydrodynamics and modelling of the freshwater-brine mixing zone in salt flats similar to the Salar de Atacama (Chile). *J. Hydrol.* **2018**, *561*, 223–235. [CrossRef]
4. Sanz, D.; Valiente, N.; Dountcheva, I.; Muñoz-Martín, A.; Cassiraga, E.; Gómez-Alday, J. Geometry of the modelled freshwater/salt-water interface under variable-density-driven flow (Pétrola Lake, SE Spain). *Hydrogeol. J.* **2022**, *30*, 975–988. [CrossRef]
5. Rhoades, J.; Raats, P.; Prather, R. Effects of liquid-phase electrical conductivity, water content, and surface conductivity on bulk soil electrical conductivity. *Soil Sci. Soc. Am. J.* **1976**, *40*, 651–655. [CrossRef]
6. Danielsen, J.E.; Auken, E.; Jørgensen, F.; Søndergaard, V.; Sørensen, K.I. The application of the transient electromagnetic method in hydrogeophysical surveys. *J. Appl. Geophys.* **2003**, *53*, 181–198. [CrossRef]
7. Jang, H.; Kim, H.J. Mapping deep-sea hydrothermal deposits with an in-loop transient electromagnetic method: Insights from 1D forward and inverse modeling. *J. Appl. Geophys.* **2015**, *123*, 170–176. [CrossRef]
8. Metwaly, M.; Elawadi, E.; Moustafa, S.S.R.; Al Arifi, N.; El Alfy, M.; Al Zaharani, E. Groundwater contamination assessment in Al-Quwy'yia area of central Saudi Arabia using transient electromagnetic and 2D electrical resistivity tomography. *Environ. Earth Sci.* **2014**, *71*, 827–835. [CrossRef]
9. Tabbagh, A.; Dabas, M. Absolute magnetic viscosity determination using time-domain electromagnetic devices. *Archaeol. Prospect.* **1996**, *3*, 199–208. [CrossRef]
10. Goldman, M.; Gvirtzman, H.; Hurwitz, S. Mapping saline groundwater beneath the Sea Galilee and its vicinity using time domain electromagnetic (TDEM) geophysical technique. *Isr. J. Earth Sci.* **2004**, *53*, 187–197. [CrossRef]

11. Tchouta, K.D.; Marie, B.; Emmanuel, M.V.Y.; Guillaume, F.; Benjamin, N.N.; Nicaise, Y.; Baba, G.I.; Anatoly, L. Contribution of time domain electromagnetic and magnetic resonance soundings to groundwater assessment at the margin of lake chad basin, cameroon. *J. Appl. Geophys.* **2019**, *170*, 103840. [CrossRef]
12. Levi, E.; Goldman, M.; Hadad, A.; Gvirtzman, H. Spatial delineation of groundwater salinity using deep time domain electromagnetic geophysical measurements: A feasibility study. *Water Resour. Res.* **2008**, *44*, W12404. [CrossRef]
13. Flores Avilés, G.P.; Descloitres, M.; Duwig, C.; Rossier, Y.; Spadini, L.; Legchenko, A.; Soruco, Á.; Argollo, J.; Pérez, M.; Medinaceli, W. Insight into the Katari-Lago Menor Basin aquifer, Lake Titicaca-Bolivia, inferred from geophysical (TDEM), hydrogeological and geochemical data. *J. S. Am. Earth. Sci.* **2020**, *99*, 102479. [CrossRef]
14. Yihdego, Y.; Webb, J. Modelling of seasonal and long-term trends in lake salinity in southwestern Victoria, Australia. *J. Environ. Manag.* **2012**, *112*, 149–159. [CrossRef] [PubMed]
15. Martinez, C. Daily activity patterns of Great Bustards Otis tarda. *Ardeola* **2000**, *47*, 57–68.
16. Nilsson, L.; Kampe-Persson, H. Changes in migration and wintering patterns of greylag geese Anser anser from southernmost Sweden during three decades. *Ornis Svec.* **2018**, *28*, 19–38. [CrossRef]
17. IGM. *Investigación Hidrogeológica de la Cuenca del Duero: Sistemas nº 8 y 12*; IGME: Madrid, Spain, 1980; p. 75.
18. IGME-DGA. *Apoyo a la Caracterización Adicional de las Masas de Agua Subterránea en Riesgo de no Cumplir los Objetivos Medioambientales en 2015. Demarcación Hidrográfica del Duero. Masa de agua Subterránea 31 Villafáfila*; IGME: Madrid, Spain, 2009; p. 84.
19. AEMET. AEMET Open Data. *Benavente*. Available online: http://www.aemet.es/es/datos_abiertos/AEMET_OpenData (accessed on 1 July 2020).
20. Huerta, P.; Armenteros, I.; Recio, C.; Carrasco-García, P.; Rueda-Gualdrón, C.; Cidón-Trigo, A. The origin of the saline waters in the Villafáfila lakes (NW Spain). A hydrogeological, hydrochemical, and geophysical approach. *Sci. Total Environ.* **2021**, *789*, 147909. [CrossRef]
21. Armenteros, I.; Huerta, P.; Cidón-Trigo, A.; Rueda-Gualdrón, M.C.; Recio, C.; Martínez-Grana, A. Hydrogeology of the lagunas de villafáfila area (Zamora). *Geogaceta* **2019**, *66*, 51–54.
22. Fernández Pérez, L.; Cabrera Lagunilla, M.P. Estudio Hidrogeológico de las lagunas de Villafáfila (Zamora). In *Geología Ambiental y Ordenación del Territorio. III Reunión Nacional*; Universitat de Valencia: Valencia, Spain, 1987; Volume 1, pp. 441–459.
23. Fitterman, D.V.; Stewart, M.T. Transient electromagnetic sounding for groundwater. *Geophysics* **1986**, *51*, 995–1005. [CrossRef]
24. Spies, B.R. Depth of investigation in electromagnetic sounding methods. *Geophysics* **1989**, *54*, 872–888. [CrossRef]
25. Nabighian, M.N. *Electromagnetic Methods in Applied Geophysics: Volume 1, Theory*; Society of Exploration Geophysicists: Houston, TX, USA, 1988.
26. Nieto, I.M.; Carrasco García, P.; Sáez Blázquez, C.; Farfán Martín, A.; González-Aguilera, D.; Carrasco García, J. Geophysical Prospecting for Geothermal Resources in the South of the Duero Basin (Spain). *Energies* **2020**, *13*, 5397. [CrossRef]
27. Hoekstra, P.; Blohm, M.W. Case histories of time-domain electromagnetic soundings in environmental geophysics. In *Geotechnical an Environmental Geophysics: Volume II: Environmental and Groundwater*; Society of Exploration Geophysicists: Houston, TX, USA, 1990; pp. 1–16.
28. Constable, S.C.; Parker, R.L.; Constable, C.G. Occam's inversion: A practical algorithm for generating smooth models from electromagnetic sounding data. *Geophysics* **1987**, *52*, 289–300. [CrossRef]
29. Martín Serrano, A.; Piles Mateo, E. Villafáfila (308). In *Mapa Geológico de España y Memoria, Escala 1:15.000*; IGME: Madrid, Spain, 1982.
30. Martín Serrano, A.; Barba Martín, A. Manganeses de la Lampreana 340. In *Mapa Geológico de España y Memoria. Escala 1:50.000*; IGME: Madrid, Spain, 1979.
31. Archie, G.E. The Electrical Resistivity Log as an Aid in Determining Some Reservoir Characteristics. *Trans. AIME* **1942**, *146*, 54–62. [CrossRef]
32. Yadav, D.; Sarin, M.; Krishnaswami, S. Hydrogeochemistry of Sambhar Salt Lake, Rajasthan: Implication to recycling of salt and annual salt budget. *J.-Geol. Soc. India* **2007**, *69*, 139–152.
33. Drever, J.I.; Smith, C.L. Cyclic wetting and drying of the soil zone as an influence on the chemistry of ground water in arid terrains. *Am. J. Sci.* **1978**, *278*, 1448–1454. [CrossRef]
34. Descloitres, M.; Chalikakis, K.; Legchenko, A.; Moussa, A.M.; Genthon, P.; Favreau, G.; Le Coz, M.; Boucher, M.; Oï, M. Investigation of groundwater resources in the Komadugu Yobe Valley (Lake Chad Basin, Niger) using MRS and TDEM methods. *J. Afr. Earth Sci.* **2013**, *87*, 71–85. [CrossRef]
35. Amato, F.; Pace, F.; Vergnano, A.; Comina, C. TDEM prospections for inland groundwater exploration in semiarid climate, Island of Fogo, Cape Verde. *J. Appl. Geophys.* **2021**, *184*, 104242. [CrossRef]
36. Martínez-Moreno, F.J.; Monteiro-Santos, F.A.; Madeira, J.; Bernardo, I.; Soares, A.; Esteves, M.; Adão, F. Water prospection in volcanic islands by Time Domain Electromagnetic (TDEM) surveying: The case study of the islands of Fogo and Santo Antão in Cape Verde. *J. Appl. Geophys.* **2016**, *134*, 226–234. [CrossRef]

ARTICULO 4 Hidrogeología del entorno de las lagunas del Oso (Ávila)

Resumen:

En las proximidades de El Oso, en la Moraña abulense, existen varios humedales siendo la laguna de El Hoyo el más importante. Las arenas miocenas y cuaternarias constituyen buenos acuíferos con flujos subterráneos que van de Sur a Norte. En las proximidades de El Oso el nivel freático está muy somero y existe una componente vertical ascendente del flujo. Las aguas son dulces y tienen una composición bicarbonata cálcico sódica. La laguna de El Hoyo tiene modificado su régimen natural por aportes de agua de sondeos cercanos. El Hoyo es una laguna de recarga durante el invierno alimentada principalmente por precipitación directa, aunque durante el verano puede recibir aportes de agua subterránea.

Sociedad Geológica España

GEOGACETA, 72, 2022

Hidrogeología del entorno de las lagunas del Oso (Ávila)

Hydrogeology of the surroundings of El Oso lakes (Ávila)

Pedro Huerta[1], Álvaro Inthirat[2], Pedro Carrasco[2], Ildefonso Armenteros[3], Clemente Recio[3], Esther Rodríguez-Jiménez[3] y Javier Carrasco García[4]

[1] Dpto. Geología, Escuela Politécnica Superior de Ávila. Universidad de Salamanca, Av. Hornos Caleros, n° 50, 05003 Ávila, Spain. phuerta@usal.es;
[2] Dpto. Ingeniería Cartográfica y del Terreno, Escuela Politécnica Superior de Ávila. Universidad de Salamanca, Av. Hornos Caleros, n° 50, 05003 Ávila, Spain. retep81@usal.es; al.inth@usal.es
[3] Dpto. Geología, Facultad de Ciencias, Universidad de Salamanca, Pza. de la Merced S/N, 37008 Salamanca, Spain. ilde@usal.es; crecio@usal.es; erj@usal.es.
[4] Técnicas Geofíscas, S.L. Paseo de San Roque 21, 3°1 05003 Ávila (Ávila). tgeofisicas@gmail.com

ABSTRACT

In the surroundings of the locality of El Oso in the region of the Moraña (Ávila), there are many wetlands. The most important is El Hoyo lake. The Miocene and Quaternary sands constitute good aquifers with northward groundwater flow. In the vicinity of El Oso the groundwater table is very shallow and groundwater shows an ascendant vertical component. Groundwaters are fresh and have a bicarbonate-calcium-sodic composition. The natural regime of El Hoyo lake has been modified by the groundwater inputs from nearby boreholes. El Hoyo is a recharge lake during the winter, fed mainly by direct precipitation, but during the summer it can receive groundwater inputs.

Key-words: *Pond, Moraña, El Hoyo lake, aquifer, Duero basin.*

RESUMEN

En las proximidades de El Oso, en la Moraña abulense, existen varios humedales siendo la laguna de El Hoyo el más importante. Las arenas miocenas y cuaternarias constituyen buenos acuíferos con flujos subterráneos que van de Sur a Norte. En las proximidades de El Oso el nivel freático está muy somero y existe una componente vertical ascendente del flujo. Las aguas son dulces y tienen una composición bicarbonata cálcico sódica. La laguna de El Hoyo tiene modificado su régimen natural por aportes de agua de sondeos cercanos. El Hoyo es una laguna de recarga durante el invierno alimentada principalmente por precipitación directa, aunque durante el verano puede recibir aportes de agua subterránea.

Palabras clave: *laguna, Moraña, laguna de El Hoyo, acuífero, Cuenca del Duero.*

Geogaceta, 72 (2022), 15-18
ISSN (versión impresa): 0213-683X
ISSN (Internet): 2173-6545

Fecha de recepción: 07/02/2022
Fecha de revisión: 22/04/2022
Fecha de aceptación: 27/05/2022

Introducción

Sobre el gran sistema acuífero de la cuenca del Duero existen muchos humedales que, si bien no tienen grandes dimensiones, son relevantes en cuanto a su papel medioambiental e interés hidrogeológico (Armenteros *et al.*, 2019; Sanz-Montero *et al.*, 2019; Mediavilla *et al.*, 2020; Huerta *et al.*, 2021). En la región abulense conocida como La Moraña existen una serie de humedales de pequeñas dimensiones, muchos de los cuales se encuentran secos durante la mayor parte del año. Uno de estos humedales es la laguna de El Hoyo o de El Oso, nombre que recibe del término municipal en el que se encuentra (El Oso). Esta laguna es la que tiene una lámina de agua más estable a lo largo del año, aunque solía secarse, casi en su totalidad, durante el verano. Actualmente su régimen natural se encuentra modificado por los aportes de aguas de sondeos de una embotelladora cercana, con los que el Ayuntamiento de El Oso pretende mantener la presencia de aves en la zona. No se conoce el caudal aportado, que suele ser variable, ni su continuidad a lo largo del año. Aunque esta laguna aparece en el catálogo regional de zonas húmedas de Castilla y León y es lugar de descanso de aves migratorias no tiene ninguna figura de protección. La proximidad del nivel freático a superficie en el entorno de la laguna de El Hoyo hace interesante estudiar el comportamiento hidrogeológico de la zona y su relación con la laguna.

Situación geográfica y geología

La zona de estudio se encuentra en el borde sur de la cuenca cenozoica del Duero. Esta zona tiene un relieve aplanado con cotas en torno a los 900 metros sobre el nivel del mar (msnm), en el que destacan algunos cerros testigo. Las rocas miocenas que aparecen en la zona están constituidas por conglomerados y arcosas con cantos de rocas graníticas y metamórficas que afloran al sur de El Oso, en la sierra de Ávila. Hacia el norte de la zona de estudio (Fig. 1) predominan las arcosas y fangos areno-limosos. En ambas zonas aparecen enrejados y nódulos de calcita formados por procesos pedogénicos.

Las rocas miocenas están cubiertas en buena parte de la zona de estudio por depósitos cuaternarios (Plio-Pleistocenos): coluviones procedentes principalmente del borde sur y de los relieves próximos; depósitos de arcosas de terrazas; depósitos de arcosas con cantos de origen fluvial. Sobre éstos se apoyan, en algunos lugares, arenas de origen eólico que forman mantos y dunas, y depósitos lacustres constituidos por arenas y lutitas con precipitados carbonáticos. Estos últimos depósitos se asignan al Holoceno (Pérez-González y Elízaga-Muñoz, 1979a; Pérez-González y Elízaga-Muñoz, 1979b) (Fig. 1). Tanto los depósitos miocenos como los cuaternarios son muy porosos y permeables, por lo que constituyen buenos acuíferos. Los humedales presentes en esta zona de la Moraña, entre los que se incluye la laguna del Hoyo tienen un origen eólico (Sanz Donaire y García Rodríguez, 1998). La laguna tiene un

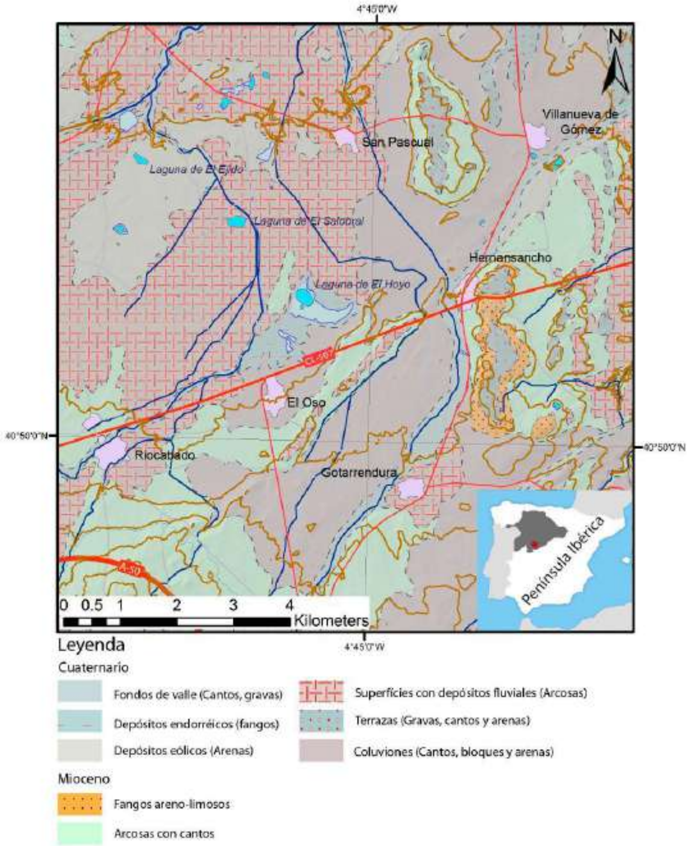

Fig. 1.- Mapa geológico de la zona de estudio. Modificado a partir de Geode Z2300 Cuenca del Duero Almazán (Pineda et al., en línea). Ver figura en color en la web.

Fig. 1.- Geological map of the study area. The map was modified from the Geode Z2300 Cuenca del Duero-Almazán (Pineda et al., en línea). See color figure in the web.

tamaño de 0.1 km^2, mientras que el área de drenaje que vierte a ella tiene un área de 4.8 km^2 (Fig.2). Su profundidad media varía entre 20 y 50 cm, aunque puede pasar de estar seca a tener 1 m de profundidad. En las proximidades de la laguna se excavaron zanjas drenantes antes de 1945 con el fin de drenar los campos que solían estar llenos de agua durante los meses de invierno.

Clima

La zona de estudio se caracteriza por tener un clima mediterráneo continentalizado, con importantes oscilaciones entre las temperaturas mínimas y máximas. Las temperaturas medias más bajas registradas en la estación meteorológica de Gotarrendura (Fig. 1) para la serie (2016-2020), son de 4,1 ºC, y se registran en enero. Las temperaturas medias más altas son de 22,5 ºC y se registran en julio. La precipitación media anual es de 321 mm, siendo abril el mes más lluvioso y agosto el menos.

Metodología

La toma de datos con los que se ha elaborado el mapa piezométrico (Fig. 2) se realizó en Julio de 2021. Se midieron pozos excavados con profundidades inferiores a 15 m con una sonda de nivel. Los pozos están abiertos en el acuífero cuaternario en su mayoría aunque muchos alcanzan el acuífero mioceno. Los muestreos de parámetros fisicoquímicos se realizaron durante julio de 2020, y febrero, abril y julio de 2021. El pH se midió con un peachímetro Hanna HI 9023 y la conductividad eléctrica (CE) y la temperatura se midieron con un conductivímetro Hanna HI 9835 con sonda de temperatura incorporada. Los análisis químicos se realizaron en el Servicio de Análisis químicos de la Universidad de Salamanca y en el Laboratorio de aguas de la Confederación Hidrográfica del Duero.

Resultados

Piezometría

El mapa piezométrico de la zona (Fig. 2) indica que el nivel freático desciende de Sur a Norte, desde los relieves formados por los depósitos aluviales miocenos hasta las zonas llanas dominadas por depósitos cuaternarios. Pasa de cotas de 940 m hasta los 890 m. En la parte norte, el nivel freático se encuentra muy próximo a la superficie del terreno. En algunos casos se encuentra a 0,3 m de profundidad en la época de estiaje. Durante la época de lluvias, muchas de estas zonas llegan a estar cubiertas en grandes extensiones por una lámina de agua con profundidades centimétricas. Las líneas de flujo tienen trayectorias de Sur a Norte, y se dirigen desde los relieves hacia los valles de los ríos.

Los pozos y sondeos abiertos a profundidades mayores de 15 m, en la zona de El Oso son surgentes (Fig. 2). Algunos de estos pozos, de los que capta agua una embotelladora, están abiertos a 80, 100 y 120 m.

En un piezómetro instalado en uno de los bordes de la laguna del Hoyo (Fig. 2), abierto a 9 m de profundidad, el agua se encuentra a unos 40-80 cm por debajo del suelo de la laguna.

La evolución de la piezometría en esta zona de La Moraña en los últimos años puede considerarse estable (MIRAME, 2022).

Características físico-químicas de las aguas

Los aguas medidas en pozos excavados (prof.< 15 m) tienen temperaturas de 16,8 ºC – 17,2 ºC. El pH varía entre 6,8 y 7,2 y la CE varía entre 500 y 1500 µS/cm. Durante los meses de verano estos valores (CE) se ven incrementados y existe un aumento hacia la zona norte. Los sondeos, abiertos a profundidades mayores a 15 m tienen temperaturas constantes a

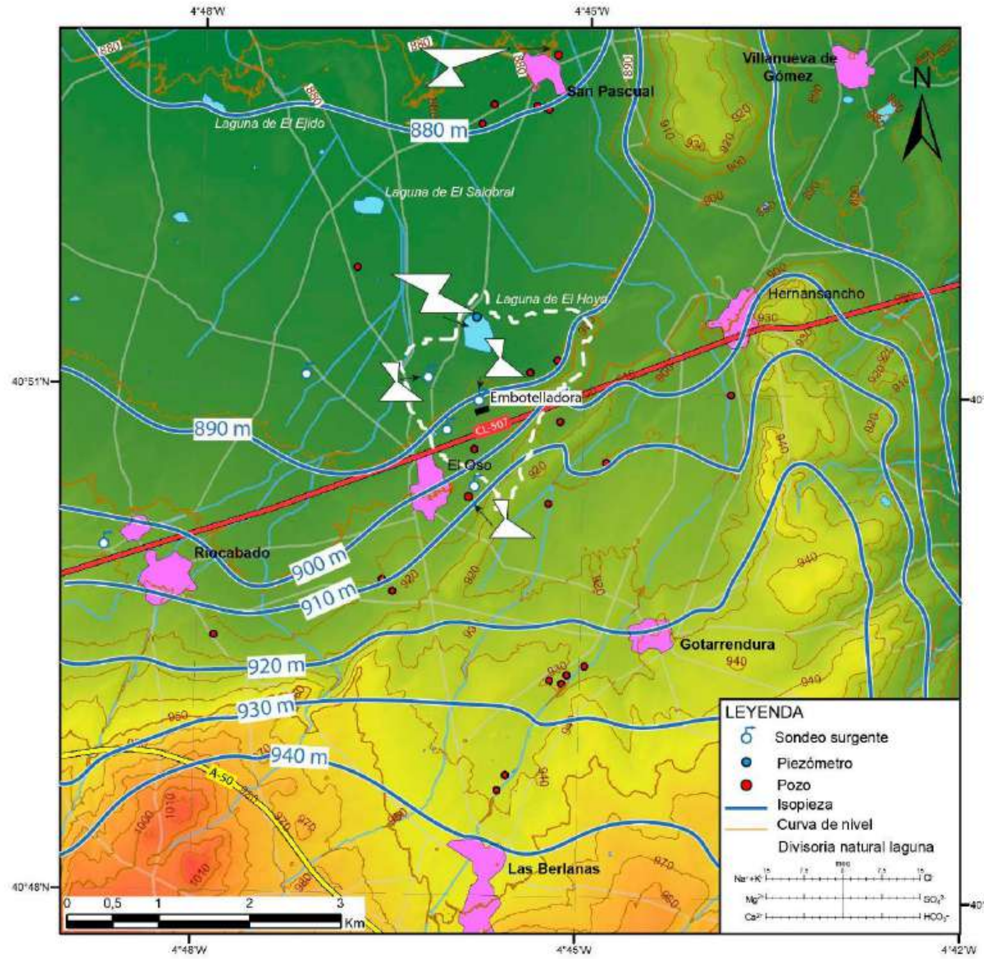

Fig. 2.- Mapa piezométrico de la zona de estudio. Elaborado a partir de pozos excavados abiertos a profundidades < 15 m en julio de 2020.
Fig. 2.- Piezometry of the study area. The map was constructed with data from dug wells (screened at depths<15 m), during July 2020.

lo largo del año de unos 16 ºC. El pH varía desde valores de 7 hasta 9 en los sondeos profundos de la embotelladora. La CE varía entre los 400 y 800 µS/cm.

Las aguas de la laguna muestran variaciones de temperatura a lo largo del año de unos 10 a 20 ºC. El pH de la laguna varía desde 7,4 hasta 9 y la CE desde 250 µS/cm en los meses de invierno a 2600 µS/cm en verano. Tanto las aguas de los pozos excavados como las de los sondeos tienen una composición química de tipo bicarbonatado cálcico sódica. Con un total de sólidos disueltos (TSD) de entre 500-800 mg/L. Los cationes principales, el Ca^{2+} y el Na^{+}, se encuentran en proporciones similares en torno al 50%. El anión principal es el HCO_3^- que representa aproximadamente el 90% de éstos. El Cl^- se encuentra en proporciones próximas al 10% mientras que la presencia del anión sulfato es mínima. Las aguas de la laguna muestran algunas diferencias, con un enriquecimiento del Na^+ y del Cl^- con respecto al resto de iones (Fig. 2).

Discusión

La principal área de recarga de los acuíferos en esta zona próxima al borde sur de la cuenca del Duero se localiza en los depósitos aluviales de dicho margen, que en la zona constituyen áreas elevadas que hacia el sur dan paso a los granitos y rocas metamórficas de la Sierra de Ávila. Es posible que existan aportes de agua subterránea desde dicha sierra a través de fracturas del basamento.

El cambio de pendiente desde los relieves de la zona sur a las llanuras de la zona norte favorece, junto con la presencia de depósitos cuaternarios, la somerización del nivel freático que se encuentra muy próximo a superficie.

La presencia de sondeos surgentes en la zona de El Oso puede estar relacionada con que se encuentren ranurados en zonas con un potencial hidráulico mayor que la cota de superficie en un acuífero arenoso homogéneo. Otra posibilidad es que existan capas lutíticas que se comporten como acuicludos o acuitardos, confinando los acuíferos en los que captan agua los sondeos. Los cambios e interdigitaciones desde posiciones proximales (al sur), a posiciones distales (al norte), de los abanicos aluviales miocenos del borde sur de la cuenca cenozoica del Duero podrían explicar esta situación. De cualquier modo parece existir una componente vertical ascendente del flujo subterráneo en esta zona. En el piezómetro situado en el borde de la laguna del Hoyo, el nivel piezométrico se encuentra por debajo del suelo de la laguna en su borde. Así que en los momentos en los que el nivel de la laguna es alto y está por encima del nivel piezométrico debe existir un aporte de agua desde la laguna al acuífero. En el estío, cuando la laguna está restringida a sus zonas centrales, el nivel de la laguna y el nivel piezométrico se igualan (Fig. 3).

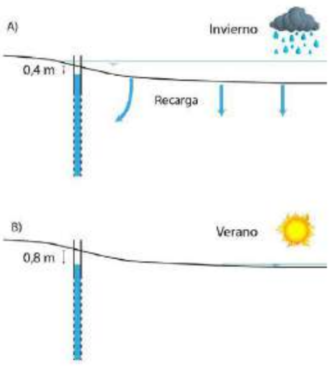

Fig. 3.- Relación entre las aguas de la laguna del Oso y el piezómetro situado en su margen durante el invierno (A) y el verano (B).
Fig. 3.- Relationship between El Oso lake waters and the piezometer placed at its margin during winter (A) and summer (B).

Si se aplica el índice de función hidrológica (IFH) que relaciona el área de la cuenca superficial con el área de la laguna y la precipitación anual efectiva (Rodríguez-Rodríguez *et al.*, 2010), el valor para la laguna del Hoyo sería próximo a 0,4. Esto podría ser indicador de que las lagunas reciben aportes de agua subterránea. Algo que realmente ocurre a través de los aportes de los sondeos. Este índice se ha desarrollado para lagunas y "playa-lakes" de la cuenca del Guadalquivir.

La composición química de las aguas puede derivar de la meteorización de silicatos del basamento como las plagioclasas y/o de la disolución de caliches presentes en la sucesión miocena.

El agua de las lagunas muestra una mayor variabilidad en los parámetros físico-químicos debido en buena medida a las variaciones estacionales en la precipitación, la temperatura y la evaporación. Esto hace que en invierno las aguas estén más diluidas, mientras que en verano estén más concentradas. Las variaciones en el pH desde valores de 7 hasta 9 se interpretan como debidos a aportes de precipitación directa para los primeros y aportes de agua de la embotelladora para los segundos.

Conclusiones

En el entorno de El Oso existen varias lagunas, siendo la más importante la laguna de El Hoyo, también conocida como laguna de El Oso. Los depósitos miocenos y cuaternarios son buenos acuíferos arenosos en los que el agua circula de sur a norte. El nivel freático se encuentra muy próximo a superficie en la zona norte y existe una componente ascendente del flujo subterráneo en la zona del Oso.

El valor de TSD de las aguas subterráneas es de 500-800 mg/L y su composición es bicarbonatada cálcico sódica. Aunque el pH en las aguas más superficiales está próximo a 7, destaca el pH 9 de los sondeos profundos de la embotelladora.

La laguna, aunque se alimenta principalmente de agua de lluvia, también recibe aportes de agua subterráneas. Actualmente su régimen natural se ha modificado por aportes de agua de sondeos con los que se pretende mantener este ecosistema en condiciones estables.

Contribución de los autores

Huerta ha realizado tareas de toma de datos, planificación y preparación del trabajo; Inthirat ha realizado tareas de toma de datos y elaboración del trabajo. Carrasco, P. Armenteros, Recio y Rodríguez-Jiménez y Carrasco, J. han participado en la toma de datos, metodología y análisis.

Agradecimientos y financiación

Este trabajo es parte del proyecto de investigación I+D+i/ PGC2018-094566-B-C21, financiado por el MCIN/AEI/10.13039/501100011033/ y FEDER "Una manera de hacer Europa". Los investigadores agradecen a la Consejería de Fomento y Medio Ambiente, Junta de Castilla y León los permisos de trabajo de campo. Los autores agradecen la labor de los editores y los comentarios de dos revisores anónimos.

Referencias

Armenteros, I., Huerta, P., Cidón-Trigo, A., Rueda-Gualdrón, M.C., Recio, C. y Martínez-Grana, A. (2019). *Geogaceta*, 66, 51-54.

Huerta, P., Armenteros, I., Recio, C., Carrasco-García, P., Rueda-Gualdrón, C. y Cidón-Trigo, A. (2021). *Science of The Total Environment*, 789, 147909.

Mediavilla, R., Santisteban, J.I., López-Cilla, I., Galán de Frutos, L. y de la Hera-Portillo, Á. (2020). *Water*, 12, 1911.

MIRAME (2022). *Confederación Hidrográfica del Duero*, http://www.mirame.chduero.es/DMADuero_09_15/index.faces, 20-02-2022.

Pérez-González, A. y Elízaga-Muñoz, E. (1979a): *Mapa Geológico de España 1:50.000, hoja nº 481 (Nava de Arévalo)*. IGME, Madrid 52 p.

Pérez-González, A. y Elízaga-Muñoz, E. (1979b): *Mapa Geológico de España 1:50.000, hoja nº 506 (Cardeñosa) y memoria*. IGME, Madrid 68 p.

Pineda, A., Huerta, P., Nozal, F., Montes, M. y López-Olmedo, F. (en línea): *Mapa Geológico Digital continuo E. 1: 50.000, Zona Cuenca del Duero-Almazán (Zona-2300)* IGME, en línea.

Rodríguez-Rodríguez, M., Moral, F., Benavente, J. y Beltrán, M. (2010). *Journal of Arid Environments*, 74, 1478-1486.

Sanz-Montero, M.E., Cabestrero, Ó. y Sánchez-Román, M. (2019). *Frontiers in Microbiology*, 10.

Sanz Donaire, J.J. y Garcia Rodríguez, M.P. (1998). *Observatorio Medioambiental*, 1, 65-92.

ARTICULO 5 Electrical-Resistivity Tomography Techniques for the Exploration of Medium- and Low-Geothermal Energy Resources

Resumen:

El crecimiento de la industria geotérmica exige la búsqueda constante de técnicas con el objetivo de reducir los esfuerzos de exploración al tiempo que se minimiza la incertidumbre del subsuelo. La exploración de los recursos geotérmicos es fundamental desde el punto de vista de la explotación, especialmente en aquellas regiones donde esta energía no está tan extendida como el resto de fuentes renovables. Esta investigación muestra cómo los métodos geoeléctricos pueden contribuir a la investigación y caracterización de recursos geotérmicos de media-baja entalpía hasta unos 800 m de profundidad. Se realizó un perfil de tomografía en una región del sur de España con evidencias previas de un potencial geotérmico moderado. Los resultados de esta campaña geofísica (junto con una caracterización geológica preliminar) permitieron obtener un perfil 2D y un modelo pseudo-3D con amplia información sobre el subsuelo en términos de composición geológica y formaciones. La interpretación de resultados geofísicos denota la existencia de una formación potencial constituida por materiales carbonatados con espesores superiores a 300 m, atravesando por diferentes fracturas. Una vez definida la ubicación ideal para la explotación geotérmica, la investigación evalúa la contribución de la posible fuente de energía, deduciendo que la extracción de energía en la zona de fracturación potencial sería el doble que la de la de las inmediaciones del yacimiento.

energies

MDPI

Article

Applying Deep Electrical-Resistivity Tomography Techniques for the Exploration of Medium- and Low-Geothermal Energy Resources

Cristina Sáez Blázquez *, Ignacio Martín Nieto, Javier Carrasco, Pedro Carrasco, Daniel Porras, Miguel Ángel Maté-González, Arturo Farfán Martín and Diego González-Aguilera

Department of Cartographic and Land Engineering, Higher Polytechnic School of Avila, University of Salamanca, Hornos Caleros 50, 05003 Avila, Spain; nachomartin@usal.es (I.M.N.); tgeofisicas@gmail.com (J.C.); retep81@usal.es (P.C.); dporras@geoland.es (D.P.); mategonzalez@usal.es (M.Á.M.-G.); afarfan@usal.es (A.F.M.); daguilera@usal.es (D.G.-A.)
* Correspondence: u107596@usal.es

Abstract: The growth of the geothermal industry demands the constant search of techniques with the aim of reducing exploration efforts whilst minimizing subsurface uncertainty. The exploration of geothermal resources is fundamental from the exploitation point of view, especially in those regions where this energy is not as widespread as the rest of renewable sources. This research shows how geoelectrical methods can contribute to the investigation and characterization of medium–low enthalpy geothermal resources until about 800 m of depth. A 2000 m long electrical-resistivity tomography profile was performed in a region of Southern Spain with previous evidence of moderate geothermal potential. Results of this geophysical campaign (together with a preliminary geological characterization) allowed for the obtainment of a 2D profile and a pseudo-3D model with extensive information about the subsoil in terms of geological composition and formations. The interpretation of geophysical results denotes the existence of a potential formation constituted by carbonate materials with thickness greater than 300 m, crossing different fractures. Once the ideal location for the geothermal exploitation is defined, the research evaluates the contribution of the possible energy source, deducing that the energy extraction in the potential fracturing area would be double that of the one in the vicinity of the site.

Keywords: geothermal resources; exploration; electrical resistivity tomography; 2D profile; potential area

check for updates

Citation: Sáez Blázquez, C.; Martín Nieto, I.; Carrasco, J.; Carrasco, P.; Porras, D.; Maté-González, M.Á.; Farfán Martín, A.; González-Aguilera, D. Applying Deep Electrical-Resistivity Tomography Techniques for the Exploration of Medium- and Low-Geothermal Energy Resources. *Energies* **2024**, *17*, 1836. https://doi.org/10.3390/en17081836

Academic Editor: Hossein Hamidi

Received: 18 March 2024
Revised: 4 April 2024
Accepted: 9 April 2024
Published: 11 April 2024

1. Introduction

Due to the current energy context and the exponential increase of the world energy demand, there is a clear need to move towards the massive use of renewable energy resources and become less dependent on social or geopolitical factors. In fact, the continuous availability of energy is considered one of the most critical aspects for society development, especially considering that, today, a significant portion of energy still derives from burning limited organic fuels. One approach to replace conventional fossil fuels and alleviate the mentioned energy issues is the introduction of renewable energy technologies. In this sense, geothermal energy appears as a potential contributor in the way of reducing the external and internal energy dependence on non-renewable systems [1], constituting one of the most efficient sources that can operate continuously to meet the energy demand 24/7 [2]. This energy can be directly used for heating and/or cooling applications, constituting one of the oldest and most versatile ways of utilizing geothermal resources [3]. In this context, the globally installed capacity for direct geothermal use worldwide was, at the end of 2019, 107,727 MWt, meaning a 52% increase over the year 2015, which is a growing annual rate of 8.7% [4]. The reason for this significant growth is, mainly, the recent technological development of geothermal heat pumps (GHPs), which generally constitute these shallow systems through the well-known ground-source or ground-water heat pump (GSHP-GWHP) technologies [5,6]. The alternative use of geothermal energy is power generation, which is usually attributed to deep and hydrothermal resources with an average growth rate of around 5% per year and a global production of 95 TWh in 2020 in more than 30 countries [7].

Despite the clear versatility of geothermal resources, when compared with other renewable solutions (e.g., biomass, hydro, solar PV, wind), geothermal falls far behind both in production and installed capacity. The principal obstacle to geothermal growth is the initial investment costs generally associated with power projects, but also for domestic heating and cooling solutions. However, numerous countries have done the required groundwork to conduct resource inventories with the aim of quantifying their potential for exploiting the different possibilities of geothermal energy [8,9].

In the particular case of Spain (where this research is focused), geothermal development is still undervalued. There are no high-enthalpy geothermal facilities operating in the country, and the shallow geothermal use is also limited. In this sense, although slower than desirable considering the existing capacity and energy requirements, the installation of GHP systems has been a growing trend in the last few years. In addition, public administrations are making a great effort to introduce GHP systems in public buildings (both in refitted and new spaces) in order to move into the concept of "Nearly Zero-Energy Buildings" (NZEBs) promoted by the European Union [10–13]. Based on the data from the World Geothermal Congresses of 2015 and 2020, the estimated uses for the country are summarized in the following Table 1.

Table 1. Estimated shallow geothermal uses for Spain [14,15].

Use	MWt	TJ/Year
Individual space heating	5.20	133.6
Greenhouse heating	22.0	165.4
Bath and swimming	3.80	92.0
Geothermal heat pumps	513.0	3542.0
Total for the country	**544.0**	**3933.0**

In spite of the clear advantages and the proven capacity to provide energy at a constant pace, as shown in the previous Table 1, the widespread production of geothermal energy in the country considered here has been limited by different factors. Among them are the lack of access to thermal supplies, the operating risks when drilling the geothermal wells, and the associated high capital costs [16,17]. When these factors are analyzed, it is common to conclude that most of these risks are mainly due to the lack of knowledge and precise characterization of the ground where the system is planned. In this sense, the in-depth evaluation of the subsoil structure and the determination of its expected thermal behavior are essential when designing the geothermal well field.

Regarding the reservoir temperature, it can be measured directly by bottom-hole temperature measurements. However, well measurements may not be representative of the entire reservoir, and geophysical prospecting appears as an effective tool for providing a more spatially complete information source. Depending on the type of geothermal system considered, the objective of these tests may be the determination of the geological structures and their distribution in depth, the estimation of the thermal properties of the existing formations, or the location of aquifers or singular structures, among many other applications [18–20]. The implementation of these techniques has proven to be useful when designing a shallow geothermal system and, thus, ensuring its correct operation during the estimated useful life period. But these prospecting systems are also essential when trying to achieve a better understanding of a deep geothermal resource. Geophysical detection and the monitoring of deep reservoirs represent a great advance in the exploration of geothermal energy and, ultimately, in the acquisition of complete and optimized information about the structure in depth and the possibilities of future geothermal exploitation [21,22].

In the context of defining new possibilities of geothermal exploitation, this research includes a deep Electrical-Resistivity Tomography (ERT) model obtained from the geophysical prospecting on a certain study case, with an already known favorable geological setting and thermal evidence. From the geophysical campaign tests, the geological and thermal characterization of the area was performed to finally evaluate the possible geothermal use. Despite the preliminary discovery of anomalous underground temperatures, there is, in the study area, a lack of knowledge about the distribution of the geothermal resource at depth and the viability of its extraction. Based on this, the importance of this research lies in achieving a greater characterization of the underground area, being the final aim of the work is to provide a new basis for possible future geothermal exploitation. In turn, this research pursues to highlight the benefits of geophysics when characterizing the underground to evaluate the proper geothermal exploitation and optimize the configuration of the global well field and the corresponding elements of the system. In this context, the present paper is organized as follows: firstly, information about the geological and geothermal conditions of the study area and the geophysical technique implemented in the prospecting campaign is included. Then, the results of the geophysical tests are presented, as well as the discussion of the main achievements derived from the experimental phase. As a final section, the paper includes the conclusions and future perspectives of applications.

2. Preliminary Study-Area Characterization

2.1. Geology and Structural Setting

As previously mentioned, the objective of this study is the analysis of the subsoil characteristics in order to clarify the possibilities of future deep–medium geothermal energy exploitation. In this context, the study focuses on a certain area located in the autonomous community of Granada (Spain), in which an electrical-resistivity tomography survey has been performed. The following Figure 1 describes the location of the study area selected in the present research.

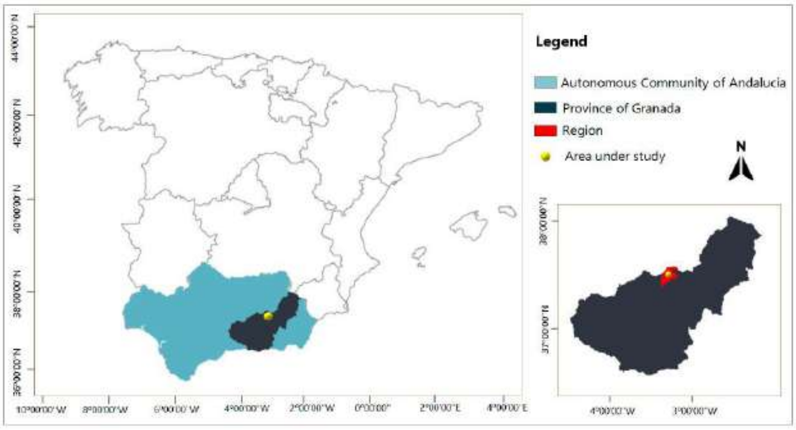

Figure 1. Location of the study area included in the evaluation of this research.

The selection of the location under study is based on the structural and geological characterization that indicated a possible formation of interest from the point of view of energy use. The area under study is located within a series of mountainous alignments to the south of the Guadalquivir Valley, known as the Baetic Mountains and, more specifically, in the region of the "Montes Orientales". The area suffered tectonic phenomena on a continental scale during most of the Mesozoic and Tertiary, related to the opening of the Atlantic and Tethys, as well as the collision of the European and African plates [23,24]. In particular, the area included in this research is located in the sub-Baetic zone, characterized by presenting practically continuous sedimentation between the Triassic and the lower Miocene. Three main domains are established from north to south in this context:

- External sub-Baetic, corresponding to an area in which limestone materials predominate, acquiring great development levels of condensation.
- Medium sub-Baetic, predominating marly materials that appear as characteristic lithologies, radiolarites, and submarine volcanic rocks.
- Internal sub-Baetic that covers a relatively slightly subsiding sector in which exclusively limestone materials outcrop.

Beyond the described sub-Baetic level, Neogene and Quaternary materials are also located in the analysed environs that appear as alluvial deposits. Figure 2 presents the geological levels that constitute the area under study [25].

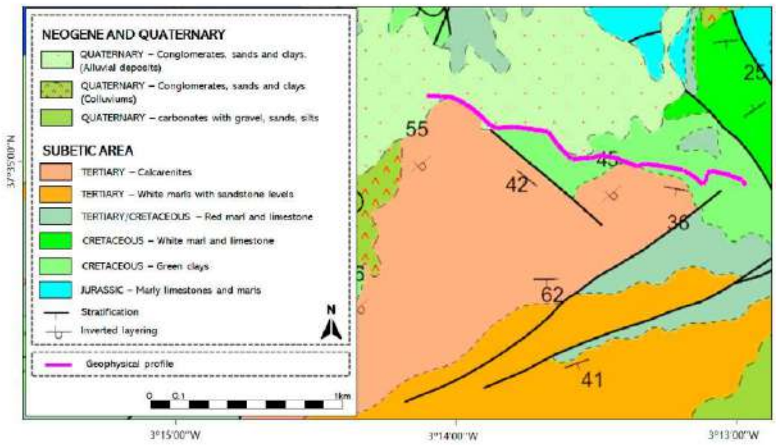

Figure 2. Geological setting of the area in which the geophysical survey was performed.

2.2. *Previous Geothermal Evidences*

In addition to the geological characterization presented above, in the vicinity of the area where the geophysical campaign has been conducted, there is an existing drilling whose open-access information is also relevant to the aim of this study. The 219 m borehole (included in Figure 3) was drilled by percussion with a downhole trephine and allowed for the deduction of the lithological column described in Table 2 [26].

During the prolonged pumping in the drilling, several measurements of the temperature of the extracted water were conducted. It was stabilized at 35.2 °C, which could preliminarily indicate the existence of a low-temperature geothermal resource (placing this temperature above the average of the place by around 15 °C). The interpretation of the borehole tests and the results of the pumping test also allowed for the conclusion that the storage formation has a calculated transmissivity of 600 m^2/day and an estimated exploitation flow of at least 60 L/s, with maximum values around 80–90 L/s.

Figure 3. Arrangement of the ERT profile in the area under study (at the **top**) execution of works in the field (at the **bottom**).

Table 2. Description of the lithological column of the existing borehole located in the study area.

Length	Geological Description
0–170 m	Alternations of light and white colors marls assigned to the middle–lower Cretaceous
170–198 m	Alternation of sandy and marl sections with limestone From the Lower Cretaceous and Upper Jurassic
198–214 m	Marls and white limestones from the Middle Jurassic
214–219 m	Tabled limestone and karstified gray dolomitic limestone

3. Materials and Methods

3.1. Geophysical Surveys-ERT

3.1.1. ERT for Geothermal Characterization Review

Based on the description of the previous Sections 2.1 and 2.2, this research aims to determine the in-depth characterization of the structure and arrangement of the subsoil materials and analyze the lateral continuity of the formation of interest, with special attention to the potential presence of fractures. With these objectives in mind, the geophysical-prospecting campaign has been raised considering the partial knowledge of the ground in the study area and the need to reach sufficient depth levels for the investigation here pursued. From the commented initial statements and, as previously mentioned, the electrical-resistivity tomography technique, it was considered as the potential method for the underground evaluation of this work.

ERT survey is widely implemented for mapping the location of potential areas for groundwater, minerals, or geothermal use [27,28]. In the specific geothermal field, different studies have focused on the delineation of geothermal reservoirs and/or associated structures such as fractures or faults as a preliminary prerequisite for a successful geothermal exploration [29]. In the evaluation of large and known geothermal areas, ERT profiles have proven to be a suitable method for obtaining a high spatial variability, where the potential zone is clearly distinguishable from those with different resistivity [30–32]. In the case of high- and medium-enthalpy geothermal systems, these present great variations in their resistivity/conductivity structure, usually associated with the occurrence of fluids but also with the presence of anomalous concentrations of hydrothermal minerals. The existence of particular fluids, such as saline fluids or meteoric water in rocks, results in enhanced electrical conductivity to a greater or lesser extent, depending on the characteristics of this fluid [33–35]. In these cases, ERT methods are an important source of information, but they also constitute a great help in those surveys where the initial thermal evidence is not so clear, but a possible state of fracturing or structural disposition could indicate the potentiality of geothermal exploitation at different scales. In the case of low- and very-low-enthalpy geothermal resources, these geophysical tools are also extremely valuable for the characterization and distribution of the ground materials and the subsequent design of the well field [18,19].

3.1.2. Fundamentals of the Method and Application on the Study Case

ETR technique provides a subsurface geoelectrical characterization by the measurement of the apparent resistivity from a tetra-electrode device, injecting current of a known intensity into two electrodes called "A" and "B" and automatically recording the potential difference between the other two electrodes "M" and "N". The process is consequently repeated by automatically varying the distances between the pairs of electrodes so that the apparent resistivity is obtained in multiple positions and levels (n). Data are subsequently processed by means of mathematical inversion algorithms, obtaining an image of resistivities and real depths of the subsoil. The depth of investigation is in fact a function of the ability of the material to identify and measure the electric potential between electrodes [36].

The methodology is based on the contrast of resistivities obtained that allows for the differentiation of the subsoil materials based on their electrical behavior; that is, their apparent resistivity value (after the inversion of the field data). However, the subsurface resistivity of a particular area can be affected by different factors such as the porosity and pore structure of the rock formations, the content of water or steam, salinity, pressure, temperature, or any other alteration between water–rock. In this sense, the pore volume, regarding the total rock volume ratio, the geometric arrangement of the pores (formation factor), the ratio of water-filled pores to empty pores, or the resistivity/conductivity of the fluid that is filling the pores [37], is particularly influential.

In the case of the present research, field works consisted of the execution of an electrical tomography profile of 2000 m in length using a hose with 21 electrodes with a separation of 100 m, and a direct and inverse pole–dipole recording device (Figure 3). Data were collected using the commercial equipment Syscal Pro multi-electrode imaging system with an automatic injection range with a 1200 W AC/DC converter. The array configuration was set with the aim of obtaining a strong signal, high-penetration capability, and high-density data. Since the data quality during the ERT acquisition depends on factors such as the noise or the resistivity of materials, the use of a high-power transmitter and an AC/CD converter increases the effective working voltage and contributes to their mitigation. One more influential factor is contact resistance, which is a function of the resistivity of the most superficial layer of the ground. If contact resistances are not allowed, longer and/or multiple linked electrodes are used at the electrode position, and if required, the galvanic contact of electrodes with the ground can be improved by adding a saltwater solution [38]. It is also convenient to mention that the location of each electrode was defined by using a handheld Global Positioning System (GPS) with a horizontal accuracy of 3 m. For the GPS coordinates, ellipsoidal altitudes were also determined since elevation values are required for the subsequent data inversion.

3.1.3. Inversion-Model Approach

Once the ERT raw data on the field (binary) were acquired, these were converted into ASCII format to numerically process the field datasets. For removing the outlier data points, X2IPI software (version 5.19) was used following the criteria of unmeasured intensities of those values lower than 100 mA [39]. In the next step, topography information was assigned to each node, and the apparent resistivity data were inverted using a linearized least-squares algorithm in order to obtain the inverted resistivity models [40].

Finally, RES2DINV software (version 5.0) was implemented for ERT data modeling. The tool is based on a finite element modeling or a difference algorithm capable of providing the forward modeling of the voltage response to the current injection. The models of resistivity developed by the software are then divided into different rectangular blocks with specific resistivity values coming from the field-measuring process. Data of apparent resistivity are finally presented as a pseudo-section, in which the apparent resistivity values are assigned to a predefined location in function of the type of array [41].

The selected inversion procedure was the smoothness-constrained least-squares optimization method, or the smooth L2 norm (function of a damping factor), which allows for the minimization of the sum of squares between the calculated apparent resistivity values and those observed, producing smooth fluctuations in resistivity within the inversion model. The process of inversion begins with the initial model parameters and the damping factors that are refined through an iterative process.

4. Results

4.1. 2D ERT Profile

Figure 4 shows the results obtained in the 2D ERT profile performed in the area under study. The geoelectrical model also includes the synthetic column crossed by the existing drilling together with the distinction of three main geological horizons and the location of the fault's structures in line with the geological characterization established in Section 2.

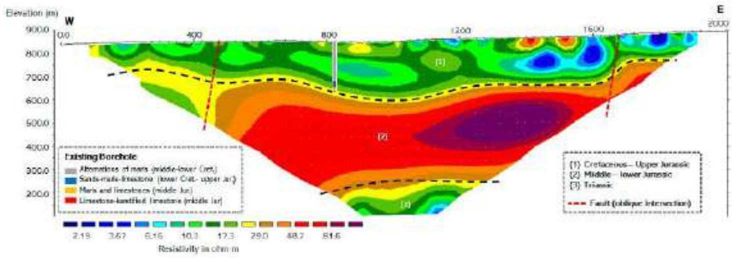

Figure 4. Electrical-resistivity tomography 2D profile in the study area. Length: 2000 m, Interelectrode span: 100 m, Number of electrodes: 21, Dispositive registration: Pole–Dipole, RMS error: 10.3%.

In the 2D model of the above Figure 4, three layers can be distinguished with the following characteristics:

- A first outcropping surface layer (1) of a relatively conductive nature, corresponding to Cretaceous and Upper Jurassic materials mainly constituted by alternations of sandy, limestone, and marly materials. As observed in the 2D profile, Layer (1) presents a more conductive character in the extreme east, indicating the majority presence of clays and marls. Regarding the thickness of the layer, it ranges between 120–250 m.
- An intermediate resistive layer (2), constituted by carbonate materials from the middle and lower Jurassic. This layer has a significant thickness higher than 300 m and presents two main fracture areas (also included in Figure 4):
    - A fracture located around Meter 450 of the 2D profile. The area is defined by the lateral change in resistivity observed in the model that descends at that point in a westerly direction. It should be noted that this fracture context agrees with the fault mapped by the consulted geological database [23], which intersects the trace of the profile at this point, but with a very oblique character.

This factor could influence the resistivity values obtained from the geophysical prospecting campaign.

- A fracture formation appearing approximately at Meter 1700 of the ERT profile, defined by the jump and elevation observed at the top of layer (2), estimated at about 80 m.

- A final conductive basal layer (3), determined by the clear decrease in resistivity, which could indicate the presence of Triassic materials.

In general, the described results indicate that there is an appropriate correlation between the data derived from the existing borehole and the geoelectrical model obtained from geophysics.

4.2. Pseudo-3D ERT Model

In addition to the previous 2D profile, a three-dimensional model has been obtained using Oasis Montaj software (Seequent). Once the profile into the tool is exported, it performs an interpolation of the areas without data from the tomography profile, located in the basal part of the ends. The final product is a 3D geoelectrical model that enables an in-depth analysis of the whole ground distribution [42]. These 3D models are included in the following Figures 5–7 in which it is possible to observe the general structure of the study area in relation to its topography and geological cartography.

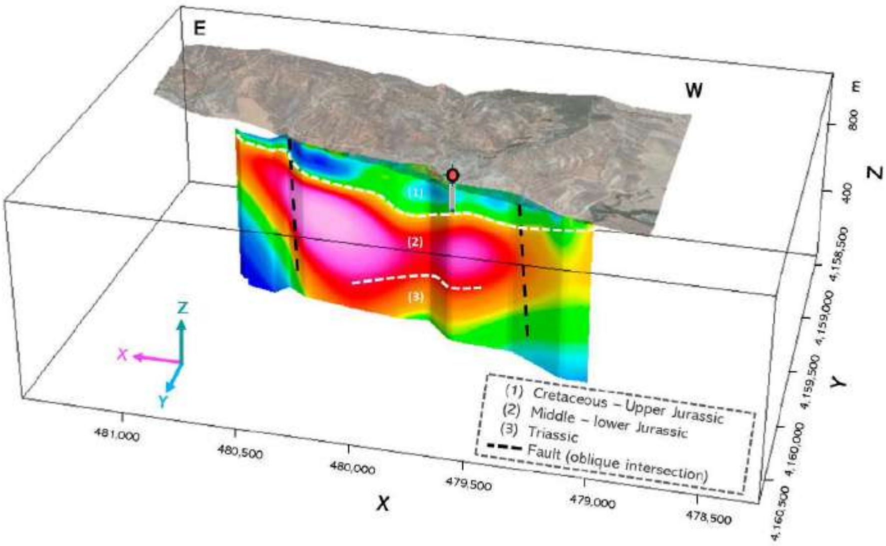

Figure 5. Pseudo 3D model with the digital Terrain Model (DTM) and the orthophoto. View from the north.

The previous Figures 5–7 show the tomography profile obtained from the geophysical campaign (depth information) overlaid with three surface visualization modes: according to the digital model of the terrain and the orthophoto, the single digital terrain model and the digital terrain model together with the geology and family of faults in the area. In all of them, the location of the existing borehole has also been included in order to facilitate the interpretation of the results.

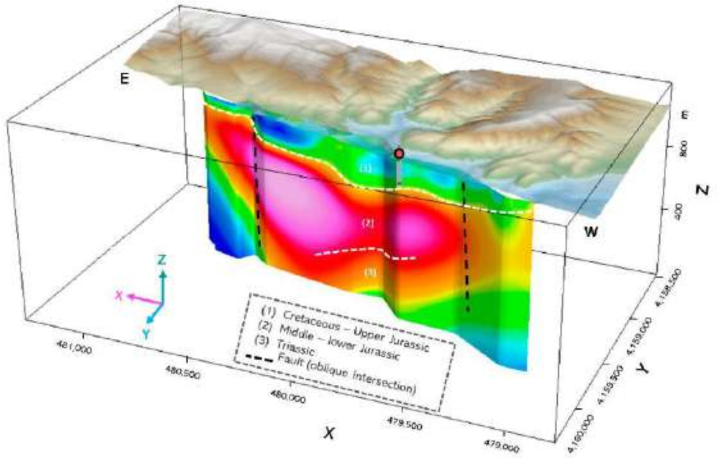

Figure 6. Pseudo-3D model with the Digital Terrain Model (DTM). View from the north.

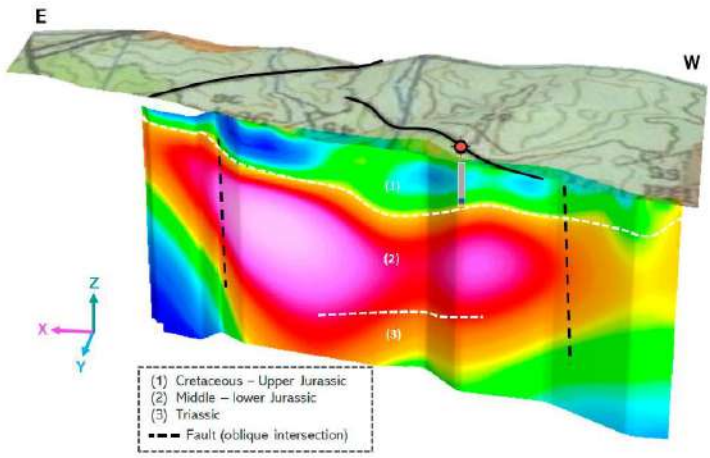

Figure 7. Pseudo-3D model with DTM and geology, highlighting the main mapped faults. View from the north.

5. Discussion

5.1. Model Validation

In certain exploration areas, there is great variability between the geological conditions and the underground distribution. In this sense, the application of geophysics is fundamental for understanding the existing structures and formations in depth. The present research investigates the potential of ERT for the exploration of low–medium enthalpy geothermal resources.

The implementation of an ERT 2000 m long profile has allowed for the penetration of the subsoil up to levels of around 800 m, meaning it is an important source of information about the composition of the materials that make up the subsoil and its distribution in the horizons. The obtained geoelectrical model must represent the subsurface and, at the same time, provide a good fit to the surface geology and lithostratigraphic units based on the existing geological cartography and the known fracture formations and faults.

According to the 1:50,000 scale cartographic layer produced by the IGME (Instituto Geologico y Minero de España) in the area under study, two families of fractures intersect the profile at the eastern and western ends of it. This source of information provides an initial basis for the nature of the characteristic geological formations of the site, which, together with the lithological column known from the borehole existing in the area, represents an important approximation to the characterization of the subsoil. The interpretation of the ERT results agrees with the existing information in the first levels of the ground, also providing additional documentation of how the geological structures are distributed in depth. Through the geophysical campaign, it has been possible to corroborate the arrangement of the fault formations at deeper levels and to characterize the subsoil at greater levels of depth. The results of the survey denote the existence of a potential formation constituted by carbonate materials from the middle and lower Jurassic with a thickness greater than 300 m, which is also crossed by the families of fractures. The set of information provided by the tests and verified by the known structures at more superficial levels makes it possible to accurately plan the most optimal location for possible geothermal exploitation in the analyzed area. The data known from the drilling report of the borehole in the area also confirm (although in much less detail) a significant coincidence in the division of layers in depth.

5.2. Geothermal Exploitation

As commented before, based on the results obtained in the geophysical model, it is possible to establish a preliminary approximation of the most appropriate scenario for future geothermal exploitation. The approach followed here is to evaluate a possible opportunity to semi-directly capture the geothermal flow that is suspected to exist in the underground study area. Due to the limitations of the geophysical techniques (which can only be solved with direct drilling), there is not total certainty about the behavior of the phenomenon, but this section tries to provide a possible exploitation pattern according to the known in-depth information.

Following the geological distribution in the ground, the geothermal drilling should reach the formation (2) of Figures 4–7 in which carbonate materials are present. These layers, characterized in their most superficial part by a certain degree of karstification, constitute a proper environment for the extraction of the required water flow by means of geothermal use. Specifically, the projected borehole should be located at the extreme west of the profile (Figure 8) in the vicinity of the fault structure, and where the formation of interest (2) does not present resistivity values as high as in the case of the existing borehole.

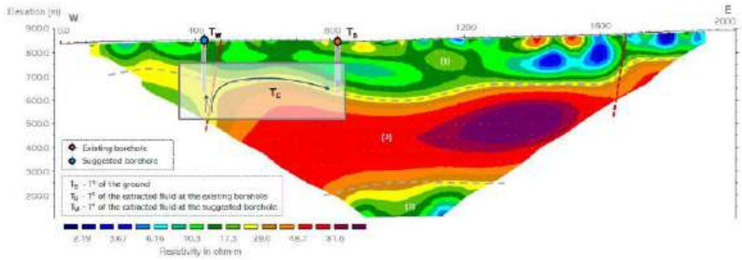

Figure 8. Location of the proposed drilling for possible geothermal exploitation.

Once the potential location for a possible geothermal use is established, an estimation of the temperature of the fluid in the considered area and the possible thermal extraction is presented in this subsection. For this, the probable flow path from the potential area (in the fault) to the existing drilling will be evaluated. Taking into account the geological distribution analyzed in this study, the probable circulation layer should be the one marked in yellow (Figure 8) that communicates the fracture with the lower end of the existing borehole. In this way, and based on the scale of Figure 8, the circulation area is approximately 400 m long and 40 m thick. From this information, and considering the porosity of the limestone formation of the reservoir, the real diameter through which the flow circulates up to the borehole is obtained (D_F of Table 3).

As a second step, it is necessary to define the initial thermal conditions of the site, such as the average temperature of the ground at the depth considered (220 m as the existing drilling). Based on previous studies, the area is not characterized by known significant geothermal anomalies, having a normal geothermal gradient of around 3 °C/100 m and with temperatures within the average values in the original geological environment [43]. The estimated ground temperature at the considered level can be also found in Table 3 as T_G.

Table 3. Principal site and fluid parameters required for the thermal characterization of the site [44].

Main Site Parameters	
Flow diameter (D_F)	3.2 m
Ground Temperature (T_G)	19.5 °C
Temperature of the water borehole (T_B)	35.2 °C
Length of the area (L_A)	400 m
Thickness of the area (T_A)	40 m
Considered depth (D_P)	220 m
Fluid Properties	
Kinematic viscosity (υ)	1×10^{-6} m^2/s
Dynamic viscosity (μ)	1×10^{-3} kg/m·s
Specific heat (c_p)	4184 J/kg·K
Thermal conductivity (k)	0.6 W/m·K

Based on the above information, the heat flux by forced convection can be evaluated, for which different parameters must be defined. The first one is the dimensionless Reynolds number (Re), required to categorize the fluid of the system and to confirm the laminar behavior of the flow (Equation (1)) [45].

$$Re = \frac{V \cdot D_F}{\upsilon} \tag{1}$$

where V is the average flow velocity (m/s).

In the present study case, the flow velocity (V) is estimated according to measurements obtained from the existing borehole, such as the transmissivity of 600 m^2/day already mentioned in Section 2.2 and the analyzed layer thickness (T_A), obtaining a maximum flow velocity of around 15 m/day. Regarding the kinematic viscosity (υ), it is consulted in standard databases for water at the temperature of the medium considered (Table 3) [43]. With all these values, a Reynolds number of 555.56 is obtained, denoting the laminar nature of the fluid in the analysed conditions of the environment.

The following parameters to calculate are the Prandtl number (Pr), which expresses a dimensionless quantity for assessing the relation between momentum transport and thermal transport capacity of the fluid, and the Nusselt number (Nu) that is basically a function of Re and Pr numbers. Both numbers are defined in Equations (2) and (3) [45].

$$Pr = \frac{\mu \cdot C_p}{k} \tag{2}$$

$$Nu = 3.66 + \frac{0.065 \cdot \left(\frac{D_F}{L_A}\right) \cdot Re \cdot Pr}{1 + 0.04 \cdot \left[\left(\frac{D_F}{L_A}\right) \cdot Re \cdot Pr\right]^{2/3}} \quad (3)$$

Considering again the standard values of μ, c_p, and k for the fluid at the analyzed conditions (Table 3) [46], Pr and the Nu numbers are estimated as 6.97 and 5.26, respectively. It is convenient to mention that Equation (3) provides an approximation to the calculation of Nu, considering that the value obtained is greater than 3.66 as the one here presented.

Once defined, the previous parameters, the thermal convection coefficient (h) (W/m^2·K) for forced convection, is expressed as follows (Equation (4)).

$$h = \frac{k}{D_F} \cdot Nu \quad (4)$$

Substituting the corresponding values, the convection coefficient h for the study conditions is 0.99 W/m^2·K. Convective heat transfer occurs from the moving of the fluid through the considered formation, according to what is known as Newton's Law of Cooling. In this way, from the calculated convection coefficient, the temperature of the water (T_W) in the suggested location of the fracture can be calculated by applying Equation (5) [47].

$$T_W = T_{G-} \left[\frac{T_G - T_B}{e^{-\frac{h \cdot A_s}{\dot{m} \cdot c_p}}} \right] \quad (5)$$

where A_s (m^2) is the area through which the fluid circulates in the formation and $\dot{m}$ (kg/s) is the mass flow rate.

Considering the geometry of the formation, as well as the density and the estimated velocity of the fluid, A_s and $\dot{m}$ can be directly obtained, being the values 3516.80 m^2 and 1.40 kg/s, respectively. Finally, applying the previous Equation (5), the water temperature in the area suggested in this study could reach the value of 48.89 °C.

On top of the above, the specific energy (E) that the increase in temperature supposes in both conditions (in the existing drilling and in the suggested one) is calculated applying the following equation.

$$E = c_p \cdot \Delta T \cdot m \quad (6)$$

where m (kg/h) is the mass of the circulating fluid, which can be calculated from the estimated flow in the existing drilling (at least 60 L/s) that, considering the density of the fluid, is means 216,000 kg/h. ΔT (°C) is the temperature increase between the ground and the temperature of the water in each assumption. These values, and the final result of applying Equation (6), are included in Table 4.

Table 4. Increase in temperature and specific energy achieved in each of the considered scenarios.

Scenario	ΔT (°C)	E (J)	E (th)
Existing drilling	15.70	1.42×10^{10}	3388.93
Suggested drilling	29.39	2.66×10^{10}	6343.99

From the previous values of Table 4, it is easily observable how the extraction of water in the area suggested in the present research supposes an increase in temperature of almost double that currently achieved in the existing borehole of the area. All this also means doubling the specific energy of the site and denoting the presence of a relevant geothermal resource of significant importance for its future use.

In relation to the previous calculations of the upwelling temperature, it should be clarified that this is one of the possible scenarios regarding the origin of the thermal anomaly measured in the well. For a deeper characterization of the resource, it would be necessary to take into account possible deviations in the geometry and properties of the geological structure that constitute the aquifer (error of the inversion process of geophysical data), or possible thermal contributions not considered in the direction of the flow prior to the emerging fracture.

6. Conclusions

In different regions of Spain, the lack of precise information on the resource and its possibilities of exploitation constitute a barrier preventing geothermal energy from making a greater contribution to meeting energy demand at present. The present study applies deep electrical-resistivity tomography to characterize a possible geothermal site. The information about the subsoil obtained from the resistivity data is in agreement with the geological structures known from the existing borehole located in the vicinity of the studied area. Beyond this contribution, the geophysical campaign has allowed to know the distribution of the geological formations and structures at greater depth and define the ideal location for better geothermal resource exploitation. In this way, and by locating the possible energy source in depth through the structuring in the form of a fault, the extraction of water in the proposed area allows us to achieve an estimated temperature of 48 °C with an energy use of practically double the current extraction in the existing borehole.

Based on all that has been evaluated in this investigation, future geothermal exploitation initiatives in the study area will be precisely planned, minimizing the possibilities of error and facilitating the corresponding exploration and implementation tasks linked to the geothermal-extraction system. Regarding future research, and since it is a promising area, it would be interesting to address the analysis of the formations that give rise to thermal anomalies on the surface through the use of more extensive geophysical techniques. In this sense, the application of the magnetotelluric method could be advisable to image the subsurface electrical resistivity and provide (by the use of the Earth's naturally occurring electromagnetic fields) useful information about the lateral and vertical resistivity variation. The investigation depth of this technique can reach several tens of kilometers in function on rock resistivity, making it a technology of great value to be applied in areas such as the one evaluated in this research, making it also possible to determine with greater precision the scope of the resource and its possibilities of use as a medium or a high-enthalpy geothermal system.

Author Contributions: Conceptualization, C.S.B. and I.M.N.; methodology, C.S.B.; software, P.C. and J.C.; validation, A.F.M. and D.G.-A.; formal analysis, C.S.B., I.M.N. and M.Á.M.-G.; investigation, C.S.B.; resources, P.C., D.P. and J.C.; data curation, P.C., D.P. and J.C.; writing—original draft preparation, C.S.B.; writing—review and editing, C.S.B.; visualization, M.Á.M.-G.; supervision, A.F.M. and D.G.-A.; project administration, C.S.B.; funding acquisition, A.F.M., C.S.B. and M.Á.M.-G. All authors have read and agreed to the published version of the manuscript.

Funding: This research was supported by the research projects support program and cofinanced by the European Regional Development Fund (ERDF) under the order of the Ministry of Education from Castilla y León (project ref.: SA102P20). "Development and integration of a new district heating system using low-energy geothermal energy (GEO-DISTRICT 3.0)" and the European Union's Horizon 2020 research and innovation programme under grant agreement nº 101091885 (Mine.io project). M.Á.M.-G. and C.S.B. acknowledge the grant RYC2021-034813-I and RYC2021-034720-I, respectively, funded by MCIN/AEI/10.13039/501100011033 and by European Union "NextGenerationEU"/PRTR.

Data Availability Statement: Data will be available when required.

Acknowledgments: Authors would also like to thank the Department of Cartographic and Land Engineering of the Higher Polytechnic School of Avila, University of Salamanca for allowing us to use their facilities and their collaboration during the experimental phase of this research.

Conflicts of Interest: The authors declare no conflicts of interest.

Nomenclature

Acronyms

GHP	Geothermal Heat Pump
GSHP	Ground-Source Heat Pump
GWHP	Ground-Water Heat Pump
NZEB	Nearly Zero-Energy Building
ERT	Electrical-Resistivity Tomography
GPS	Global Positioning System
IGME	Instituto Geológico y Minero de España
D_F	Flow diameter
T_G	Ground Temperature
T_B	Temperature of the water borehole
T_W	Temperature of the water
L_A	Length of the area
T_A	Thickness of the area
D_P	Considered depth
υ	Kinematic viscosity
v	Flow velocity
μ	Dynamic viscosity
c_P	Specific heat
k	Thermal conductivity
Re	Reynolds number
Pr	Prandtl number
Nu	Nusselt number
h	Thermal convection coefficient
A_s	Area of circulation of the fluid in the formation
$\dot{m}$	Mass flow rate
E	Specific energy
m	Mass of the circulating fluid

References

1. Fridleifsson, I.B. Geothermal energy for the benefit of the people. *Renew. Sustain. Energy Rev.* **2001**, *5*, 299–312. [CrossRef]
2. García-Gil, A.; Goetzl, G.; Kłonowski, M.R.; Borovic, S.; Boon, D.P.; Abesser, C.; Janza, M.; Herms, I.; Petitclerc, E.; Erlström, M.; et al. Governance of shallow geothermal energy resources. *Energy Policy* **2020**, *138*, 111283. [CrossRef]
3. Dickson, M.H.; Fanelli, M. *Geothermal Energy: Utilization and Technology*; Routledge: London, UK, 2013; ISBN 978-1-84407-184-5.
4. Lund, J.W.; Toth, A.N. Direct utilization of geothermal energy 2020 worldwide review. *Geothermics* **2021**, *90*, 101915. [CrossRef]
5. Sáez Blázquez, C.; Martín Nieto, I.; Farfán Martín, A.; González-Aguilera, D.; Carrasco García, P. Comparative analysis of different methodologies used to estimate the ground thermal conductivity in low enthalpy geothermal systems. *Energies* **2019**, *12*, 1672. [CrossRef]
6. Limberger, J.; Boxem, T.; Pluymaekers, M.; Bruhn, D.; Manzella, A.; Calcagno, P.; Beekman, F.; Cloetingh, S.; van Wees, J.-D. Geothermal energy in deep aquifers: A global assessment of the resource base for direct heat utilization. *Renew. Sustain. Energy Rev.* **2018**, *82*, 961–975. [CrossRef]
7. Rybach, L. Global Status, Development and Prospects of Shallow and Deep Geothermal Energy. *Int. J. Terr. Heat Flow Appl. Geotherm.* **2022**, *5*, 20–25. [CrossRef]
8. Lund, J.W.; Huttrer, G.W.; Toth, A.N. Characteristics and trends in geothermal development and use, 1995 to 2020. *Geothermics* **2022**, *105*, 102522. [CrossRef]
9. Blázquez, C.S.; Borge-Diez, D.; Nieto, I.M.; Martín, A.F.; González-Aguilera, D. Multi-parametric evaluation of electrical, biogas and natural gas geothermal source heat pumps. *Renew. Energy* **2021**, *163*, 1682–1691. [CrossRef]
10. D'Agostino, D.; Mazzarella, L. What is a Nearly zero energy building? Overview, implementation and comparison of definitions. *J. Build. Eng.* **2019**, *21*, 200–212. [CrossRef]
11. Blázquez, C.S.; Borge-Diez, D.; Nieto, I.M.; Martín, A.F.; González-Aguilera, D. Technical optimization of the energy supply in geothermal heat pumps. *Geothermics* **2019**, *81*, 133–142. [CrossRef]
12. Magrini, A.; Lentini, G.; Cuman, S.; Bodrato, A.; Marenco, L. From nearly zero energy buildings (NZEB) to positive energy buildings (PEB): The next challenge-The most recent European trends with some notes on the energy analysis of a forerunner PEB example. *Dev. Built Environ.* **2020**, *3*, 100019. [CrossRef]
13. Sorman, A.H.; García-Muros, X.; Pizarro-Irizar, C.; González-Eguino, M. Lost (and found) in Transition: Expert stakeholder insights on low-carbon energy transitions in Spain. *Energy Res. Soc. Sci.* **2020**, *64*, 101414. [CrossRef]

14. Arrizabalaga, I.; De Gregorio, M.; De Santiago, C.; García de la Noceda, C.; Pérez, P.; Urchueguía, J.F. Country update for the Spanish geothermal sector. In Proceedings of the World Geothermal Congress, Melbourne, Australia, 19–24 April 2015; pp. 19–24.
15. Arrizabalaga, I.; De Gregorio, M.; De Santiago, C.; García de la Noceda, C.; Pérez, P.; Urchueguía, J.F. Country update for the Spanish geothermal sector. In Proceedings of the World Geothermal Congress, Reykjavik, Iceland, 27 April–1 May 2020; p. 12.
16. Vivas, C.; Salehi, S.; Tuttle, J.D.; Rickard, B. Challenges and opportunities of geothermal drilling for renewable energy generation. *GRC Trans.* **2020**, *44*, 904–918.
17. Anderson, A.; Rezaie, B. Geothermal technology: Trends and potential role in a sustainable future. *Appl. Energy* **2019**, *248*, 18–34. [CrossRef]
18. Blázquez, C.S.; Nieto, I.M.; González, M.Á.M.; García, P.C.; Martín, A.F.; González-Aguilera, D. Geophysical exploration for shallow geothermal applications: A case study in Artà, (Balearic Islands, Spain). *Geothermics* **2022**, *105*, 102517. [CrossRef]
19. Sáez Blázquez, C.; Carrasco García, P.; Nieto, I.M.; Maté-González, M.Á.; Martín, A.F.; González-Aguilera, D. Characterizing geological heterogeneities for geothermal purposes through combined geophysical prospecting methods. *Remote Sens.* **2020**, *12*, 1948. [CrossRef]
20. Carrier, A.; Fischanger, F.; Gance, J.; Cocchiararo, G.; Morelli, G.; Lupi, M. Deep electrical resistivity tomography for the prospection of low-to medium-enthalpy geothermal resources. *Geophys. J. Int.* **2019**, *219*, 2056–2072. [CrossRef]
21. Nieto, I.M.; Carrasco García, P.; Sáez Blázquez, C.; Farfán Martín, A.; González-Aguilera, D.; Carrasco García, J. Geophysical prospecting for geothermal resources in the south of the Duero Basin (Spain). *Energies* **2020**, *13*, 5397. [CrossRef]
22. Ismail, N.; Syukri, M.; Idroes, R. Deep and shallow structures of geothermal Seulawah Agam based on electromagnetic and magnetic data. *Geomate J.* **2019**, *16*, 141–147. [CrossRef]
23. Mohamed, M.A.; Pajares, A.J.M.; Moreno, J.L.; Herrador, M.B.; Álvarez, F.P.; Reyes, J.M.G. Phylogenetic relationships of "Erysimum"(Brassicaceae) from the Baetic Mountains (SE Iberian Peninsula). In *Anales del Jardín Botánico de Madrid*; Real Jardín Botánico: Madrid, Spain, 2014; Volume 71, p. 5. [CrossRef]
24. Sala, M. Baetic Cordillera and Guadalquivir Basin. In *Geomorphology of Europe*; Palgrave: London, UK, 1984; pp. 323–340. [CrossRef]
25. Albir, A.E.; López Olmedo, F.L.; Díaz de Neira, J.A. Mapa y memoria explicativa de la Hoja 970, El Rubio. MAGNA. IGME. 1981.
26. Guzmán, S.J. *Sondeo de Agua Minero Industrial de Origen Termal "Alamedilla 1" Capacity Report*; Junta de Andalucía: Andalusia, Spain, 2015.
27. Lévy, L.; Maurya, P.K.; Byrdina, S.; Vandemeulebrouck, J.; Sigmundsson, F.; Árnason, K.; Ricci, T.; Deldicque, D.; Roger, M.; Gibert, B.; et al. Electrical resistivity tomography and time-domain induced polarization field investigations of geothermal areas at Krafla, Iceland: Comparison to borehole and laboratory frequency-domain electrical observations. *Geophys. J. Int.* **2019**, *218*, 1469–1489. [CrossRef]
28. Singh, S.; Gautam, P.K.; Bagchi, D.; Singh, S.; Kumar, S.; Kannaujiya, S. 2D electrical resistivity imaging for geothermal groundwater characterization and rejuvenation of the Gaurikund hot spring in the Main Central Thrust (MCT) zone of the Garhwal Himalaya, Uttrakhand, India. *Groundw. Sustain. Dev.* **2021**, *15*, 100686. [CrossRef]
29. Kumar, D.; Thiagarajan, S.; Rai, S.N. Deciphering geothermal resources in Deccan Trap region using electrical resistivity tomography technique. *J. Geol. Soc. India* **2011**, *78*, 541–548. [CrossRef]
30. Vanhooren, L.; Fontaine, O.; Caudron, C.; Vrancken, E.; Dekoninck, W.; De Lathauwer, H.; Hermans, T. *Characterization and Monitoring of the Gunnuhver Geothermal Site Using Electrical Methods (No. EGU23-12873)*; Copernicus Meetings; EGU: Vienna, Austria, 2023. [CrossRef]
31. Cheng, Y.; Wang, C.; Da, W.; Kong, Y.; Hu, X. Anatomy of the convective geothermal system from geophysical and hydrochemical data: A case study from the Changshou geothermal field, South China. *Geophysics* **2023**, *88*, 1–43. [CrossRef]
32. Ussher, G.; Harvey, C.; Johnstone, R.; Anderson, E. Understanding the resistivities observed in geothermal systems. In Proceedings of the World Geothermal Congress, Kyushu, Japan, 28 May–10 June 2000; pp. 1915–1920.
33. Marwan, M.; Isa, M.; Idroes, R.; Nursyafira, N.; Idris, S.; Yanis, M.; Ghani, A.A.; Paembonan, A.Y. Geoelectrical Model of Geothermal Spring in ie Jue Seulawah Deriving from 2D Vlf-Em and dc Resistivity Methods. *J. Appl. Eng. Sci.* **2023**, *21*, 59–69. [CrossRef]
34. Abdullah, A.I.; Musa, M.D.T.; Uno, I.; Jayadi, H. Resistivity model of hallow subsurface to find the path of geothermal manifestation in Bora Village of Sigi Regency of Central Sulawesi. *J. Phys. Conf. Ser.* **2019**, *1242*, 012048. [CrossRef]
35. Cumming, W.; Mackie, R. Resistivity imaging of geothermal resources using 1D, 2D and 3D MT inversion and TDEM static shift correction illustrated by a Glass Mountain case history. In Proceedings of the World Geothermal Congress, Bali, Indonasia, 25–30 April 2010; pp. 25–29.
36. Arjwech, R.; Everett, M.E. Application of 2D electrical resistivity tomography to engineering projects: Three case studies. *Songklanakarin J. Sci. Technol.* **2015**, *37*, 675–681.
37. Zhou, B.; Bouzidi, Y.; Ullah, S.; Asim, M. A full-range gradient survey for 2D electrical resistivity tomography. *Near Surf. Geophys.* **2020**, *18*, 609–626. [CrossRef]
38. Carrasco García, P. Avance en Técnicas Geofísicas Para la Caracterización del Subsuelo Mediante Innovación y el Uso de Herramientas de Gestión de Información Espacial. Ph.D. Thesis, Escuela Politécnica Superior de Ávila, Univ de Salamanca, Ávila, Spain, 2013; p. 523.
39. Robain, H.; Bobachev, A. X2IPI Toolbox for 2D DC measurements with SYSCAL equipment. *User manual*, 2002; 25p.

40. Loke, M.H.; Dahlin, T. A comparison of the Gauss–Newton and quasi-Newton methods in resistivity imaging inversion. *J. Appl. Geophys.* **2002**, *49*, 149–162. [CrossRef]
41. Telford, W.M.; Telford, W.M.; Geldart, L.P.; Sheriff, R.E. *Applied Geophysics*; Cambridge University Press: Cambridge, UK, 1990; ISBN 1139642928/9781139642927.
42. Arifin, M.H.; Kayode, J.S.; Ismail, K.I.; Abdullah, M.; Embrandiri, A.; Nazer, S.M.; Azmi, A. Data for the industrial and municipal environmental wastes hazard contaminants assessment with integration of RES2D techniques and Oasis Montaj software. *Data Brief* **2020**, *33*, 106595. [CrossRef]
43. Galindo-Zaldívar, J.; Jabaloy, A.; Serrano, I.; Morales, J.; González-Lodeiro, F.; Torcal, F. Recent and present-day stresses in the Granada Basin (Betic Cordilleras): Example of a late Miocene-present-day extensional basin in a convergent plate boundary. *Tectonics* **1999**, *18*, 686–702. [CrossRef]
44. Mao, Y.; Zhang, Y. Thermal conductivity, shear viscosity and specific heat of rigid water models. *Chem. Phys. Lett.* **2012**, *542*, 37–41. [CrossRef]
45. Abraham, J.P.; Sparrow, E.M.; Tong, J.C.K. Heat transfer in all pipe flow regimes: Laminar, transitional/intermittent, and turbulent. *Int. J. Heat Mass Transf.* **2009**, *52*, 557–563. [CrossRef]
46. Crittenden, J.C.; Trussell, R.R.; Hand, D.W.; Howe, K.J.; Tchobanoglous, G. *MWH's Water Treatment: Principles and Design*, 3rd ed.; John Wiley & Sons: Hoboken, NJ, USA, 1861; ISBN 978-0-470-40593-0.
47. Domenico, P.A.; Palciauskas, V.V. Theoretical analysis of forced convective heat transfer in regional ground-water flow. *Geol. Soc. Am. Bull.* **1973**, *84*, 3803–3814. [CrossRef]

CAPÍTULO 3
CONCLUSIONES Y LÍNEAS FUTURAS

3 Conclusiones y líneas futuras

En este apartado se presentan las conclusiones principales derivadas de los trabajos de investigación expuestos en las secciones anteriores, junto con una propuesta de posibles líneas de investigación futuras que podrían ampliar y complementar el trabajo realizado hasta la fecha.

3.1. Conclusiones

Las principales conclusiones obtenidas en los diferentes trabajos de investigación presentados en esta tesis doctoral:

- Se ha confirmado que las técnicas geofísicas asociadas a programas de gestión de información geoespacial forman una potente herramienta, económica y no intrusiva, para la delimitación y gestión de recursos hidrogeológicos e hidrogeotérmicos.
- Se ha evidenciado que la combinación de métodos geofísicos, ofrece una visión integral y detallada de las formaciones geológicas y acuíferas. Esta integración permite una identificación más precisa de zonas estratégicas para la explotación de acuíferos y mejora la precisión en la planificación de perforaciones.
- La utilización de drones equipados con magnetómetros ha demostrado ser una herramienta eficaz para la cartografía espacial rápida y detallada de áreas de difícil acceso. Esto no solo facilita la identificación de unidades litológicas, sino que también optimiza los recursos y el tiempo invertido en la exploración hidrogeofísica.
- Las investigaciones geofísicas realizadas han permitido desarrollar formas de monitorear las variaciones estacionales de la salinidad del agua subterráneas, proporcionando información crucial sobre la interacción entre aguas subterráneas y superficiales. Este conocimiento es esencial para la gestión sostenible de los recursos hídricos en áreas con variaciones climáticas significativas.
- Las investigaciones llevadas a cabo han resaltado la importancia de los humedales como sistemas de recarga y almacenamiento de agua subterránea. Los estudios han mostrado que estos humedales, alimentados por aguas subterráneas y precipitaciones, desempeñan un papel crucial en la regulación del nivel freático y la calidad del agua.
- Se ha demostrado que la aplicación de técnicas como la tomografía eléctrica permite la identificación de recursos hidrogeotérmicos de media y baja entalpía. Los resultados han proporcionado modelos detallados del subsuelo, identificando formaciones carbonatadas y fracturadas que indican un alto potencial para la explotación hidrogeotérmica.

3.2. Líneas futuras

La presente Tesis Doctoral ha brindado la oportunidad de identificar diversas estructuras hidrogeológicas en diferentes formas, las cuales tienen potencial para ser ampliadas y perfeccionadas. Además, se ha planteado la posibilidad de investigar otras estructuras que aún no han sido exploradas, lo que podría ser el punto de partida para futuras investigaciones. En este contexto, se anticipa abordar las siguientes cuestiones en el futuro:

- **Estudios que alcancen mayor profundidad para la resolución de problemas actuales en acuíferos a grandes profundidades:** La realización de investigaciones más exhaustivas y detalladas es crucial para abordar los desafíos actuales en la gestión de acuíferos profundos. Se recomienda explorar técnicas avanzadas y metodologías innovadoras que no han sido empleadas en los estudios previos de esta tesis. Esto podría incluir la implementación de métodos geofísicos de alta resolución, el uso de tecnologías de perforación más avanzadas y la aplicación de modelos hidrogeológicos que proporcionen una visión más precisa y completa de los sistemas acuíferos a gran profundidad, como por ejemplo el método magnetotelúrico.

- **Aplicación de métodos en otros enclaves no descritos para su aportación a la comunidad científica:** Es fundamental ampliar el ámbito de estudio a otras regiones geográficas y tipos de acuíferos que no han sido abordados en esta tesis. La aplicación de los métodos desarrollados y probados en este trabajo en nuevos enclaves permitirá validar su eficacia y adaptar las técnicas a diferentes contextos hidrogeológicos. Esta expansión contribuirá significativamente al cuerpo de conocimiento científico, ofreciendo nuevas perspectivas y soluciones a problemas hidrogeológicos en diversas áreas.

- **Aplicación de métodos aerotransportados para mejorar la eficiencia en zonas de difícil acceso:** La utilización de tecnologías aerotransportadas, como drones equipados con sensores geofísicos, puede mejorar en gran medida la forma en que se realizan estudios hidrogeológicos. Estos métodos permiten realizar trabajos de campo de manera más eficiente y con mayor rapidez, especialmente en áreas de difícil acceso. Además, pueden ser igualmente efectivos en zonas más accesibles, optimizando los recursos y reduciendo los tiempos de trabajo. La implementación de estas tecnologías puede facilitar la recolección de datos de alta calidad y su análisis en tiempo real, mejorando así la eficiencia y precisión de los estudios.

- **Aplicación de futuros softwares para mejorar la representación de resultados y el tratamiento de datos:** El desarrollo y aplicación de software avanzado en el campo de la geofísica pueden proporcionar mejoras significativas en la visualización y análisis de datos. Herramientas de modelado y simulación más sofisticadas, junto con algoritmos de procesamiento de datos más eficientes, permitirán una interpretación más precisa y detallada de los resultados. La integración de inteligencia artificial y aprendizaje automático en estos softwares puede ofrecer nuevas capacidades para identificar patrones y tendencias en los datos hidrogeológicos, facilitando así la toma de decisiones informadas.

- **Ampliación de los resultados indirectos con resultados directos para una mayor comprensión hidrogeológica:** Es esencial complementar los datos obtenidos mediante métodos indirectos (como las técnicas geofísicas) con datos directos (como muestras de agua y análisis químicos). Este enfoque integrado proporcionará una comprensión más completa y precisa de los sistemas acuíferos. Los estudios combinados permiten validar y calibrar los modelos hidrogeológicos, ofreciendo una visión más holística del comportamiento de los acuíferos y sus interacciones con el entorno. La incorporación de resultados directos mejorará la confiabilidad de las predicciones y la efectividad de las estrategias de gestión de los recursos hídricos subterráneos.

CAPÍTULO 4
REFERENCIAS

Drone Magnetic and Time Domain Electromagnetic Exploration in Metamorphic Formations: Tool for the Identification of Strategic Sites for Aquifer Exploitation

D'Odorico, P.; Chicarelli, D.D.; Rosa, L.; Bini, A.; Zilberman, D.; Rulli, M.C. The global value of water in agriculture. Proc. Natl. Acad. Sci. USA 2020, 117, 21985–21993

Basso, B.; Kendall, A.D.; Hyndman, D.W. The future of agriculture over the Ogallala Aquifer: Solutions to grow crops more efficiently with limited water. Earth's Future 2013, 1, 39–41. Appl. Sci. 2023, 13, 10949 15 of 16

Smidt, S.J.; Haacker, E.M.K.; Kendall, A.D.; Deines, J.M.; Pei, L.; Cotterman, K.A.; Li, H.; Liu, X.; Basso, B.; Hyndman, D.W. Complex water management in modern agriculture: Trends in the water-energy-food nexus over the High Plains Aquifer. Sci. Total Environ. 2016, 566–567, 988–1001.

Othman, A.; Sultan, M.; Becker, R.; Alsefry, S.; Alharbi, T.; Gebremichael, E.; Alharbi, H.; Abdelmohsen, K. Use of Geophysical and Remote Sensing Data for Assessment of Aquifer Depletion and Related Land Deformation. Surv. Geophys. 2018, 39, 543–566.

Calderón Palma, H.; Bentley, L.R. A regional-scale groundwater flow model for the Leon-Chinandega aquifer, Nicaragua. Hydrogeol. J. 2007, 15, 1457–1472.

Rad, M.R.; Brozovic, N.; Foster, T.; Mieno, T. Effects of instantaneous groundwater availability on irrigated agriculture and implications for aquifer management. Resour. Energy Econ. 2020, 59, 101129.

Ofterdinger, U.; MacDonald, A.M.; Comte, J.C.; Young, M.E. Groundwater in fractured bedrock environments: Managing catchment and subsurface resources- an introduction. Geol. Soc. Lond. Spec. Publ. 2019, 479, 1–9.

Font Capó, J.; Vázquez Suñe, E.; Carrera, J.; Herms, I. Groundwater characterization of a heterogenous granitic rock massif for shallow tunneling. Geol. Acta Int. Earth Sci. J. 2012, 10, 395–408. Available online: https://dialnet.unirioja.es/servlet/articulo?codigo=4138023 (accessed on 17 August 2023).

Gobashy, M.M.; Metwally, A.M.; Abdelazeem, M.; Soliman, K.S.; Abdelhalim, A. Geophysical Exploration of Shallow Groundwater Aquifers in Arid Regions: A Case Study of Siwa Oasis, Egypt. Nat. Resour. Res. 2021, 30, 3355–3384.

Nabighian, M.N.; Grauch, V.J.S.; Hansen, R.O.; LaFehr, T.R.; Li, Y.; Peirce, J.W.; Phillips, J.D.; Ruder, M.E. The historical development of the magnetic method in exploration. Geophysics 2005, 70, 33–61.

IGME MAGNA. Geological and Mining Institute of Spain (IGME). Hoja de Usagre (855). In Mapa Geológico de España (E. 1:50.000); Servicio de Publicaciones del Ministerio de Industria y Energía: Madrid, Spain, 1981.

BD Puntos de Agua v2.0 IGME. Available online: https://info.igme.es/BDAguas/ (accessed on 19 August 2023).

Hernandez-Lopez, D.; Felipe-Garcia, B.; Gonzalez-Aguilera, D.; Arias-Perez, B. An automatic approach to UAV flight planning and control for photogrammetric applications. Am. Soc. Photogramm. Remote Sens. 2013, 1, 87–98.

Elwaheidi, M. Geophysical Imaging of a Buried Tertiary Valley Aquifer in an Arid Region Using Time Domain Electromagnetic Method. J. Geosci. Environ. 2020, 8, 195–206.

Hamada, L.R.; Porsani, J.L.; Bortolozo, C.A.; Rangel, R.C. TDEM and VES soundings applied to a hydrogeological study in the central region of the Taubaté Basin, Brazil. First Break 2018, 36, 49–54.

Cunningham, M.; Samson, C.;Wood, A.; Cook, I. Aeromagnetic Surveying with a Rotary-Wing Unmanned Aircraft System: A Case Study from a Zinc Deposit in Nash Creek, New Brunswick, Canada. Pure Appl. Geophys. 2018, 175, 3145–3158.

Walter, C.A.; Braun, A.; Fotopoulos, G. Impact of three-dimensional attitude variations of an unmanned aerial vehicle magnetometry system on magnetic data quality. Geophys. Prospect. 2019, 67, 465–479.

Mu, Y.; Chen, L.; Xiao, Y. Small Signal Magnetic Compensation Method for UAV-Borne Vector Magnetometer System. IEEE Trans. Instrum. Meas. 2023, 72, 1–7.

Walter, C.A.; Braun, A.; Fotopoulos, G. High-resolution unmanned aerial vehicle aeromagnetic surveys for mineral exploration targets. Geophys. Prospect. 2020, 68, 334–349.

Zheng, Y.; Li, S.; Xing, K.; Zhang, X. Unmanned Aerial Vehicles for Magnetic Surveys: A Review on Platform Selection and Interference Suppression. Drones 2021, 5, 93.

Huerta, P.; Carrasco-García, P.; Armenteros, I.; Recio, C.; Carrasco-García, J.; Rodríguez-Jiménez, E. TDEM Soundings as a Tool to Determine Seasonal Variations of Groundwater Salinity (Villafáfila Lakes, Spain). Water 2022, 14, 2402.

Nieto, I.M.; Carrasco García, P.; Sáez Blázquez, C.; Farfán Martín, A.; González-Aguilera, D.; Carrasco García, J. Geophysical Prospecting for Geothermal Resources in the South of the Duero Basin (Spain). Energies 2020, 13, 5397.

Sheriff, R.E. Geophysical Methods, 1st ed.; Prentice Hall: Englewood Cliffs, NJ, USA, 1989.

Porras, D.; Carrasco, J.; Carrasco, P.; Alfageme, S.; Gonzalez-Aguilera, D.; Lopez Guijarro, R. Drone Magnetometry in Mining Research. An Application in the Study of Triassic Cu-Co-Ni Mineralizations in the Estancias Mountain Range, Almería (Spain). Drones 2021, 5, 151.

Carrasco-García, J.; Porras-Sanchiz, D.; Carrasco-García, P.; Herrero-Pacheco, J.L.; Martín-Nieto, I.; Benito-Herrero, J.M.; Huerta-Hurtado, P. Time-Domain Electromagnetics as a Geophysical Tool in Hydrogeological Exploitation Projects in Mesozoic Formations. Appl. Sci. 2022, 12, 8655.

Subasinghe, N.D.; Charles, W.K.D.G.D.R.; De Silva, S.N. Analytical Signal and Reduction to Pole Interpretation of Total Magnetic Field Data at Eppawala Phosphate Deposit. J. Geosci. Environ. Prot. 2014, 2, 3.

Munazyi, D.; Suparman, R.; Abiyudo, R. Application of Magnetic Method (Reduced to Pole and Analytic Signal) to Extract Specific Geology Information (Young Lava, Alteration and Quarternary Older Rock). Case Study: Mount Lamongan. In Proceedings of the 4th Indonesia International Geothermal Convention & Exhibition 2016, Cendrawasih Hall—Jakarta Convention Center, Jakarta, Indonesia, 10–12 August 2016.

Telford,W.M.; Geldart, L.P.; Sheriff, R.E. Applied Geophysics; Cambridge University Press: Cambridge, UK, 1990.

Clark, D.A.; Emerson, D.W. Notes on Rock Magnetization Characteristics in Applied Geophysical Studies. Explor. Geophys. 1991, 22, 547–555. Appl. Sci. 2023, 13, 10949 16 of 16

MacLeod, I.N.; Ellis, R.G. Magnetic Vector Inversion, a Simple Approach to the Challenge of Varying Direction of Rock Magnetization. Australian Society of Exploration Geophysicists, Extended Abstracts. 2013, pp. 1–4, Melbourne. Available online: https://www.semanticscholar.org/paper/Magnetic-Vector-Inversion-%2C-a-simple-approach-to-of-Macleod-Ellis/9cd186fe7e6843baeb43c706d80fc64ffed3109a (accessed on 1 December 2021).

Porras, D.; Carrasco, J.; Carrasco, P.; Herrero-Pacheco, J.L. Deep TDEM Study for Structural and Mining Purposes: A Case Study of the Barbastro Saline-Evaporitic Formation, Spain. Appl. Sci. 2023, 13, 6385.

Mendoza, R.; Rey, J.; Martínez, J.; Hidalgo, M.C.; Sandoval, S.S. Geophysical characterisation of geologic features with mining implications from ERT, TDEM and seismic reflection (Mining District of Linares-La Carolina, Spain). Ore Geol. Rev. 2021, 139, 104581.

Howard, K.W.F. Sustainable cities and the groundwater governance challenge. Environ. Earth Sci. 2015, 73, 2543–2554.

Madramootoo, C.A. Sustainable groundwater use in agriculture. Irrig. Drain. 2012, 61, 26–33.

Mahmoud, M.A. Groundwater and Agriculture in the Nile Delta. In Groundwater in the Nile Delta. The Handbook of Environmental Chemistry; Negm, A., Ed.; Springer: Berlin/Heidelberg, Germany, 2017; Volume 73.

Chevalier, R. Alumbramiento de Aguas Ocultas; Sintes: Barcelona, Spain, 1984.

Layade, G.O.; Adegoke, J.A.; Oladewa, F.C. Hydro geophysical Investigation for groundwater development at Gbongudu Area, Akobo Ojurin, Ibadan, Southwestern Nigeria. J. Appl. Sci. Environ. Manag. 2017, 21, 527–535.

Soomro, A.; Qureshi, A.L.; Jamali, M.A.; Ashraf, A. Groundwater investigation through vertical electrical sounding at hilly area from Nooriabad toward Karachi. Acta Geophys. 2019, 67, 247–261.

Varamashvili, N.D.; Tarkhan-Mouravi, A.G.; Ghlonti, N.Y. Efficiency of Vertical Electrical Sounding inWater Prospecting Problems in Adjara Region (Khelvachauri Municipality). J. Georgian Geophys. Soc. 2021, 24.

Fitterman, D.V.; Stewart, M.T. Transient electromagnetic sounding for groundwater. Geophysics 1986, 51, 995–1005.

Amato, F.; Pace, F.; Vergnano, A.; Comina, C. TDEM prospections for inland groundwater exploration in semiarid climate, Island of Fogo, Cape Verde. J. Appl. Geophys. 2021, 184, 104242.

Descloitres, M.; Chalikakis, K.; Legchenko, A.; Moussa, A.M.; Genthon, P.; Favreau, G.; Le Coz, M.; Boucher, M.; Oï, M. Investigation of groundwater resources in the Komadugu Yobe Valley (Lake Chad Basin, Niger) using MRS and TDEM methods. J. Afr. Earth Sci. 2013, 87, 71–85.

Guevara Mansilla, O.; Ventura Houle, R.; Andrade Limas, E.C. Uso de sondeos electromagnéticos en la caracterización hidrológica del acuífero del altiplano de Tula, Tamaulipas. Investig. Y Cienc. Univ. Autónoma Aguascalientes 2017, 70, 23–30.

Huerta, P.; Carrasco-García, P.; Armenteros, I.; Recio, C.; Carrasco-García, J.; Rodríguez-Jiménez, E. TDEM Soundings as a Tool to Determine Seasonal Variations of Groundwater Salinity (Villafáfila Lakes, Spain). Water 2022, 14, 2402.

Martínez-Moreno, F.J.; Monteiro-Santos, F.A.; Madeira, J.; Bernardo, I.; Soares, A.; Esteves, M.; Adão, F. Water prospection in volcanic islands by Time Domain Electromagnetic (TDEM) surveying: The case study of the islands of Fogo and Santo Antão in Cape Verde. J. Appl. Geophys. 2016, 134, 226–234.

Goy, A.; Gomez, J.J.; y Yébenes, A. El Pliensbachiense y Toarciense en la Rambla del Salto (Sierra Palomera, Teruel). Estud. Geol. 1976, 32, 391–423.

Vilas, L.; Mas, R.; García, A.; Arias, C.; Alonso, A.; Meléndez, N.; y Rincón, R. El Cretácico de España; Universidad Complutense de Madrid: Madrid, Spain, 1982; p. 457514.

Mozal Martín, F.; y Rubio Pascual, F.J. Mapa Geológico de España 1:50.000, Hoja nº 404 (Ayllón) y Memoria; IGME: Madrid, Spain, 1997; 119p.

Confederación Hidrográfica del Duero Borehole Control Piezometric Information. 2019. Available online: https://www.chduero.es/documents/20126/0/Piezometria_Red_Nivel_CHD.xlsx/5088b7a0-39ca-09da-eaca-edf17b423388?t=1641227734531 (accessed on 10 April 2022).

Carrasco García, P. Avance en Técnicas Geofísicas para la Caracterización del Subsuelo Mediante Innovación y el uso de Herramientas de Gestión de Información Espacial. Ph.D. Thesis, Escuela Politécnica Superior de Ávila, Universidad de Salamanca, Salamanca, Spain, 2013.

McNeill, J.D. Applications of Transient Electromagnetic Technics; Technical Note TN-7; Geonics Ltd.: Mississauga, ON, Canada, 1980; 17p.

Navarro Luna, R.A. Aplicación de Pruebas Electromagnéticas en el Dominio de Tiempo (TDEM) para Caracterización de Recursos Hídricos en Venezuela. Ph.D. Thesis, Universidad Simón Bolívar, Barranquilla, Colombia, 2006; 86p.

Nieto, I.M.; Carrasco García, P.; Sáez Blázquez, C.; Farfán Martín, A.; González-Aguilera, D.; Carrasco García, J. Geophysical Prospecting for Geothermal Resources in the South of the Duero Basin (Spain). Energies 2020, 13, 5397. Appl. Sci. 2022, 12, 8655 13 of 13

Sheriff, R.E. Geophysical Methods, 1st ed.; Prentice Hall: Englewood Cliffs, NJ, USA, 1989.

Ward, S.H.;Wannamaker, P.E. The MT/AMT Electromagnetic Method in Geothermal Exploration; Report 5; UNU-GTP: Reykjavik, Iceland, 1983; 107p.

Constable, S.C.; Parker, R.L.; Constable, C.G. Occam's inversion: A practical algorithm for generating smooth models from electromagnetic sounding data. Geophysics 1987, 52, 289–300.

TDEM Soundings as a Tool to Determine Seasonal Variations of Groundwater Salinity (Villafáfila Lakes, Spain)

Kohfahl, C.; Rodriguez, M.; Fenk, C.; Menz, C.; Benavente, J.; Hubberten, H.; Meyer, H.; Paul, L.; Knappe, A.; López-Geta, J.A.; et al. Characterising flow regime and interrelation between surface-water and ground-water in the Fuente de Piedra salt lake basin by means of stable isotopes, hydrogeochemical and hydraulic data. J. Hydrol. 2008, 351, 170–187.

Cartwright, I.; Hall, S.; Tweed, S.; Leblanc, M. Geochemical and isotopic constraints on the interaction between saline lakes and groundwater in southeast Australia. Hydrogeol. J. 2009, 17, 1991.

Marazuela, M.A.; Vázquez-Suñé, E.; Custodio, E.; Palma, T.; García-Gil, A.; Ayora, C. 3D mapping, hydrodynamics and modelling of the freshwater-brine mixing zone in salt flats similar to the Salar de Atacama (Chile). J. Hydrol. 2018, 561, 223–235.

Sanz, D.; Valiente, N.; Dountcheva, I.; Muñoz-Martín, A.; Cassiraga, E.; Gómez-Alday, J. Geometry of the modelled freshwater/salt-water interface under variable-density-driven flow (Pétrola Lake, SE Spain). Hydrogeol. J. 2022, 30, 975–988.

Rhoades, J.; Raats, P.; Prather, R. Effects of liquid-phase electrical conductivity, water content, and surface conductivity on bulk soil electrical conductivity. Soil Sci. Soc. Am. J. 1976, 40, 651–655.

Danielsen, J.E.; Auken, E.; Jørgensen, F.; Søndergaard, V.; Sørensen, K.I. The application of the transient electromagnetic method in hydrogeophysical surveys. J. Appl. Geophys. 2003, 53, 181–198.

Jang, H.; Kim, H.J. Mapping deep-sea hydrothermal deposits with an in-loop transient electromagnetic method: Insights from 1D forward and inverse modeling. J. Appl. Geophys. 2015, 123, 170–176.

Metwaly, M.; Elawadi, E.; Moustafa, S.S.R.; Al Arifi, N.; El Alfy, M.; Al Zaharani, E. Groundwater contamination assessment in Al-Quwy'yia area of central Saudi Arabia using transient electromagnetic and 2D electrical resistivity tomography. Environ. Earth Sci. 2014, 71, 827–835.

Tabbagh, A.; Dabas, M. Absolute magnetic viscosity determination using time-domain electromagnetic devices. Archaeol. Prospect. 1996, 3, 199–208.

Goldman, M.; Gvirtzman, H.; Hurwitz, S. Mapping saline groundwater beneath the Sea Galilee and its vicinity using time domain electromagnetic (TDEM) geophysical technique. Isr. J. Earth Sci. 2004, 53, 187–197. Water 2022, 14, 2402 14 of 14

Tchouta, K.D.; Marie, B.; Emmanuel, M.V.Y.; Guillaume, F.; Benjamin, N.N.; Nicaise, Y.; Baba, G.I.; Anatoly, L. Contribution of time domain electromagnetic and magnetic resonance soundings to groundwater assessment at the margin of lake chad basin, cameroon. J. Appl. Geophys. 2019, 170, 103840.

Levi, E.; Goldman, M.; Hadad, A.; Gvirtzman, H. Spatial delineation of groundwater salinity using deep time domain electromagnetic geophysical measurements: A feasibility study. Water Resour. Res. 2008, 44, W12404.

Flores Avilés, G.P.; Descloitres, M.; Duwig, C.; Rossier, Y.; Spadini, L.; Legchenko, A.; Soruco, Á.; Argollo, J.; Pérez, M.; Medinaceli, W. Insight into the Katari-Lago Menor Basin aquifer, Lake Titicaca-Bolivia, inferred from geophysical (TDEM), hydrogeological and geochemical data. J. S. Am. Earth. Sci. 2020, 99, 102479.

Yihdego, Y.; Webb, J. Modelling of seasonal and long-term trends in lake salinity in southwestern Victoria, Australia. J. Environ. Manag. 2012, 112, 149–159.

Martinez, C. Daily activity patterns of Great Bustards Otis tarda. Ardeola 2000, 47, 57–68.

Nilsson, L.; Kampe-Persson, H. Changes in migration and wintering patterns of greylag geese Anser anser from southernmost Sweden during three decades. Ornis Svec. 2018, 28, 19–38.

IGM. Investigación Hidrogeológica de la Cuenca del Duero: Sistemas nº 8 y 12; IGME: Madrid, Spain, 1980; p. 75.

IGME-DGA. Apoyo a la Caracterización Adicional de las Masas de Agua Subterránea en Riesgo de no Cumplir los Objetivos Medioambientales en 2015. Demarcación Hidrográfica del Duero. Masa de agua Subterránea 31 Villafáfila; IGME: Madrid, Spain, 2009; p. 84.

AEMET.AEMET Open Data. Benavente. Available online: http://www.aemet.es/es/datos_abiertos/AEMET_OpenData (accessed on 1 July 2020).

Huerta, P.; Armenteros, I.; Recio, C.; Carrasco-García, P.; Rueda-Gualdrón, C.; Cidón-Trigo, A. The origin of the saline waters in the Villafáfila lakes (NW Spain). A hydrogeological, hydrochemical, and geophysical approach. Sci. Total Environ. 2021, 789, 147909.

Armenteros, I.; Huerta, P.; Cidón-Trigo, A.; Rueda-Gualdrón, M.C.; Recio, C.; Martínez-Grana, A. Hydrogeology of the lagunas de villafáfila area (Zamora). Geogaceta 2019, 66, 51–54.

Fernández Pérez, L.; Cabrera Lagunilla, M.P. Estudio Hidrogeológico de las lagunas de Villafáfila (Zamora). In Geología Ambiental y Ordenación del Territorio. III Reunión Nacional; Universitat de Valencia: Valencia, Spain, 1987; Volume 1, pp. 441–459.

Fitterman, D.V.; Stewart, M.T. Transient electromagnetic sounding for groundwater. Geophysics 1986, 51, 995–1005.

Spies, B.R. Depth of investigation in electromagnetic sounding methods. Geophysics 1989, 54, 872–888.

Nabighian, M.N. Electromagnetic Methods in Applied Geophysics: Volume 1, Theory; Society of Exploration Geophysicists: Houston, TX, USA, 1988.

Nieto, I.M.; Carrasco García, P.; Sáez Blázquez, C.; Farfán Martín, A.; González-Aguilera, D.; Carrasco García, J. Geophysical Prospecting for Geothermal Resources in the South of the Duero Basin (Spain). Energies 2020, 13, 5397.

Hoekstra, P.; Blohm, M.W. Case histories of time-domain electromagnetic soundings in environmental geophysics. In Geotechnical an Environmental Geophysics: Volume II:

Environmental and Groundwater; Society of Exploration Geophysicists: Houston, TX, USA, 1990; pp. 1–16.

Constable, S.C.; Parker, R.L.; Constable, C.G. Occam's inversion: A practical algorithm for generating smooth models from electromagnetic sounding data. Geophysics 1987, 52, 289–300.

Martín Serrano, A.; PilesMateo, E. Villafáfila (308). InMapa Geológico de España y Memoria, Escala 1:15.000; IGME:Madrid, Spain, 1982.

Martín Serrano, A.; Barba Martín, A. Manganeses de la Lampreana 340. In Mapa Geológico de España y Memoria. Escala 1:50.000; IGME: Madrid, Spain, 1979.

Archie, G.E. The Electrical Resistivity Log as an Aid in Determining Some Reservoir Characteristics. Trans. AIME 1942, 146, 54–62.

Yadav, D.; Sarin, M.; Krishnaswami, S. Hydrogeochemistry of Sambhar Salt Lake, Rajasthan: Implication to recycling of salt and annual salt budget. J.-Geol. Soc. India 2007, 69, 139–152.

Drever, J.I.; Smith, C.L. Cyclic wetting and drying of the soil zone as an influence on the chemistry of ground water in arid terrains. Am. J. Sci. 1978, 278, 1448–1454.

Descloitres, M.; Chalikakis, K.; Legchenko, A.; Moussa, A.M.; Genthon, P.; Favreau, G.; Le Coz, M.; Boucher, M.; Oï, M. Investigation of groundwater resources in the Komadugu Yobe Valley (Lake Chad Basin, Niger) using MRS and TDEM methods. J. Afr. Earth Sci. 2013, 87, 71–85.

Amato, F.; Pace, F.; Vergnano, A.; Comina, C. TDEM prospections for inland groundwater exploration in semiarid climate, Island of Fogo, Cape Verde. J. Appl. Geophys. 2021, 184, 104242.

Martínez-Moreno, F.J.; Monteiro-Santos, F.A.; Madeira, J.; Bernardo, I.; Soares, A.; Esteves, M.; Adão, F. Water prospection in volcanic islands by Time Domain Electromagnetic (TDEM) surveying: The case study of the islands of Fogo and Santo Antão in Cape Verde. J. Appl. Geophys. 2016, 134, 226–234.

Hidrogeología del entorno de las lagunas del Oso (Ávila)

Armenteros, I., Huerta, P., Cidón-Trigo, A., Rueda-Gualdrón, M.C., Recio, C. y Martínez-Grana, A. (2019). Geogaceta, 66, 51-54.

Huerta, P., Armenteros, I., Recio, C., Carrasco-García, P., Rueda-Gualdrón, C. y Cidón-Trigo, A. (2021). Science of The Total Environment, 789, 147909.

Mediavilla, R., Santisteban, J.I., López-Cilla, I., Galán de Frutos, L. y de la Hera-Portillo, Á. (2020). Water, 12, 1911. MIRAME (2022). Confederación Hidrográfica del Duero, http://www.mirame.chduero.es/DMADuero_09_15/index.faces, 20-02-2022.

Pérez-González, A. y Elízaga-Muñoz, E. (1979a): Mapa Geológico de España 1:50.000, hoja nº 481 (Nava de Arévalo). IGME, Madrid 52 p.

Pérez-González, A. y Elízaga-Muñoz, E. (1979b): Mapa Geológico de España 1:50.000, hoja nº 506 (Cardeñosa) y memoria. IGME, Madrid 68 p.

Pineda, A., Huerta, P., Nozal, F., Montes, M. y López-Olmedo, F. (en línea): Mapa Geológico Digital continuo E. 1: 50.000, Zona Cuenca del Duero-Almazán (Zona-2300) IGME, en línea.

Rodríguez-Rodríguez, M., Moral, F., Benavente, J. y Beltrán, M. (2010). Journal of Arid Environments, 74, 1478-1486.

Sanz-Montero, M.E., Cabestrero, Ó. y Sánchez-Román, M. (2019). Frontiers in Microbiology, 10.

Sanz Donaire, J.J. y García Rodríguez, M.P. (1998). Observatorio Medioambiental, 1, 65-92.

Applying Deep Electrical-Resistivity Tomography Techniques for the Exploration of Medium- and Low-Geothermal Energy Resources

Fridleifsson, I.B. Geothermal energy for the benefit of the people. Renew. Sustain. Energy Rev. 2001, 5, 299–312.

García-Gil, A.; Goetzl, G.; Kłonowski, M.R.; Borovic, S.; Boon, D.P.; Abesser, C.; Janza, M.; Herms, I.; Petitclerc, E.; Erlström, M.; et al. Governance of shallow geothermal energy resources. Energy Policy 2020, 138, 111283.

Dickson, M.H.; Fanelli, M. Geothermal Energy: Utilization and Technology; Routledge: London, UK, 2013; ISBN 978-1-84407-184-5.

Lund, J.W.; Toth, A.N. Direct utilization of geothermal energy 2020 worldwide review. Geothermics 2021, 90, 101915.

Sáez Blázquez, C.; Martín Nieto, I.; Farfán Martín, A.; González-Aguilera, D.; Carrasco García, P. Comparative analysis of different methodologies used to estimate the ground thermal conductivity in low enthalpy geothermal systems. Energies 2019, 12, 1672.

Limberger, J.; Boxem, T.; Pluymaekers, M.; Bruhn, D.; Manzella, A.; Calcagno, P.; Beekman, F.; Cloetingh, S.; van Wees, J.-D. Geothermal energy in deep aquifers: A global assessment of the resource base for direct heat utilization. Renew. Sustain. Energy Rev. 2018, 82, 961–975.

Rybach, L. Global Status, Development and Prospects of Shallow and Deep Geothermal Energy. Int. J. Terr. Heat Flow Appl. Geotherm. 2022, 5, 20–25.

Lund, J.W.; Huttrer, G.W.; Toth, A.N. Characteristics and trends in geothermal development and use, 1995 to 2020. Geothermics 2022, 105, 102522.

Blázquez, C.S.; Borge-Diez, D.; Nieto, I.M.; Martín, A.F.; González-Aguilera, D. Multi-parametric evaluation of electrical, biogás and natural gas geothermal source heat pumps. Renew. Energy 2021, 163, 1682–1691.

D'Agostino, D.; Mazzarella, L. What is a Nearly zero energy building? Overview, implementation and comparison of definitions. J. Build. Eng. 2019, 21, 200–212.

Blázquez, C.S.; Borge-Diez, D.; Nieto, I.M.; Martín, A.F.; González-Aguilera, D. Technical optimization of the energy supply in geothermal heat pumps. Geothermics 2019, 81, 133–142.

Magrini, A.; Lentini, G.; Cuman, S.; Bodrato, A.; Marenco, L. From nearly zero energy buildings (NZEB) to positive energy buildings (PEB): The next challenge-The most recent European trends with some notes on the energy analysis of a forerunner PEB example. Dev. Built Environ. 2020, 3, 100019.

Sorman, A.H.; García-Muros, X.; Pizarro-Irizar, C.; González-Eguino, M. Lost (and found) in Transition: Expert stakeholder insights on low-carbon energy transitions in Spain. Energy Res. Soc. Sci. 2020, 64, 101414. Energies 2024, 17, 1836 15 of 16

Arrizabalaga, I.; De Gregorio, M.; De Santiago, C.; García de la Noceda, C.; Pérez, P.; Urchueguía, J.F. Country update for the Spanish geothermal sector. In Proceedings of the World Geothermal Congress, Melbourne, Australia, 19–24 April 2015; pp. 19–24.

Arrizabalaga, I.; De Gregorio, M.; De Santiago, C.; García de la Noceda, C.; Pérez, P.; Urchueguía, J.F. Country update for the Spanish geothermal sector. In Proceedings of the World Geothermal Congress, Reykjavik, Iceland, 27 April–1 May 2020; p. 12.

Vivas, C.; Salehi, S.; Tuttle, J.D.; Rickard, B. Challenges and opportunities of geothermal drilling for renewable energy generation. GRC Trans. 2020, 44, 904–918.

Anderson, A.; Rezaie, B. Geothermal technology: Trends and potential role in a sustainable future. Appl. Energy 2019, 248, 18–34.

Blázquez, C.S.; Nieto, I.M.; González, M.Á.M.; García, P.C.; Martín, A.F.; González-Aguilera, D. Geophysical exploration for shallow geothermal applications: A case study in Artà, (Balearic Islands, Spain). Geothermics 2022, 105, 102517.

Sáez Blázquez, C.; Carrasco García, P.; Nieto, I.M.; Maté-González, M.Á.; Martín, A.F.; González-Aguilera, D. Characterizing geological heterogeneities for geothermal purposes through combined geophysical prospecting methods. Remote Sens. 2020, 12, 1948.

Carrier, A.; Fischanger, F.; Gance, J.; Cocchiararo, G.; Morelli, G.; Lupi, M. Deep electrical resistivity tomography for the prospection of low-to medium-enthalpy geothermal resources. Geophys. J. Int. 2019, 219, 2056–2072.

Nieto, I.M.; Carrasco García, P.; Sáez Blázquez, C.; Farfán Martín, A.; González-Aguilera, D.; Carrasco García, J. Geophysical prospecting for geothermal resources in the south of the Duero Basin (Spain). Energies 2020, 13, 5397.

Ismail, N.; Syukri, M.; Idroes, R. Deep and shallow structures of geothermal Seulawah Agam based on electromagnetic and magnetic data. Geomate J. 2019, 16, 141–147.

Mohamed, M.A.; Pajares, A.J.M.; Moreno, J.L.; Herrador, M.B.; Álvarez, F.P.; Reyes, J.M.G. Phylogenetic relationships of “Erysimum”(Brassicaceae) from the Baetic Mountains (SE Iberian Peninsula). In Anales del Jardín Botánico de Madrid; Real Jardín Botánico: Madrid, Spain, 2014; Volume 71, p. 5.

Sala, M. Baetic Cordillera and Guadalquivir Basin. In Geomorphology of Europe; Palgrave: London, UK, 1984; pp. 323–340.

Albir, A.E.; López Olmedo, F.L.; Díaz de Neira, J.A. Mapa y memoria explicativa de la Hoja 970, El Rubio. MAGNA. IGME. 1981.

Guzmán, S.J. Sondeo de Agua Minero Industrial de Origen Termal “Alamedilla 1” Capacity Report; Junta de Andalucía: Andalusia, Spain, 2015.

Lévy, L.; Maurya, P.K.; Byrdina, S.; Vandemeulebrouck, J.; Sigmundsson, F.; Árnason, K.; Ricci, T.; Deldicque, D.; Roger, M.; Gibert, B.; et al. Electrical resistivity tomography and time-domain induced polarization field investigations of geotermal areas at Krafla, Iceland: Comparison to borehole and laboratory frequency-domain electrical observations. Geophys. J. Int. 2019, 218, 1469–1489.

Singh, S.; Gautam, P.K.; Bagchi, D.; Singh, S.; Kumar, S.; Kannaujiya, S. 2D electrical resistivity imaging for geotermal groundwater characterization and rejuvenation of the Gaurikund hot spring in the Main Central Thrust (MCT) zone of the Garhwal Himalaya, Uttrakhand, India. Groundw. Sustain. Dev. 2021, 15, 100686.

Kumar, D.; Thiagarajan, S.; Rai, S.N. Deciphering geothermal resources in Deccan Trap region using electrical resistivity tomography technique. J. Geol. Soc. India 2011, 78, 541–548.

Vanhooren, L.; Fontaine, O.; Caudron, C.; Vrancken, E.; Dekoninck, W.; De Lathauwer, H.; Hermans, T. Characterization and Monitoring of the Gunnuhver Geothermal Site Using Electrical Methods (No. EGU23-12873); Copernicus Meetings; EGU: Vienna, Austria, 2023.

Cheng, Y.;Wang, C.; Da,W.; Kong, Y.; Hu, X. Anatomy of the convective geothermal system from geophysical and hydrochemical data: A case study from the Changshou geothermal field, South China. Geophysics 2023, 88, 1–43.

Ussher, G.; Harvey, C.; Johnstone, R.; Anderson, E. Understanding the resistivities observed in geothermal systems. In Proceedings of the World Geothermal Congress, Kyushu, Japan, 28 May–10 June 2000; pp. 1915–1920.

Marwan, M.; Isa, M.; Idroes, R.; Nursyafira, N.; Idris, S.; Yanis, M.; Ghani, A.A.; Paembonan, A.Y. Geoelectrical Model of Geothermal Spring in ie Jue Seulawah Deriving from 2D Vlf-Em and dc Resistivity Methods. J. Appl. Eng. Sci. 2023, 21, 59–69.

Abdullah, A.I.; Musa, M.D.T.; Uno, I.; Jayadi, H. Resistivity model of hallow subsurface to find the path of geotermal manifestation in Bora Village of Sigi Regency of Central Sulawesi. J. Phys. Conf. Ser. 2019, 1242, 012048.

Cumming, W.; Mackie, R. Resistivity imaging of geothermal resources using 1D, 2D and 3D MT inversion and TDEM static shift correction illustrated by a Glass Mountain case history. In Proceedings of the World Geothermal Congress, Bali, Indonasia, 25–30 April 2010; pp. 25–29.

Arjwech, R.; Everett, M.E. Application of 2D electrical resistivity tomography to engineering projects: Three case studies. Songklanakarin J. Sci. Technol. 2015, 37, 675–681.

Zhou, B.; Bouzidi, Y.; Ullah, S.; Asim, M. A full-range gradient survey for 2D electrical resistivity tomography. Near Surf. Geophys. 2020, 18, 609–626.

Carrasco García, P. Avance en Técnicas Geofísicas Para la Caracterización del Subsuelo Mediante Innovación y el Uso de Herramientas de Gestión de Información Espacial. Ph.D. Thesis, Escuela Politécnica Superior de Ávila, Univ de Salamanca, Ávila, Spain, 2013; p. 523.

Robain, H.; Bobachev, A. X2IPI Toolbox for 2D DC measurements with SYSCAL equipment. User manual, 2002; 25p. Energies 2024, 17, 1836 16 of 16

Loke, M.H.; Dahlin, T. A comparison of the Gauss–Newton and quasi-Newton methods in resistivity imaging inversion. J. Appl. Geophys. 2002, 49, 149–162.

Telford,W.M.; Telford,W.M.; Geldart, L.P.; Sheriff, R.E. Applied Geophysics; Cambridge University Press: Cambridge, UK, 1990; ISBN 1139642928/9781139642927.

Arifin, M.H.; Kayode, J.S.; Ismail, K.I.; Abdullah, M.; Embrandiri, A.; Nazer, S.M.; Azmi, A. Data for the industrial and municipal environmental wastes hazard contaminants assessment with integration of RES2D techniques and Oasis Montaj software. Data Brief 2020, 33, 106595.

Galindo-Zaldívar, J.; Jabaloy, A.; Serrano, I.; Morales, J.; González-Lodeiro, F.; Torcal, F. Recent and present-day stresses in the Granada Basin (Betic Cordilleras): Example of a late Miocene-present-day extensional basin in a convergent plate boundary. Tectonics 1999, 18, 686–702.

Mao, Y.; Zhang, Y. Thermal conductivity, shear viscosity and specific heat of rigid water models. Chem. Phys. Lett. 2012, 542, 37–41.

Abraham, J.P.; Sparrow, E.M.; Tong, J.C.K. Heat transfer in all pipe flow regimes: Laminar, transitional/intermittent, and turbulent. Int. J. Heat Mass Transf. 2009, 52, 557–563.

Crittenden, J.C.; Trussell, R.R.; Hand, D.W.; Howe, K.J.; Tchobanoglous, G. MWH's Water Treatment: Principles and Design, 3rd ed.; John Wiley & Sons: Hoboken, NJ, USA, 1861; ISBN 978-0-470-40593-0.

Domenico, P.A.; Palciauskas, V.V. Theoretical analysis of forced convective heat transfer in regional ground-water flow. Geol. Soc. Am. Bull. 1973, 84, 3803–3814.

CAPÍTULO 5

ÍNDICES DE CALIDAD DE LAS REVISTAS

Products

Journal Citation Reports™ Journals Categories Pub My favorites Sign In Register

Home > Journal profile

JCR Year
2022

Favorite Export

Applied Sciences-Basel

Open Access since 2011

ISSN
N/A

EISSN
2076-3417

JCR ABBREVIATION
APPL SCI-BASEL

ISO ABBREVIATION
Appl. Sci.-Basel

Journal information

EDITION
Science Citation Index Expanded (SCIE)

CATEGORY
CHEMISTRY, MULTIDISCIPLINARY - SCIE

MATERIALS SCIENCE, MULTIDISCIPLINARY - SCIE

PHYSICS, APPLIED - SCIE

ENGINEERING, MULTIDISCIPLINARY - SCIE

LANGUAGES	REGION	1ST ELECTRONIC JCR YEAR
English	SWITZERLAND	2014

Publisher information

PUBLISHER	ADDRESS	PUBLICATION FREQUENCY
MDPI	ST ALBAN-ANLAGE 66, CH-4052 BASEL, SWITZERLAND	24 issues/year

Journal's performance

Journal Impact Factor

The Journal Impact Factor (JIF) is a journal-level metric calculated from data indexed in the Web of Science Core Collection. It should be used with careful attention to the many factors that influence citation rates, such as the volume of publication and citations characteristics of the subject area and type of journal. The Journal Impact Factor can complement expert opinion and informed peer review. In the case of academic evaluation for tenure, it is inappropriate to use a journal-level metric as a proxy measure for individual researchers, institutions, or articles. Learn more

2022 JOURNAL IMPACT FACTOR
2.7
View calculation

JOURNAL IMPACT FACTOR WITHOUT SELF CITATIONS
2.4
View calculation

Journal Impact Factor Trend 2022 Export

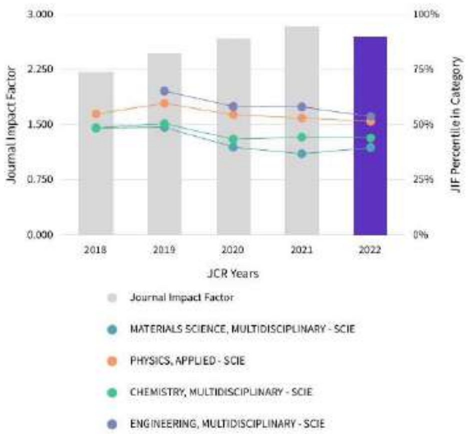

View all years

Journal Impact Factor contributing items Export

Citable items (21,030) Citing Sources (6,128)

TITLE	CITATION COUNT
A Novel K-Means Clustering Algorithm with a Noise Algorithm for Capturing...	110
Observation of Potential Contaminants in Processed Biomass Using Fourier...	89
A Novel Transfer Learning Based Approach for Pneumonia Detection in...	88
Sentence Representation Method Based on Multi-Layer Semantic Network	78
The Impact of Drought in Plant Metabolism: How to Exploit Tolerance...	77
Diversity of Synthetic Dyes from Textile Industries, Discharge Impacts and...	75
A Novel Advancing Signal Processing Method Based on Coupled Multi-Stab...	66
Transfer Learning with Deep Convolutional Neural Network (CNN)...	61
A Review of the Potential Climate Change Impacts and Adaptation...	60
Peak Fitting Applied to Fourier Transform Infrared and Raman...	57

View All in Web of Science

Journal Citation Indicator (JCI)

Export

0.57

The Journal Citation Indicator (JCI) is the average Category Normalized Citation Impact (CNCI) of citable items (articles & reviews) published by a journal over a recent three year period. The average JCI in a category is 1. Journals with a JCI of 1.5 have 50% more citation impact than the average in that category. It may be used alongside other metrics to help you evaluate journals. Learn more

Total Citations

Export

98,949

The total number of times that a journal has been cited by all journals included in the database in the JCR year. Citations to journals listed in JCR are compiled annually from the JCR years combined database, regardless of which JCR edition lists the journal.

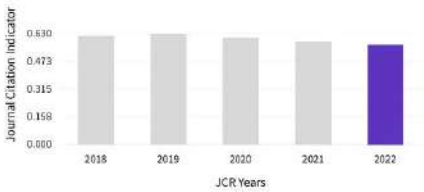

View all years

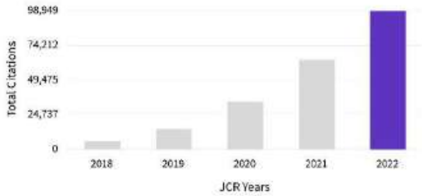

View all years

Citation distribution

Export

The Citation Distribution shows the frequency with which items published in the year or two years prior were cited in the JCR data year (i.e., the component of the calculation of the JIF). The graph has similar functionality as the JIF Trend graph, including hover-over data descriptions for each data point, and an interactive legend where each data element's legend can be used as a toggle. You can view Articles, Reviews, or Non-Citable (other) items to the JIF numerator. Learn more

ARTICLE CITATION MEDIAN

1

REVIEW CITATION MEDIAN

4

UNLINKED CITATIONS

714

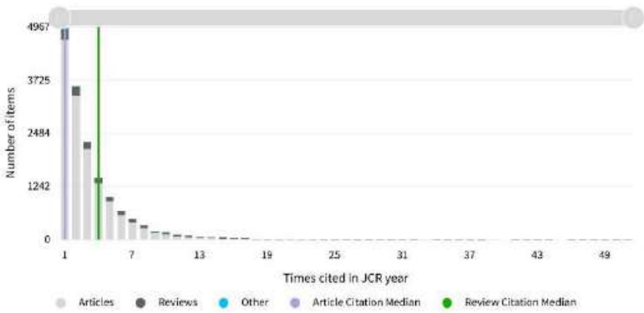

TIMES CITED

0

ARTICLES

5,064

REVIEWS

169

OTHER

200

Open Access (OA)

Export

The data included in this tile summarizes the items published in the journal in the JCR data year and in the previous two years. This three-year set of published items is used to provide descriptive analysis of the content and community of the journal. Learn more

Items

TOTAL CITABLE	% OF CITABLE OA
33,771	99.30%

Citations*

TOTAL CITABLE	% OF CITABLE OA
65,765	99.08%

15

CITABLE

GOLD OPEN ACCESS
33,535 / 97.59%

SUBSCRIPTION AND FREE TO READ
236 / 0.69%

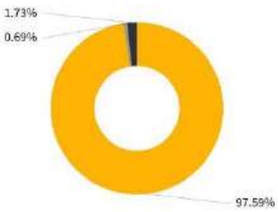

NON-CITABLE

OTHER (NON CITABLE ITEMS)
593 / 1.73%

CITABLE

GOLD OPEN ACCESS
65,163 / 97.52%

SUBSCRIPTION AND FREE TO READ
602 / 0.90%

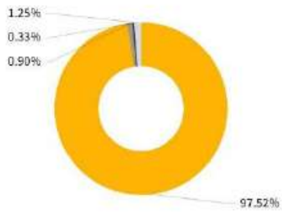

NON-CITABLE

OTHER (NON CITABLE ITEMS)
223 / 0.33%

UNLINKED CITATIONS
835 / 1.25%

*Citations in 2022 to items published in [2020 - 2022]

Rank by Journal Impact Factor

Journals within a category are sorted in descending order by Journal Impact Factor (JIF) resulting in the Category Ranking below. A separate rank is shown for each category in which the journal is listed in JCR. Data for the most recent year is presented at the top of the list, with other years shown in reverse chronological order. Learn more

EDITION
Science Citation Index Expanded (SCIE)

CATEGORY
MATERIALS SCIENCE, MULTIDISCIPLINARY

208/344

JCR YEAR	JIF RANK	JIF QUARTILE	JIF PERCENTILE
2022	208/344	Q3	39.7
2021	218/345	Q3	36.96
2020	201/334	Q3	39.97
2019	161/314	Q3	48.89

EDITION
Science Citation Index Expanded (SCIE)

CATEGORY
PHYSICS, APPLIED

78/160

JCR YEAR	JIF RANK	JIF QUARTILE	JIF PERCENTILE
2022	78/160	Q2	51.6
2021	76/161	Q2	53.11
2020	73/160	Q2	54.69
2019	63/155	Q2	59.68

Rank by Journal Citation Indicator (JCI)

15

Journals within a category are sorted in descending order by Journal Citation Indicator (JCI) resulting in the Category Ranking below. A separate rank is shown for each category in which the journal is listed in JCR. Data for the most recent year is presented at the top of the list, with other years shown in reverse chronological order. Learn more

TEGORY
IATERIALS SCIENCE, MULTIDISCIPLINARY
:12/424

R YEAR	JCI RANK	JCI QUARTILE	JCI PERCENTILE
ı22	212/424	Q2	50.12
ı21	195/414	Q2	53.02
ı20	173/384	Q2	55.08
ı19	149/375	Q2	60.40
ı18	142/361	Q2	60.80
ı17	165/343	Q2	52.04

CATEGORY
PHYSICS, APPLIED
79/178

JCR YEAR	JCI RANK	JCI QUARTILE	JCI PERCENTILE
2022	79/178	Q2	55.90
2021	75/178	Q2	58.15
2020	63/171	Q2	63.45
2019	62/170	Q2	63.82
2018	63/169	Q2	63.02
2017	82/165	Q2	50.61

Citation network

Cited Half-life

2.4 years

The Cited Half-Life is the median age of the items in this journal that were cited in the JCR year. Half of a journal's cited items were published more recently than the cited half-life.

TOTAL NUMBER OF CITES

98,949

NON SELF-CITATIONS

88,372

SELF-CITATIONS

10,577

Citing Half-life

6.3 years

The Citing Half-Life is the median age of items in other publications cited by this journal in the JCR year.

TOTAL NUMBER OF CITES

576,866

NON SELF-CITATIONS

566,289

SELF-CITATIONS

10,577

Cited Half-life Data   Citing Half-life Data

Export

15

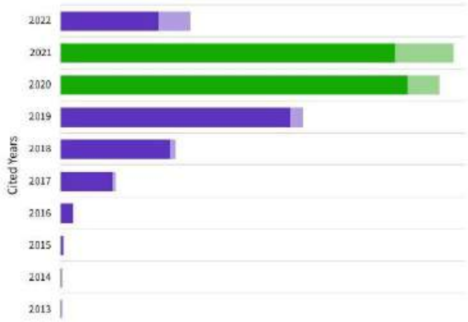

CITED YEAR	# OF CITES FROM 2022	CUMULATIVE %	# OF CITING SOURCES
All years	**98,949 citations**	**100.00%**	**6,782 sources**
2022	9,637 citations	9.74%	1,688 sources
2021	29,106 citations	39.15%	4,034 sources
2020	28,080 citations	67.53%	4,356 sources
2019	17,984 citations	85.71%	3,446 sources
2018	8,530 citations	94.33%	2,275 sources
2017	4,062 citations	98.43%	1,440 sources
2016	969 citations	99.41%	536 sources
2015	223 citations	99.64%	167 sources
2014	79 citations	99.72%	68 sources

Journal Citation Relationships

Cited Data Citing Data

Top 20 journals citing APPL SCI-BASEL by number of citations

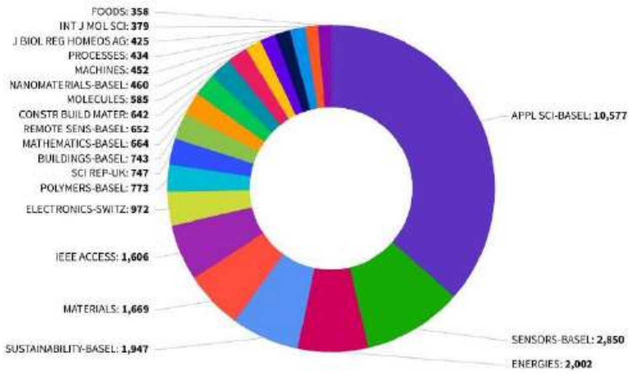

Content metrics

Source data

This tile shows the breakdown of document types published by the journal. Citable Items are Articles and Reviews. For the purposes of calculating JIF, a JCR year considers the publications of that journal in the two prior years. Learn more

12,741 total citable items

	ARTICLES	REVIEWS	COMBINED(C)	OTHER DOCUMENT TYPES(D)	PERCEI
NUMBER IN JCR YEAR 2022 (A)	12,099	642	12,741	303	98%
NUMBER OF REFERENCES (B)	506,501	66,283	572,784	4,082	99%
RATIO (B/A)	41.9	103.2	45.0	13.5	

Average JIF Percentile

Export

The Average Journal Impact Factor Percentile takes the sum of the JIF Percentile rank for each category under consideration, then calculates the average of those values. Learn more

ALL CATEGORIES AVERAGE
47.3

EDITION
Science Citation Index Expanded

MATERIALS SCIENCE, MULTIDISCIPLINARY
39.7

CHEMISTRY, MULTIDISCIPLINARY
44.1

ENGINEERING, MULTIDISCIPLINARY

Contributions by organizations

Export

Organizations that have contributed the most papers to the journal in the most recent three-year period. Learn more

RANK	ORGANIZATION	COUNT
1	CHINESE ACADEMY OF SCIENCES	811
2	EGYPTIAN KNOWLEDGE BANK (EKB)	421
3	CONSIGLIO NAZIONALE DELLE RICERCHE (CNR)	382
4	CENTRE NATIONAL DE LA RECHERCHE SCIENTIFIQUE (CNRS)	350
5	KING SAUD UNIVERSITY	281
-	RUSSIAN ACADEMY OF SCIENCES	281
7	CENTRAL SOUTH UNIVERSITY	273

Contributions by country/region

Export

Countries or Regions that have contributed the most papers to the journal in the most recent three-year period. Learn more

RANK	COUNTRY / REGION	COUNT
1	CHINA MAINLAND	9116
2	South Korea	4428
3	Italy	3398
4	Spain	2460
5	USA	2018
6	Poland	1726
7	GERMANY (FED REP GER)	1422
8	Taiwan	1333
9	Saudi Arabia	1250

Additional metrics

15 ?

Eigenfactor Score

0.11103

The Eigenfactor Score is a reflection of the density of the network of citations around the journal using 5 years of cited content as cited by the Current Year. It considers both the number of citations and the source of those citations, so that highly cited sources will influence the network more than less cited sources. The Eigenfactor calculation does not include journal self-citations. Learn more

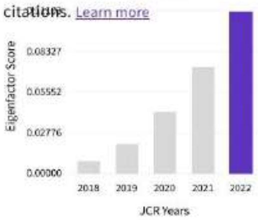

Normalized Eigenfactor

24.16562

The Normalized Eigenfactor Score is the Eigenfactor score normalized, by rescaling the total number of journals in the JCR each year, so that the average journal has a score of 1. Journals can then be compared and influence measured by their score relative to 1. Learn more

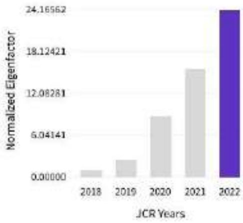

Article influence score

0.414

The Article Influence Score normalizes the Eigenfactor Score according to the cumulative size of the cited journal across the prior five years. The mean Article Influence Score for each article is 1.00. A score greater than 1.00 indicates that each article in the journal has above-average influence. Learn more

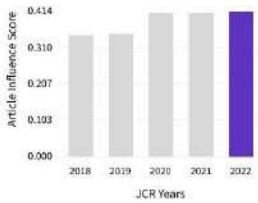

5 Year Impact Factor

2.9

View Calculation

Immediacy Index

0.8

View Calculation

Products

Journal Citation Reports™ Journals Categories Pub My favorites Sign In Register

Home > Journal profile

JCR Year 2022

Favorite Export

Water

Open Access since 2009

ISSN
N/A

EISSN
2073-4441

JCR ABBREVIATION
WATER-SUI

ISO ABBREVIATION
Water

Journal information

EDITION
Science Citation Index Expanded (SCIE)

CATEGORY
WATER RESOURCES - SCIE

ENVIRONMENTAL SCIENCES - SCIE

LANGUAGES	REGION	1ST ELECTRONIC JCR YEAR
English	SWITZERLAND	2012

Publisher information

PUBLISHER	ADDRESS	PUBLICATION FREQUENCY
MDPI	ST ALBAN-ANLAGE 66, CH-4052 BASEL, SWITZERLAND	24 issues/year

Journal's performance

Journal Impact Factor

The Journal Impact Factor (JIF) is a journal-level metric calculated from data indexed in the Web of Science Core Collection. It should be used with careful attention to the many factors that influence citation rates, such as the volume of publication and citations characteristics of the subject area and type of journal. The Journal Impact Factor can complement expert opinion and informed peer review. In the case of academic evaluation for tenure, it is inappropriate to use a journal-level metric as a proxy measure for individual researchers, institutions, or articles. Learn more

2022 JOURNAL IMPACT FACTOR
3.4
View calculation

JOURNAL IMPACT FACTOR WITHOUT SELF CITATIONS
2.9
View calculation

Journal Impact Factor Trend 2022 Export

Journal Impact Factor contributing items Export

Citable items (7,057) Citing Sources (2,334)

TITLE	CITATION COUNT
Advanced Oxidation Processes for the Removal of Antibiotics from Water. An...	145

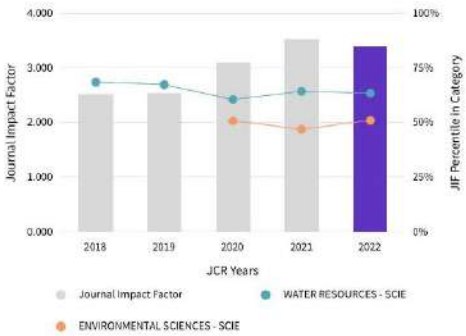

View all years

Role of Nanomaterials in the Treatment of Wastewater: A Review	114	˅
Adsorption of Methylene Blue in Water onto Activated Carbon by Surfactant...	93	˅
Antimicrobials and Antibiotic-Resistant Bacteria: A Risk to the Environment a...	64	˅
A Comprehensive Review on Membrane Fouling: Mathematical Modelling,...	44	˅
Oily Wastewater Treatment: Overview of Conventional and Modern Methods...	44	˅
Comparative Analysis of Drought Indicated by the SPI and SPEI at Vario...	43	˅
Comparative Analysis of Recurrent Neural Network Architectures for...	43	˅
Research Trends in the Use of Remote Sensing for Inland Water Quality...	41	˅
A Review of SWAT Model Application in Africa	40	˅

View All in Web of Science

Journal Citation Indicator (JCI)

Export

0.66

The Journal Citation Indicator (JCI) is the average Category Normalized Citation Impact (CNCI) of citable items (articles & reviews) published by a journal over a recent three year period. The average JCI in a category is 1. Journals with a JCI of 1.5 have 50% more citation impact than the average in that category. It may be used alongside other metrics to help you evaluate journals. Learn more

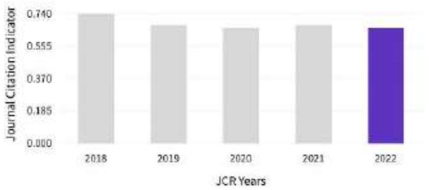

View all years

Total Citations

Export

52,504

The total number of times that a journal has been cited by all journals included in the database in the JCR year. Citations to journals listed in JCR are compiled annually from the JCR years combined database, regardless of which JCR edition lists the journal.

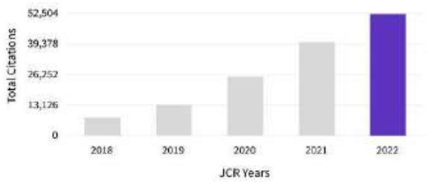

View all years

Citation distribution

Export

The Citation Distribution shows the frequency with which items published in the year or two years prior were cited in the JCR data year (i.e., the component of the calculation of the JIF). The graph has similar functionality as the JIF Trend graph, including hover-over data descriptions for each data point, and an interactive legend where each data element's legend can be used as a toggle. You can view Articles, Reviews, or Non-Citable (other) items to the JIF numerator. Learn more

ARTICLE CITATION MEDIAN

2

REVIEW CITATION MEDIAN

5

UNLINKED CITATIONS

316

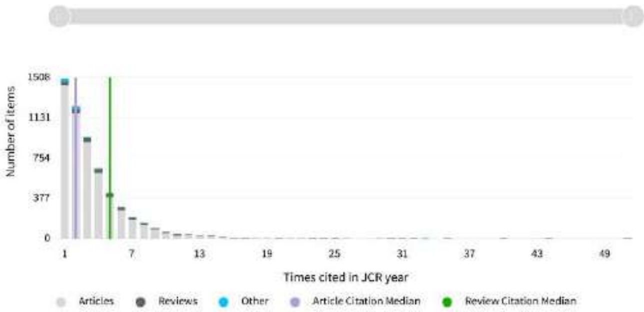

TIMES CITED

0

ARTICLES

1,190

REVIEWS

28

OTHER

105

Open Access (OA)

Export

The data included in this tile summarizes the items published in the journal in the JCR data year and in the previous two years. This three-year set of published items is used to provide descriptive analysis of the content and community of the journal. Learn more

Items

TOTAL CITABLE	% OF CITABLE OA
11,097	99.38%

Citations*

TOTAL CITABLE	% OF CITABLE OA
26,791	99.38%

CITABLE

GOLD OPEN ACCESS
11,028 / 96.84%

SUBSCRIPTION AND FREE TO READ
69 / 0.61%

NON-CITABLE

OTHER (NON CITABLE ITEMS)
291 / 2.56%

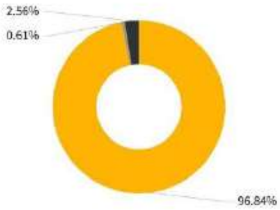

CITABLE

GOLD OPEN ACCESS
26,626 / 96.91%

SUBSCRIPTION AND FREE TO READ
165 / 0.60%

NON-CITABLE

OTHER (NON CITABLE ITEMS)
298 / 1.08%

UNLINKED CITATIONS
387 / 1.41%

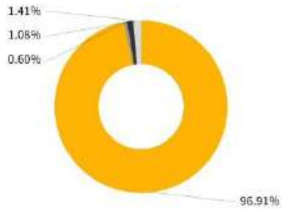

*Citations in 2022 to items published in [2020 - 2022]

Rank by Journal Impact Factor

Journals within a category are sorted in descending order by Journal Impact Factor (JIF) resulting in the Category Ranking below. A separate rank is shown for each category in which the journal is listed in JCR. Data for the most recent year is presented at the top of the list, with other years shown in reverse chronological order. Learn more

EDITION
Science Citation Index Expanded (SCIE)

CATEGORY
ENVIRONMENTAL SCIENCES

135/275

JCR YEAR	JIF RANK	JIF QUARTILE	JIF PERCENTILE
2022	135/275	Q2	51.1
2021	148/279	Q3	47.13
2020	135/274	Q2	50.91
2019	N/A	N/A	N/A

EDITION
Science Citation Index Expanded (SCIE)

CATEGORY
WATER RESOURCES

38/103

JCR YEAR	JIF RANK	JIF QUARTILE	JIF PERCENTILE
2022	38/103	Q2	63.6
2021	36/100	Q2	64.50
2020	39/98	Q2	60.71
2019	31/94	Q2	67.55

Rank by Journal Citation Indicator (JCI)

Journals within a category are sorted in descending order by Journal Citation Indicator (JCI) resulting in the Category Ranking below. A separate rank is shown for each category in which the journal is listed in JCR. Data for the most recent year is presented at the top of the list, with other years shown in reverse chronological order. Learn more

CATEGORY
ENVIRONMENTAL SCIENCES
156/334

JCR YEAR	JCI RANK	JCI QUARTILE	JCI PERCENTILE
2022	156/334	Q2	53.44
2021	142/325	Q2	56.46
2020	135/306	Q2	56.05
2019	127/302	Q2	58.11
2018	112/297	Q2	62.46
2017	114/286	Q2	60.31

CATEGORY
WATER RESOURCES
56/131

JCR YEAR	JCI RANK	JCI QUARTILE	JCI PERCENTILE
2022	56/131	Q2	57.63
2021	53/124	Q2	57.66
2020	56/120	Q2	53.75
2019	56/119	Q2	53.36
2018	49/117	Q2	58.55
2017	54/117	Q2	54.27

Citation network

Cited Half-life

2.9 years

The Cited Half-Life is the median age of the items in this journal that were cited in the JCR year. Half of a journal's cited items were published more recently than the cited half-life.

TOTAL NUMBER OF CITES

52,504

NON SELF-CITATIONS

45,361

SELF-CITATIONS

7,143

Citing Half-life

7.4 years

The Citing Half-Life is the median age of items in other publications cited by this journal in the JCR year.

TOTAL NUMBER OF CITES

236,717

NON SELF-CITATIONS

229,574

SELF-CITATIONS

7,143

Cited Half-life Data

Citing Half-life Data

Export

15

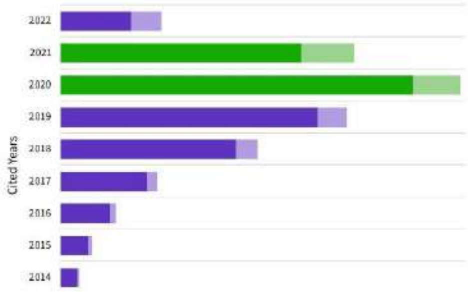

CITED YEAR	# OF CITES FROM 2022	CUMULATIVE %	# OF CITING SOURCES
All years	**52,504 citations**	**100.00%**	**3,254 sources** ›
2022	3,495 citations	6.66%	604 sources ›
2021	10,153 citations	25.99%	1,433 sources ›
2020	13,828 citations	52.33%	1,818 sources ›
2019	9,902 citations	71.19%	1,520 sources ›
2018	6,813 citations	84.17%	1,192 sources ›
2017	3,344 citations	90.54%	829 sources ›
2016	1,923 citations	94.20%	562 sources ›
2015	1,104 citations	96.30%	395 sources ›

Journal Citation Relationships

Cited Data Citing Data

Top 20 journals citing WATER-SUI by number of citations

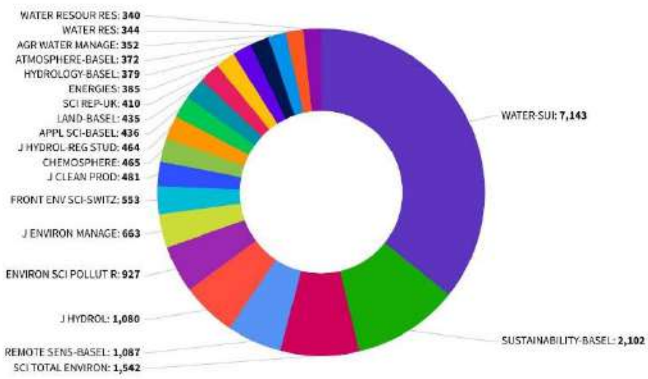

Content metrics

Source data

Average JIF Percentile ⤓ Export

This tile shows the breakdown of document types published by the journal. Citable Items are Articles and Reviews. For the purposes of calculating JIF, a JCR year considers the publications of that journal in the two prior years. Learn more

4,040 total citable items

	ARTICLES	REVIEWS	COMBINED(C)	OTHER DOCUMENT TYPES(O)	PERCEI
NUMBER IN JCR YEAR 2022 (A)	3,817	223	4,040	97	98%
NUMBER OF REFERENCES (B)	207,130	28,127	235,257	1,460	99%
RATIO (B/A)	54.3	126.1	58.2	15.1	

The Average Journal Impact Factor Percentile takes the sum of the JIF Percentile rank for each category under consideration, then calculates the average of those values. Learn more

ALL CATEGORIES AVERAGE
57.4

EDITION
Science Citation Index Expanded

ENVIRONMENTAL SCIENCES
51.1

WATER RESOURCES
63.6

Contributions by organizations

Export

Organizations that have contributed the most papers to the journal in the most recent three-year period. Learn more

RANK	ORGANIZATION	COUNT
1	CHINESE ACADEMY OF SCIENCES	594
2	HOHAI UNIVERSITY	288
3	CENTRE NATIONAL DE LA RECHERCHE SCIENTIFIQUE (CNRS)	220
4	EGYPTIAN KNOWLEDGE BANK (EKB)	187
5	CHINA INSTITUTE OF WATER RESOURCES & HYDROPOWER	179

Contributions by country/region

Export

Countries or Regions that have contributed the most papers to the journal in the most recent three-year period. Learn more

RANK	COUNTRY / REGION	COUNT
1	CHINA MAINLAND	3542
2	USA	1445
3	Italy	904
4	Spain	690
5	GERMANY (FED REP GER)	588
6	South Korea	519
7	Poland	388
8	England	383
9	Canada	381

Additional metrics

Eigenfactor Score

Normalized Eigenfactor

Article influence score

0.05670

The Eigenfactor Score is a reflection of the density of the network of citations around the journal using 5 years of cited content as cited by the Current Year. It considers both the number of citations and the source of those citations, so that highly cited sources will influence the network more than less cited sources. The Eigenfactor calculation does not include journal self-citations. Learn more

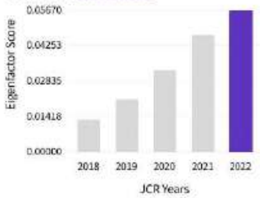

12.34147

The Normalized Eigenfactor Score is the Eigenfactor score normalized, by rescaling the total number of journals in the JCR each year, so that the average journal has a score of 1. Journals can then be compared and influence measured by their score relative to 1. Learn more

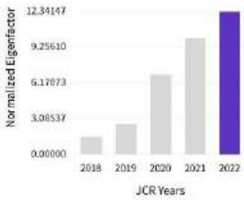

0.517

The Article Influence Score normalizes the Eigenfactor Score according to the cumulative size of the cited journal across the prior five years. The mean Article Influence Score for each article is 1.00. A score greater than 1.00 indicates that each article in the journal has above-average influence. Learn more

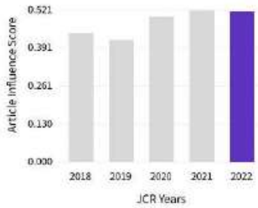

5 Year Impact Factor

3.5

View Calculation

The 5-year Impact Factor is the average number of times articles from the journal published in the past five years have been cited in the JCR year. It is calculated by dividing the number of citations in the JCR year by the total number of articles published in the five previous years. Learn more

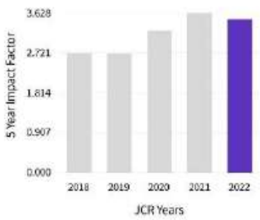

Immediacy Index

0.9

View Calculation

The Immediacy Index is the count of citations in the current year to the journal that reference content in this same year. Journals that have a consistently high Immediacy Index attract citations rapidly. Learn more

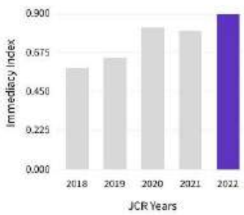

Geogaceta

Scopus coverage years: from 2017 to 2023
Publisher: Sociedad Geologica de Espana
ISSN: 0213-683X E-ISSN: 2173-6545
Subject area: Earth and Planetary Sciences: Geology
Source type: Journal

CiteScore 2022
0.4

SJR 2022
0.182

SNIP 2022
0.159

CiteScore

CiteScore 2022

0.4 = 72 Citations 2019 - 2022 / 166 Documents 2019 - 2022

Calculated on 05 May, 2023

CiteScoreTracker 2023

0.4 = 67 Citations to date / 172 Documents to date

Last updated on 05 April, 2024 • Updated monthly

CiteScore rank 2022

Category	Rank	Percentile
Earth and Planetary Sciences Geology	#261/284	8th

CiteScore trend

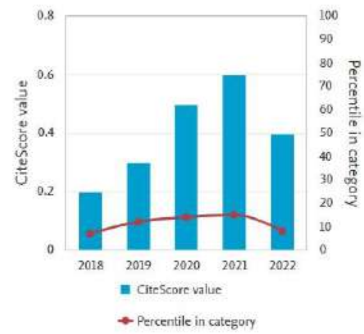

Products

Journal Citation Reports™ Journals Categories Pub My favorites Sign In Register

Home > Journal profile

JCR Year
2022

Favorite Export

Energies

Open Access since 2008

ISSN
N/A

EISSN
1996-1073

JCR ABBREVIATION
ENERGIES

ISO ABBREVIATION
Energies

Journal information

EDITION
Science Citation Index Expanded (SCIE)

CATEGORY
ENERGY & FUELS - SCIE

LANGUAGES	REGION	1ST ELECTRONIC JCR YEAR
English	SWITZERLAND	2010

Publisher information

PUBLISHER	ADDRESS	PUBLICATION FREQUENCY
MDPI	ST ALBAN-ANLAGE 66, CH-4052 BASEL, SWITZERLAND	24 issues/year

Journal's performance

Journal Impact Factor

The Journal Impact Factor (JIF) is a journal-level metric calculated from data indexed in the Web of Science Core Collection. It should be used with careful attention to the many factors that influence citation rates, such as the volume of publication and citations characteristics of the subject area and type of journal. The Journal Impact Factor can complement expert opinion and informed peer review. In the case of academic evaluation for tenure, it is inappropriate to use a journal-level metric as a proxy measure for individual researchers, institutions, or articles. Learn more

2022 JOURNAL IMPACT FACTOR
3.2
View calculation

JOURNAL IMPACT FACTOR WITHOUT SELF CITATIONS
2.5
View calculation

Journal Impact Factor Trend 2022 Export

Journal Impact Factor contributing items Export

Citable items (15,245) Citing Sources (3,303)

TITLE	CITATION COUNT
Internet of Things (IoT) and the Energy Sector	94

15

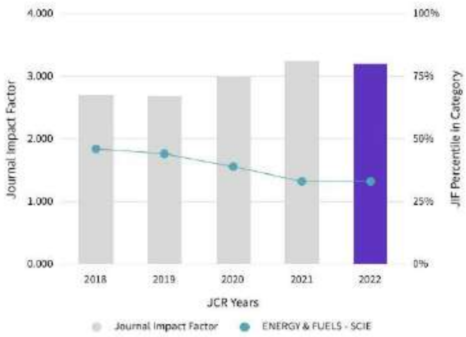

View all years

A Novel Approach of Design and Analysis of a Hexagonal Fractal Anten...	87	˅
Sustainable Solutions for Green Financing and Investment in...	81	˅
Ammonia as Effective Hydrogen Storage: A Review on Production,...	69	˅
Decarbonization of the Iron and Steel Industry with Direct Reduction of Iron...	63	˅
Do Perceived Risk, Perception of Self-Efficacy, and Openness to Technolog...	55	˅
Performance Comparison and Current Challenges of Using Machine Learnin...	54	˅
Revisiting the Role of Fiscal Policy, Financial Development, and Foreign...	52	˅
Characterization of Hybrid-nano/Paraffin Organic Phase Change...	50	˅
Do Environment-Related Policy Instruments and Technologies Facilit...	50	˅

View All in Web of Science

Journal Citation Indicator (JCI)

Export

0.46

The Journal Citation Indicator (JCI) is the average Category Normalized Citation Impact (CNCI) of citable items (articles & reviews) published by a journal over a recent three year period. The average JCI in a category is 1. Journals with a JCI of 1.5 have 50% more citation impact than the average in that category. It may be used alongside other metrics to help you evaluate journals. Learn more

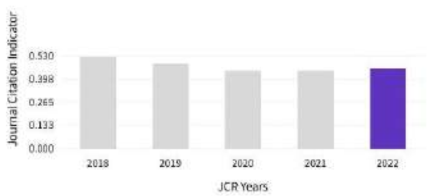

View all years

Total Citations

Export

103,643

The total number of times that a journal has been cited by all journals included in the database in the JCR year. Citations to journals listed in JCR are compiled annually from the JCR years combined database, regardless of which JCR edition lists the journal.

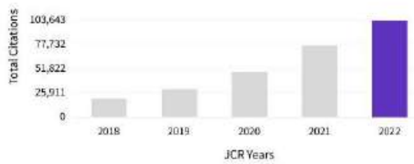

View all years

15

Citation distribution

Export

The Citation Distribution shows the frequency with which items published in the year or two years prior were cited in the JCR data year (i.e., the component of the calculation of the JIF). The graph has similar functionality as the JIF Trend graph, including hover-over data descriptions for each data point, and an interactive legend where each data element's legend can be used as a toggle. You can view Articles, Reviews, or Non-Citable (other) items to the JIF numerator. Learn more

ARTICLE CITATION MEDIAN

2

REVIEW CITATION MEDIAN

5

UNLINKED CITATIONS

541

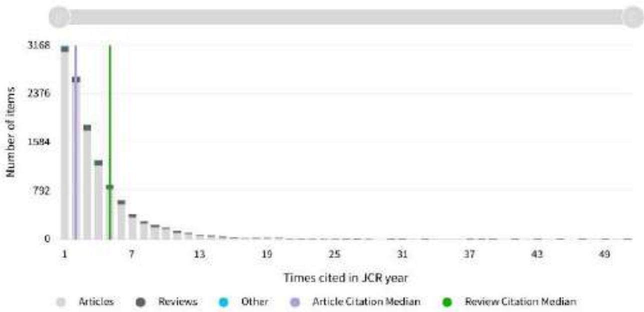

TIMES CITED

0

ARTICLES

2,868

REVIEWS

52

OTHER

73

Open Access (OA)

Export

The data included in this tile summarizes the items published in the journal in the JCR data year and in the previous two years. This three-year set of published items is used to provide descriptive analysis of the content and community of the journal. Learn more

Items

TOTAL CITABLE	% OF CITABLE OA
24,643	99.47%

Citations*

TOTAL CITABLE	% OF CITABLE OA
57,942	99.32%

CITABLE

GOLD OPEN ACCESS
24,513 / 98.01%

SUBSCRIPTION AND FREE TO READ
130 / 0.52%

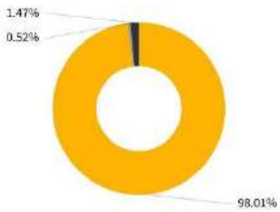

NON-CITABLE

OTHER (NON CITABLE ITEMS)
367 / 1.47%

CITABLE

GOLD OPEN ACCESS
57,548 / 97.90%

SUBSCRIPTION AND FREE TO READ
394 / 0.67%

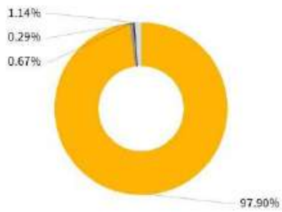

NON-CITABLE

OTHER (NON CITABLE ITEMS)
170 / 0.29%

UNLINKED CITATIONS
670 / 1.14%

*Citations in 2022 to items published in [2020 - 2022]

Rank by Journal Impact Factor

Journals within a category are sorted in descending order by Journal Impact Factor (JIF) resulting in the Category Ranking below. A separate rank is shown for each category in which the journal is listed in JCR. Data for the most recent year is presented at the top of the list, with other years shown in reverse chronological order. Learn more

EDITION
Science Citation Index Expanded (SCIE)

CATEGORY
ENERGY & FUELS

80/119

JCR YEAR	JIF RANK	JIF QUARTILE	JIF PERCENTILE
2022	80/119	Q3	33.2
2021	80/119	Q3	33.19
2020	70/114	Q3	39.04
2019	63/112	Q3	44.20

Rank by Journal Citation Indicator (JCI)

Journals within a category are sorted in descending order by Journal Citation Indicator (JCI) resulting in the Category Ranking below. A separate rank is shown for each category in which the journal is listed in JCR. Data for the most recent year is presented at the top of the list, with other years shown in reverse chronological order. Learn more

CATEGORY

ENERGY & FUELS

99/155

JCR YEAR	JCI RANK	JCI QUARTILE	JCI PERCENTILE
2022	99/155	Q3	36.45
2021	93/145	Q3	36.21
2020	81/133	Q3	39.47
2019	73/132	Q3	45.08
2018	70/131	Q3	46.95
2017	68/126	Q3	46.43

Citation network

Cited Half-life

2.7 years

The Cited Half-Life is the median age of the items in this journal that were cited in the JCR year. Half of a journal's cited items were published more recently than the cited half-life.

TOTAL NUMBER OF CITES

103,643

NON SELF-CITATIONS

81,849

SELF-CITATIONS

21,794

Citing Half-life

5.7 years

The Citing Half-Life is the median age of items in other publications cited by this journal in the JCR year.

TOTAL NUMBER OF CITES

481,423

NON SELF-CITATIONS

459,629

SELF-CITATIONS

21,794

Cited Half-life Data

Citing Half-life Data

Export

15

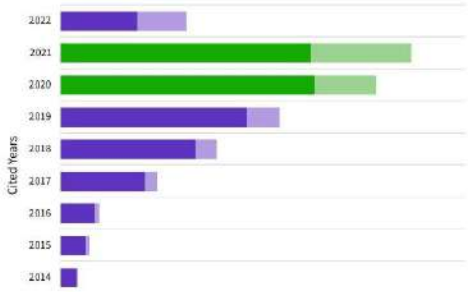

CITED YEAR	# OF CITES FROM 2022	CUMULATIVE %	# OF CITING SOURCES
All years	**103,643 citations**	**100.00%**	**4,260 sources** ›
2022	9,355 citations	9.03%	1,043 sources ›
2021	26,006 citations	34.12%	2,267 sources ›
2020	23,421 citations	56.72%	2,430 sources ›
2019	16,267 citations	72.41%	2,121 sources ›
2018	11,592 citations	83.60%	1,730 sources ›
2017	7,181 citations	90.52%	1,376 sources ›
2016	2,897 citations	93.32%	833 sources ›

Journal Citation Relationships

Cited Data Citing Data

Top 20 journals citing ENERGIES by number of citations

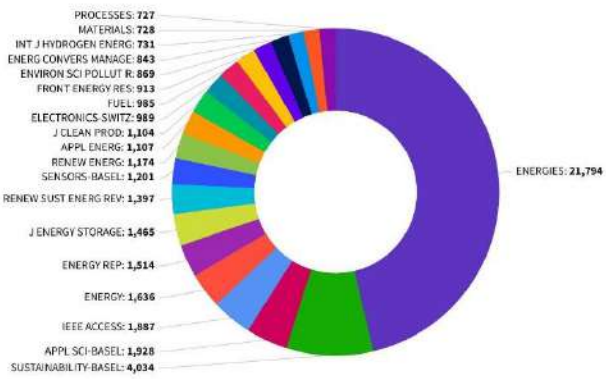

Content metrics

Source data

Average JIF Percentile

Export

This tile shows the breakdown of document types published by the journal. Citable Items are Articles and Reviews. For the purposes of calculating JIF, a JCR year considers the publications of that journal in the two prior years. Learn more

9,398 total citable items

	ARTICLES	REVIEWS	COMBINED(C)	OTHER DOCUMENT TYPES(D)	PERCE
NUMBER IN JCR YEAR 2022 (A)	8,569	829	9,398	257	97%
NUMBER OF REFERENCES (B)	378,136	99,611	477,747	3,676	99%
RATIO (B/A)	44.1	120.2	50.8	14.3	

The Average Journal Impact Factor Percentile takes the sum of the JIF Percentile rank for each category under consideration, then calculates the average of those values. Learn more

ALL CATEGORIES AVERAGE

33.2

EDITION

Science Citation Index Expanded

ENERGY & FUELS

33.2

Contributions by organizations

Export

Organizations that have contributed the most papers to the journal in the most recent three-year period. Learn more

RANK	ORGANIZATION	COUNT
1	AGH UNIVERSITY OF KRAKOW	537
2	WARSAW UNIVERSITY OF TECHNOLOGY	360
3	CHINESE ACADEMY OF SCIENCES	355
4	SILESIAN UNIVERSITY OF TECHNOLOGY	335
5	EGYPTIAN KNOWLEDGE BANK (EKB)	320
6	CHINA UNIVERSITY OF PETROLEUM	287

Contributions by country/region

Export

Countries or Regions that have contributed the most papers to the journal in the most recent three-year period. Learn more

RANK	COUNTRY / REGION	COUNT
1	CHINA MAINLAND	5814
2	Poland	4278
3	Italy	1871
4	USA	1767
5	South Korea	1731
6	GERMANY (FED REP GER)	1224
7	Spain	1148
8	England	1125
9	Saudi Arabia	704

Additional metrics

Eigenfactor Score

Normalized Eigenfactor

Article influence score

0.09910

The Eigenfactor Score is a reflection of the density of the network of citations around the journal using 5 years of cited content as cited by the Current Year. It considers both the number of citations and the source of those citations, so that highly cited sources will influence the network more than less cited sources. The Eigenfactor calculation does not include journal self-citations. Learn more

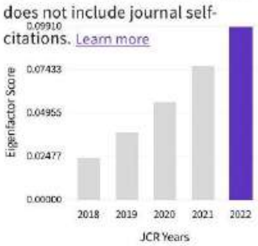

21.56905

The Normalized Eigenfactor Score is the Eigenfactor score normalized, by rescaling the total number of journals in the JCR each year, so that the average journal has a score of 1. Journals can then be compared and influence measured by their score relative to 1. Learn more

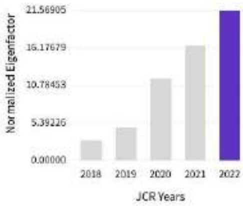

0.439

The Article Influence Score normalizes the Eigenfactor Score according to the cumulative size of the cited journal across the prior five years. The mean Article Influence Score for each article is 1.00. A score greater than 1.00 indicates that each article in the journal has above-average influence. Learn more

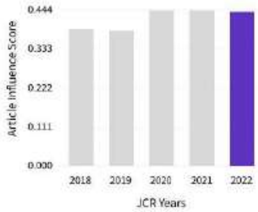

5 Year Impact Factor

3.3

View Calculation

The 5-year Impact Factor is the average number of times articles from the journal published in the past five years have been cited in the JCR year. It is calculated by dividing the number of citations in the JCR year by the total number of articles published in the five previous years. Learn more

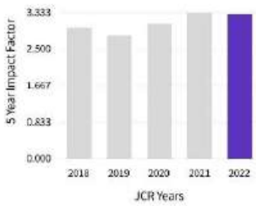

Immediacy Index

1.0

View Calculation

The Immediacy Index is the count of citations in the current year to the journal that reference content in this same year. Journals that have a consistently high Immediacy Index attract citations rapidly. Learn more

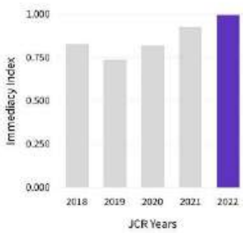

15